KU LEUVEN

ARENBERG DOCTORAL SCHOOL
Faculty of Engineering Science

Multimodal epileptic seizure detection: towards a wearable solution

Kaat Vandecasteele

Supervisors:
Prof. dr. ir. S. Van Huffel
Prof. dr. W. Van Paesschen
Prof. dr. ir. B. Hunyadi

Dissertation presented in partial fulfillment of the requirements for the degree of Doctor of Engineering Science (PhD): Electrical Engineering

April 2021

Multimodal epileptic seizure detection: towards a wearable solution

Kaat VANDECASTEELE

Examination committee:
Prof. dr. ir. Y. Willems, chair
Prof. dr. ir. S. Van Huffel, supervisor
Prof. dr. W. Van Paesschen, supervisor
Prof. dr. ir. B. Hunyadi, supervisor
(TU Delft, The Netherlands)
Prof. dr. L. Lagae
Prof. dr. ir. J. Suykens
Prof. dr. ir. M. De Vos
Prof. dr. S. Beniczky
(Aarhus University Hospital, Denmark)

Dissertation presented in partial fulfillment of the requirements for the degree of Doctor of Engineering Science (PhD): Electrical Engineering

April 2021

© 2021 KU Leuven – Faculty of Engineering Science
Uitgegeven in eigen beheer, Kaat Vandecasteele, Kasteelpark Arenberg 10 box 2446, B-3001 Leuven (Belgium), B-3001 Leuven (Belgium)

Alle rechten voorbehouden. Niets uit deze uitgave mag worden vermenigvuldigd en/of openbaar gemaakt worden door middel van druk, fotokopie, microfilm, elektronisch of op welke andere wijze ook zonder voorafgaande schriftelijke toestemming van de uitgever.

All rights reserved. No part of the publication may be reproduced in any form by print, photoprint, microfilm, electronic or any other means without written permission from the publisher.

Preface

The foundations of this thesis were already established in my last year of the master 'biomedical engineering'. I did my master thesis 'online multimodal seizure detection for children' within the group of Prof. Sabine Van Huffel under guidance of daily mentor Thomas De Cooman. When I heard Prof. Sabine van Huffel was looking for a PhD student working on seizure detection, I was immediately interested. The position looked even more interesting as it was part of an ICON project, a collaboration with partners from industry. Although I expected to have low chances, Prof. Sabine Van Huffel made me very happy to offer me the PhD position.

First of all, I would like to thank Prof. Sabine Van Huffel for giving me the opportunity to work on this PhD thesis. Even though you had many PhD students, projects and responsibilities, you kept track of my research, provided a lot of feedback and guided me towards the right direction. Not only the research results and outcomes were important but you kept also an eye on the well-being of every PhD student. The efforts you did to create a nice working atmosphere at BIOMED, are really appreciated and successful. We were every year welcome in your house during the Christmas party and pizza evening to welcome the new students. Those parties together with the speeches you gave, created a sort of bonding between the colleagues and a warm atmosphere.

I can hardly thank enough my daily supervisor, Prof. Borbála Hunyadi, for all the guidance during those four and a half years. I consider myself very lucky and my path towards the end would have been way more difficult or maybe impossible without your help. Whenever I got stuck and I had no idea how to proceed, you always came up with a solution. I learned a lot from your critical mindset during those years. When you were on pregnancy leave or when you joined TU Delft, I still could ask you advice but I had to be more independent. To be honest, I was a bit afraid of those periods, but in the end it was a very good lesson. When I had some problems, I forced myself to think 'What would Bori's advice be?'. This helped me to develop a more creative and

critical mindset.

This thesis would not be possible without the help of the clinical partners. I would like to thank all the collaborators of UZ Leuven in the group of Prof. Wim Van Paesschen, especially Evy, Lauren and Jaiver. This collaboration was crucial for me and our research team. Of course, the datasets are needed, but also the feedback and insides in the clinical point of view are key to develop novel and smart algorithms. Furthermore, I really appreciate the time and effort for the visualisation studies.

I would like to thank all the partners from the SeizeIT consortium from UCB, Byteflies, and Pilipili, especially Kasper, Gergely, Luís, Valentina, Hans & Hans, Jonathan, Waverlee, Lars, Benjamin and Brecht. I also would like to thank Steven, our former valorisation manager. This project was important for me to see the usefulness and application of my research, which was a very important driver. I really hope the algorithms I developed will be used one day to monitor seizures in patients during daily life. I hope epilepsy patients will have an improved quality of life, due to the device and the SeizeIT consortium.

I would also like to thank the other members of my examination committee: Prof. Yves Willems for accepting the invitation to be the chair of the defense. Prof. Lieven Lagae and Prof. Johan Suykens to be assessors and improve my research work by giving your critical opinions and asking questions. Prof. Maarten de Vos and Prof. Sándor Beniczky, it was an honour to have you as external jury members. Maarten, you were more than only a jury member of my PhD. Thanks for the additional guidance the last year of my PhD and steering our SeizeIT algorithm development team to a next level.

Next, I would like to thank all the collaborators of the Flanders AI research program involved in the use case 'Clinical Decision Support: Epilepsy monitoring' to improve the current state-of-the-art seizure detection algorithms.

BIOMED would not be BIOMED without such a nice colleagues. The first day of my PhD was the same day as the reflection day of August 2016. I remember that I was so surprised about the craziness and kindness of all of you. Mario, you were the first one that started to talk to me. It was directly clear that you were a very open and kind person. I actually was happy you were talking a lot so that I didn't need to say much. Carolina, Alex and Bori, you were very welcoming for new people in the group. Furthermore, you had an important role in the research group to guide all the PhD students. Ofelie, John and Dorien, I enjoyed all our runs/walks and especially the talks on our way. Jonathan M., we already knew each other from the master and started the PhD at the same time. It was nice that you had the same PhD timeline so we could complain a bit and encourage each other. Amalia, you are really

an enthusiastic person and always with a smile on your face! Rob, the parties you organized such as the cryptocoin party were remarkable. Furthermore, you definitely boosted the presentation and design skills of BIOMED. Lieven, I enjoyed playing badminton together at ESAT sportsday. Griet, Laure & Margot, there was always such a nice atmosphere in your office, full of laughter. Nick, Abhi, Christos, Jonathan D., thank you very much for the wonderful Neureka challenge collaboration. Thanks to you, we won this challenge! It was nice having some team work in my PhD career. Jasper, Simon V., Neetha, Dries, Simon G., Pooya and Cem, it was nice to have some talks with you about whatever. Tim, Thomas, Nithin, Elisabeth, Laura, Joran, Luis, Constantinos, and all the new people that recently joined, you started your PhD in a very nice research group. Unfortunately due to my pregnancy leave and the Covid lockdown periods, we didn't spend a lot of time together.

Special thanks to my office mates Abhi, Jonathan D., Ying, Thomas D., Christos and Amir. Abhi, thank you very much for the talks and helping me out with ESAT servers and other technical issues I had. By the way, your knowledge on cultural and historical sites in Belgium is remarkable. Jonathan D., I got to know you as a collaborator from Byteflies and one year later you became my office mate! I really appreciated all our discussions and got a lot of inspiration from it. Ying, it was nice having you in the office. Thomas, thanks for all the good advice during my PhD and also during my master thesis. Christos, it was very nice you joined the epilepsy SeizeIT team. Whatever question I had, you could always give very valuable advice. Amir, I really appreciated all your advice and guidance regarding deep learning. You have very good teaching skills. I was blessed with such a smart and nice office mates. As last, Miguel and Jingwei, I am happy that SeizeIT is in good hands.

Ook wil ik mijn mama en papa bedanken samen met mijn zussen: Leen, Tine en Joke. Jullie hebben me altijd aangemoedigd om het beste van mezelf te geven. Ik kijk er altijd naar uit om zondagmiddag te komen eten. Ook bedankt om af en toe eens op Elise te passen zodat ik nog wat extra tijd had om me te concentreren op mijn doctoraat.

En als laatste wil ik mijn eigen gezinnetje bedanken. Benjamin, wat een geluk dat ik jou ben tegen gekomen! Bedankt voor al je liefde en steun, zeker tijdens de laatste maanden van mijn doctoraat. Elise en ons kindje in mijn buik, ik hoop dat jullie ooit dit boekje zullen vastpakken en lezen, dan zal ik heel trots zijn. Dankzij jullie kan ik mijn gedachten snel verzetten als ik eens een moeilijkere dag heb. Af en toe was het wel eens een uitdaging om onze jobs te combineren met de sluiting en verstrengde regels van de crèche tijdens de Corona periode, maar moeilijk gaat ook! Ik kijk al uit naar onze mooie toekomst samen!

Kaat Vandecasteele, April 2021

Abstract

Epilepsy is one of the most common neurological disorders, which affects almost 1% of the population worldwide. Anti-epileptic drugs provide adequate treatment for about 70% of epilepsy patients. The remaining 30% of the patients continue to have seizures, which drastically affects their quality of life. In order to obtain efficacy measures of therapeutic interventions for these patients, an objective way to count and document seizures is needed. However, in an outpatient setting, one of the major problems is that seizure diaries kept by patients are unreliable.

Automated seizure detection systems could help to objectively quantify seizures. Those detection systems are typically based on full scalp Electroencephalography (EEG). In an outpatient setting, full scalp EEG is of limited use because patients will not tolerate wearing a full EEG cap for long time periods during daily life. There is a need for ambulatory seizure detection systems using wearable sensors. In this thesis, the focus lies on focal seizures, since for this group no existing non-invasive effective solutions for seizure detection in a daily life environment are on the market. The aim of this thesis is the development of an offline seizure detection algorithm to construct automatically a seizure diary. There were three major contributions: seizure detection using Electrocardiography (ECG)/ Photoplethysmography (PPG), seizure detection using behind-the-ear EEG and multimodal seizure detection using ECG and behind-the-ear EEG.

Focal seizures, especially temporal focal seizures, most common in the population of focal epilepsy, are associated with changes in the autonomic nervous system, in particular the cardiovascular system. It has been shown that temporal lobe seizures are often accompanied with a strong heart rate increase. Those heart rate increases can be measured using Electrocardiography (ECG) . Most of the published articles use ECG recorded with wired electrodes using hospital equipment. However, a wearable solution is preferred. Furthermore, ECG electrodes can be uncomfortable and can cause skin irritation after a few days. Another way to measure heart rate is by a photoplethysmography (PPG) sensor

in a smartwatch. PPG makes use of reflected light to measure changes in light absorption, caused by changes in the blood volume due to heart beats. The seizure detection performance of a wearable PPG and ECG device were compared with that of ECG recorded with wired hospital equipment. The sensitivities of ECG measured with the hospital system, the wearable ECG device and the wearable PPG device were respectively 57%, 70% and 32%, with corresponding false alarms per hour of 1.92, 2.11 and 1.80. Whereas seizure detection performance using the wrist-worn PPG device was considerably lower, the performance using the wearable ECG was proven to be similar to that of the hospital ECG.

Seizure detection systems based on only the heart rate have around 2 false alarms per hour, which is too high for practical use. Behind-the-ear EEG channels can also be recorded with a wearable device. Firstly, the recognition of ictal patterns using only behind-the-ear EEG channels was investigated resulting in 65.7% sensitivity and 94.4% specificity. Secondly, an automated seizure detection algorithm was developed using only those behind-the-ear EEG channels. By using the behind-the-ear seizure annotations, the automated algorithm obtained 64.1% sensitivity and 2.8 false alarms per 24 hours with the patient-independent model. The patient-specific model achieved 69.1% sensitivity and 0.49 false alarms per 24 hours.

In most cases, seizure detection algorithms in literature are developed using only one modality. However, combining different modalities can lead to a better performance. A multimodal automated seizure detection algorithm integrating behind-the-ear EEG and ECG was developed to detect focal seizures. In this framework, we quantified the added value of ECG compared to only behind-the-ear channels using a multicenter dataset. The multimodal algorithm outperformed the EEG-based seizure detection in two out of the three databases with an increase in sensitivity of 10% and 8% for the same false alarm rate.

Beknopte samenvatting

Epilepsie is één van de meest voorkomende neurologische aandoeningen, die bijna 1% van de bevolking wereldwijd treft. Anti-epileptica zorgen voor een adequate behandeling van ongeveer 70% van de epilepsiepatiënten. De overige 30% van de patiënten krijgt nog steeds aanvallen, wat hun kwaliteit van leven drastisch beïnvloedt. Om de werkzaamheid van anti-epileptica voor deze patiënten op te volgen, is een objectieve manier nodig om aanvallen te registreren en documenteren. In een thuisomgeving is één van de grootste problemen echter dat de aanvalsdagboeken die door patiënten worden bijgehouden, onbetrouwbaar zijn.

Geautomatiseerde systemen voor het detecteren van aanvallen zijn nodig om aanvallen objectief te kwantificeren. Die detectiesystemen zijn meestal gebaseerd op elektro-encefalografie (EEG), waarbij electroden verspreid over het volledige hoofd, worden geplaatst. In een thuisomgeving is zo een volledige EEG van beperkt nut omdat patiënten niet tolereren om gedurende lange tijd dit apparaat te dragen tijdens het dagelijks leven. Er is behoefte aan ambulante aanvalsdetectiesystemen met draagbare sensoren. In dit proefschrift ligt de focus op focale aanvallen, aangezien er voor deze groep geen bestaande effectieve en niet-invasieve oplossingen voor het opsporen van aanvallen in een dagelijkse omgeving op de markt zijn. Het doel van dit proefschrift is de ontwikkeling van een offline algoritme voor het detecteren van aanvallen om automatisch een aanvalsdagboek te maken. Er waren drie belangrijke bijdragen: detectie van aanvallen met behulp van elektrocardiografie (ECG)/ photoplethysmografie (PPG), detectie van aanvallen met behulp van EEG opgemeten achter het oor, en multimodale detectie van aanvallen met behulp van ECG en EEG opgemeten achter het oor.

Focale aanvallen, vooral temporale focale aanvallen, die het meest voorkomen bij de populatie van focale epilepsie, zijn geassocieerd met veranderingen in het autonome zenuwstelsel, in het bijzonder het cardiovasculaire systeem. Het is aangetoond dat aanvallen van de temporale kwab vaak gepaard gaan

met een sterke verhoging van de hartslag. Die hartslagverhogingen kunnen worden gemeten met behulp van elektrocardiografie (ECG). De meeste van de gepubliceerde artikelen gebruiken ECG signalen die zijn opgenomen met bedrade elektroden gebruik makende van ziekenhuisapparatuur. Een draagbare oplossing heeft echter de voorkeur. Bovendien kunnen ECG elektroden ongemakkelijk zijn en na een paar dagen huidirritatie veroorzaken. Een andere manier om hartslag te meten, is door een photoplethysmografie (PPG) sensor in een smartwatch te gebruiken. PPG maakt gebruik van gereflecteerd licht om veranderingen in lichtabsorptie te meten, veroorzaakt door veranderingen in het bloedvolume als gevolg van hartslagen. De accuraatheid van aanvalsdetectie met een draagbare PPG en ECG sensor werden vergeleken met die van ECG gemeten met ziekenhuisapparatuur. De sensitiviteiten van ECG gemeten met het ziekenhuissysteem, de draagbare ECG sensor en de draagbare PPG sensor waren respectievelijk 57%, 70% en 32%, met bijbehorend 1,92, 2,11 en 1,80 valse alarmen per uur. De accuraatheid van de PPG sensor voor het detecteren van aanvallen was aanzienlijk lager, terwijl de accuraatheid van de draagbare ECG sensor vergelijkbaar was met dat van het ECG apparaat van het ziekenhuis.

Aanvalsdetectiesystemen op basis van alleen de hartslag hebben ongeveer 2 valse alarmen per uur, wat te hoog is voor praktisch gebruik. EEG kanalen achter het oor kunnen ook worden opgemeten met een draagbaar apparaat. Ten eerste werd de herkenning van ictale patronen met deze EEG kanalen onderzocht, resulterend in 65,7% sensitiviteit en 94,4% specificiteit. Ten tweede werd een geautomatiseerd algoritme voor het detecteren van aanvallen ontwikkeld met alleen die specifieke EEG kanalen achter het oor. Bij gebruik van de annotaties van herkende epileptische aanvallen, behaalde het geautomatiseerde algoritme 64,1% sensitiviteit en 2,8 valse alarmen per 24 uur met het patiënt-onafhankelijke model. Het patiënt-specifieke model behaalde een sensitiviteit van 69,1% en 0,49 valse alarmen per 24 uur.

In de meeste gevallen worden algoritmen voor het detecteren van aanvallen in de literatuur ontwikkeld met behulp van slechts één modaliteit. Het combineren van verschillende modaliteiten kan echter leiden tot betere performanties. Een multimodaal geautomatiseerd algoritme voor het detecteren van aanvallen dat de informatie van EEG opgemeten achter het oor en ECG combineert, werd ontwikkeld om focale aanvallen te detecteren. In dit kader hebben we de toegevoegde waarde van ECG vergeleken met EEG kanalen achter het oor met behulp van een multicenter dataset. Het multimodale algoritme presteerde beter dan de EEG-gebaseerde aanvalsdetectie in twee van de drie databases met een toename in sensitiviteit van 10% en 8% voor hetzelfde aantal valse alarmen.

Nomenclature

Abbreviations

ACC	Accelerometry
AEDs	Anti-epileptic drugs
ANS	Autonomic Nervous System
BSS	Blind Source Separation
CCA	Canonical Correlation Analysis
CNN	Convolutional Neural Networks
DBS	Deep Brain Stimulation
DL	Deep Learning
ECG	Electrocardiography
EDA	Electrodermal Activity
EEG	Electroencephalography
EEMD	Ensemble Empirical Mode Decomposition
EMD	Empirical Mode Decomposition
FA	Focal Aware
FAR	False Alarm Rate
F-BTC	Focal to Bilateral Tonic Clonic
FIA	Focal Impaired Awareness
FN	False Negative
FP	False Positive
GC	Generalized Clonic
GTC	Generalized Tonic-Clonic
GT	Generalized Tonic
GRU	Gated Recurrent Unit
HR	Heart Rate
HRV	Heart Rate Variability
ICA	Independent Component Analysis
LD	Light Detector

LED	Light Emitting Diode
LSTM	Long Short Term Memory
MNA	Motion and Noise Artifacts
MWF	Multichannel Wiener Filter
PI	Patient-Independent
PPG	Photoplethysmography
PPV	Positive Predictive Value
PRV	Pulse Rate Variability
PS	Patient-Specific
RD	Recording Duration
RF	Random Forest
RNN	Recurrent Neural Networks
ROC	Receiver Operating Characteristic
RRMSE	Relative Root Mean Squared Error
SD	Seizure Duration
Se	Sensitivity
sEMG	Surface Electromyography
SNRs	Signal to Noise Ratios
SUDEP	Sudden Unexpected Death in Epilepsy
SVM	Support Vector Machines
TP	True Positive
TLE	Temporal Lobe Epilepsy
vEEG	Video-electroencephalography
VNS	Vagus-nerve Stimulation

Contents

Abstract v

Beknopte samenvatting vii

Contents xi

List of Figures xvii

List of Tables xxi

1 Introduction 1
- 1.1 Problem statement . . . 1
- 1.2 Outline of the thesis . . . 2
- 1.3 Collaborations . . . 3

2 Epilepsy and monitoring solutions 5
- 2.1 The brain: physiology and anatomy . . . 5
- 2.2 The autonomic nervous system . . . 7
- 2.3 Epilepsy . . . 8
  - 2.3.1 Definition and diagnosis . . . 8
  - 2.3.2 Seizure classification . . . 10
  - 2.3.3 Treatment . . . 10
  - 2.3.4 Mortality risk for patients with epilepsy . . . 12
  - 2.3.5 Seizure monitoring . . . 12
- 2.4 Modalities for automated seizure detection . . . 14
  - 2.4.1 Electroencephalography (EEG) . . . 14
  - 2.4.2 Behind-the-ear EEG . . . 15
  - 2.4.3 Electrocardiography (ECG) . . . 17
  - 2.4.4 Photoplethysmography (PPG) . . . 20
  - 2.4.5 Quality of PPG measured at different places on the body 21
  - 2.4.6 Others . . . 21

2.5 Existing wearable seizure detection devices 22
2.5.1 Epi-Care 22
2.5.2 Empatica 23
2.5.3 Nightwatch 23
2.5.4 Brain Sentinel 23
2.5.5 EDDI 23
2.5.6 Devices for focal seizures 24

3 Machine Learning Methods **25**
3.1 Machine Learning techniques: feature-based models 25
3.1.1 Support Vector Machines 26
3.1.2 Random Forest 28
3.2 Machine Learning techniques: Deep Learning models 28
3.2.1 Convolutional Neural Networks (CNN) 29
3.2.2 Recurrent Neural Networks (RNN) 30
3.3 Imbalanced data set 31
3.4 Normalization method: Median decaying memory 32
3.5 Cross-validation 32
3.6 Performance metrics 33

4 Data description **37**
4.1 SeizeIT1 37
4.1.1 Data description 37
4.1.2 Experimental setup 38
4.2 SeizeIT2 40
4.2.1 Data description 40
4.2.2 Experimental setup 41
4.3 European Epilepsiae Dataset 42
4.3.1 Data description 42
4.3.2 Experimental setup 43
4.4 Temple University Seizure Corpus (TUSZ) 44

5 Automated algorithms **45**
5.1 Electroencephalography (EEG) 45
5.1.1 Seizure detection based on Full scalp EEG 45
5.1.2 Seizure detection based on reduced EEG channels . . . 49
5.1.3 Personalization of seizure detection algorithms 50
5.1.4 Motion and muscle artifact removal 51
5.2 Electrocardiography (ECG) 51
5.2.1 Seizure detection algorithms based on ECG 51
5.2.2 Personalization of seizure detection algorithms 52
5.2.3 Artifact detection and quality assessment of ECG . . . 53
5.3 Photoplethysmography (PPG) 53

5.3.1 Seizure detection algorithms based on PPG 53
5.3.2 Personalization of seizure detection algorithms 54
5.3.3 Artifact detection and quality assessment of PPG 54
5.4 Multimodal seizure detection 55

6 Seizure detection based on wearable ECG/PPG 57
6.1 Abstract 57
6.2 Introduction 58
6.3 Data Acquisition 59
6.4 Methodology 61
6.4.1 HRV/PRV Extraction from ECG/PPG 61
6.4.2 Seizure Detection Algorithm 62
6.4.3 Evaluation Criteria 62
6.4.4 Evaluation of Sensitivity and False Alarms 62
6.5 Results 63
6.5.1 Sensitivity 63
6.5.2 False Alarms 63
6.6 Discussion 66
6.6.1 Sensitivity 66
6.6.2 False Alarms 68
6.6.3 Limitations and Further Work 68
6.7 Conclusions 69

7 Seizure detection based on behind-the-ear EEG 71
7.1 Abstract 71
7.1.1 Objective 71
7.1.2 Methods 72
7.1.3 Results 72
7.1.4 Significance 72
7.2 Introduction 72
7.3 Data Acquisition 74
7.4 Methodology 74
7.4.1 Visual seizure recognition 74
7.4.2 Autmodated seizure detection 74
7.5 Results 78
7.5.1 Visual seizure recognition 78
7.5.2 Automated seizure detection 80
7.6 Discussion 81
7.6.1 Visual seizure recognition 81
7.6.2 Automated seizure detection 82
7.6.3 Clinical use of algorithm 83
7.6.4 Future work 84

8 Multimodal seizure detection based on ECG and behind-the-ear EEG 85
8.1 Abstract . . . 85
8.1.1 Objective . . . 85
8.1.2 Methods . . . 86
8.1.3 Results . . . 86
8.1.4 Significance . . . 86
8.2 Introduction . . . 86
8.3 Data Acquisition . . . 87
8.4 Methodology . . . 88
8.4.1 Unimodal EEG-based seizure detection algorithm using only behind-the-ear/temporal EEG electrodes . . . 89
8.4.2 Unimodal ECG-based seizure detection algorithm . . . 90
8.4.3 Multimodal seizure detection algorithm . . . 91
8.4.4 Performance evaluation . . . 92
8.5 Results . . . 92
8.5.1 Performance of the Unimodal models: EEG and ECG . 92
8.5.2 Performance of the Multimodal model . . . 93
8.6 Discussion . . . 94

9 Conclusions and future directions 99
9.1 Conclusions . . . 99
9.1.1 Seizure detection based on wearable ECG/PPG . . . 99
9.1.2 Seizure detection based on behind-the-ear EEG . . . 100
9.1.3 Multimodal seizure detection based on behind-the-ear EEG and ECG . . . 101
9.2 Future directions . . . 101
9.2.1 Future directions for the SeizeIT device . . . 101
9.2.2 Future directions for algorithm development . . . 102

A SeizeIT2 analysis 107
A.1 SeizeIT1: Analysis using two behind-the-ear channels . . . 107
A.2 SeizeIT2: Comparison between hospital equipment and Sensor Dot (SD) . . . 107

B Motion and noise artifact removal using behind-the-ear EEG channels 109
B.1 Simulation study . . . 109
B.1.1 Methods . . . 109
B.1.2 Simulated dataset . . . 110
B.1.3 Results and discussion . . . 110
B.2 Application to seizure detection . . . 112
B.2.1 Methods . . . 112
B.2.2 Results and discussion . . . 112
B.3 Conclusion . . . 113

C Multimodal seizure detection: Appendix **115**
C.1 The unimodal ECG-based algorithm: Comparison with state-of-the-art . . . 115
C.1.1 Methods . . . 115
C.1.2 Results . . . 115
C.1.3 Discussion . . . 116
C.2 The unimodal ECG-based algorithm: Extracted features . . . 117
C.2.1 Time domain HRV features . . . 117
C.2.2 Frequency domain HRV features . . . 119
C.2.3 Features Jeppesen et al. [115] . . . 120
C.2.4 Features Doyle et al. [64] . . . 120
C.2.5 Features De Cooman et al. [53] . . . 120
C.2.6 Circadian Rhythm Features . . . 122
C.2.7 Features related to the noise level [180] . . . 122
C.2.8 Point process features [40] . . . 123
C.2.9 Features Osorio et al. [181, 182] . . . 123
C.2.10 Features Ungureanu et al. [244] . . . 124
C.3 Detected seizures in function of seizure type and localization . 124
C.4 Probable reasons why seizures are not detected with EEG, while they are detected with ECG . . . 124

D Artifact detection of wrist photplethysmograph signals **127**
D.1 Abstract . . . 127
D.2 Introduction . . . 128
D.3 Methodology . . . 129
D.3.1 Data acquisition . . . 129
D.3.2 Feature extraction . . . 129
D.3.3 LS-SVM based classification of MNA . . . 131
D.3.4 Feature selection . . . 131
D.3.5 Reference signal: ECG . . . 132
D.4 Results and discussion . . . 133
D.4.1 Feature selection . . . 133
D.4.2 Classification performance . . . 133
D.4.3 Overall data quality . . . 136
D.4.4 Limitations and further work . . . 137
D.5 Conclusions . . . 138

Bibliography **141**

Curriculum vitae **169**

List of publications **171**

List of Figures

2.1 Digram of a neuron. Taken from [109] 6
2.2 Synaptic transmission. Taken from Wikipedia.org 6
2.3 Brain anatomy. Taken from [196] 7
2.4 Different lobes of the brain. Taken from [159] 8
2.5 The autonomic nervous system. Taken from [152] 9
2.6 ILEA Classification of Seizure Types. Taken from [76] 11
2.7 Placement of the standard electrodes of the 10-20 system (A: lateral view, B: frontal view, C: from the top, taken from [216] 15
2.8 Example of Focal Impaired Awareness (FIA) seizure with the onset in the temporal lobe, right hemisphere with the full EEG set-up. The EEG is plotted in a window of 10s with the seizure onset at the start (3:29:26). 16
2.9 Behind-the-ear electroencephalographic setup. Left panel shows extra behind-the-ear electrodes glued to the skin. Right panel shows bipolar channel derivations. 16
2.10 Example of Focal Impaired Awareness (FIA) seizure with the onset in the temporal lobe, right hemisphere with the behind-the-ear EEG set-up. Unilateral L: OorLiTop - OorLiAchter, Unilateral R: OorReTop - OorReAchter, CrossheadOorLiTop - OorReTop, Crosshead 1: OorLiAchter - OorReAchter, Crosshead 2: OorLiTop - OorReTop 17
2.11 The effect of a seizure on ECG: (**a**) Electrocardiography (ECG) signal (bandpass filtered 1–40 Hz). (**b**) Heart rate (HR; red line indicates seizure onset as annotated by a clinician on the basis of electroencephalography (EEG)). 18
2.12 Electrode placement for a 12-lead ECG configuration, with electrodes on right arn (RA), left arm (LA), left leg (LL), Right leg (RL) and chest electrodes V1 to V6. Taken from [88] 19
2.13 Characteristic waves and segments of a normal electrocardiogram. Two heart cycles are indicated. Taken from [258] 19

2.14 The basic principle of PPG measurements. Taken from [234] . 20

3.1 Example of a Random Forest classifier. Taken from [110] 28
3.2 Artificial neural network. Taken from wikipedia.com 29
3.3 Illustration of a neuron. Taken from [7] 29
3.4 Architecture of a CNN. Taken from [242] 30
3.5 A recurrent neural netork. Taken from [161] 30
3.6 Leave-one-patient-out (LOPO) cross-validation 33
3.7 Example of a seizure reference annotation and an hypothesis [Taken from [278]] 34

4.1 Behind-the-ear electroencephalographic setup. Left panel shows extra behind-the-ear electrodes glued to the skin. Right panel shows bipolar channel derivations. Reproduced with permission from Gu et al. [96] 39
4.2 Left temporal lobe seizure recorded with behind-the-ear electroencephalographic (EEG) setup. The four bipolar EEG channels are shown over a period of 10 seconds: (1) crosshead 1, (2) crosshead 2, (3) unilateral left, (4) unilateral right. The bipolar EEG channels were filtered with a bandpass filter (1-25 Hz). The black horizontal line at 300 seconds depicts the seizure onset . 39
4.3 SeizeIT2: position of the behind-the-ear electrodes. Reproduced from the SeizeIT2 - EIT Health Consortium RedCap website [104] 41
4.4 Byteflies Sensor Dots. Reproduced from the Byteflies website [32] 41
4.5 SeizeIT2: splitter configuration. Reproduced from the SeizeIT2 - EIT Health Consortium RedCap website [104] 42

5.1 Neureka challenge: pipeline of the algorithm 48

6.1 The sensitivity and false alarm rate for different thresholds of the support vector machine (SVM) classifier. 64
6.2 Sensitivity versus seizure duration. 65
6.3 Number of and reason for missed seizures (HRD: heart rate decrease; No HRC: no heart rate change; Small HRI: small heart rate increase: MA: notion artifacts; Interf: interference). 65
6.4 Comparison of motion artifacts: hospital electrocardiography (ECG) and wearable ECG (red line indicates annotated seizure start). 67

7.1 Sensitivities for the different seizure types (A), localizations (B), lateralizations (C) and seizure durations in seconds (D) are plotted for the patient-independent model with aim I and visual recognition study. The sensitivities were calculated as percentage recognized seizures in that category over whole the database. bi, bilateral; FA, focal aware; F-BTC, focal to bilateral tonic-clonic; FIA, focal impaired awareness; L, left; NC, not clear; par, parietal; R, right; temp, temporal 80

8.1 The behind-the-ear EEG and ECG are shown during a temporal focal impaired awareness seizures from the right hemisphere. The top figure contains 4 channels: crosshead (cross), left channel, right channel and ECG. The amplitude of the ECG signal is decreased with a factor 10. The seizure onset is depicted with a vertical black line at 10 seconds. The left bottom figure shows the extracted heart rate in beats per minute during the seizure. A heart rate increase from 40 to 80 beats per minute is observed. The right bottom figure shows a close-up of the behind-the-ear EEG channel during 20 – 30 seconds after the seizure onset. . . 88
8.2 A schematic overview of the different steps in the automated seizure detection algorithm. 89
8.3 Sensitivity in function of FAR for the different datasets. The blue graph depicts the unimodal results of EEG, the red one the results of ECG. On those graphs, the sensitivities at a FAR at 0.2 FP/hour, 0.5 FP/hour and 1 FP/hour are depicted with circles. The black points are the results of the multimodal algorithm at three discrete thresholds (square: 0.2 FP/hour, diamond: 0.5 FP/hour and star: 1FP/hour). For comparison, the results on the EEG graph with the same FAR are indicated with blue marks. 93

B.1 Examples of EEG signals 111
B.2 Results of the simulation study: RMSSA [left] and correlation [right] between the reconstructed signal and the clean EEG signal 111

C.1 Performance comparison of our proposed ECG-based seizure detection algorithm. The sensitivity versus FAR is plotted together with the standard deviation on the sensitivity [dotted lines]. The sensitivity and FAR is shown for two state-of-the-art solutions: Fürbass [82] and De Cooman et al. [53], the dotted lines indicate the standard deviation in two directions: the FAR and sensitivity. 116

C.2 Percentage of detected seizures at a FAR of 1/hour is displayed for the four groups: Seizures detected with both EEG and ECG, only with EEG, only with ECG or seizures not detected neither with EEG nor with ECG in function of Seizure type (A) and in function of localization (B). The number of seizures in each group is indicated in the legend. 125

D.1 Flowchart: Backwards wrapper feature selection 132
D.2 ACM axis 134
D.3 Classification performance 135
D.4 Example: Clean (blue) and MNA (red) PPG segments with 3 axis ACM 136
D.5 Example: Clean (blue) and MNA, caused by finger motion, (red) PPG 137

List of Tables

4.1 SeizeIT1: An overview of the seizure types, origins and hemispheres (n=Number of seizures, FA= Focal Aware, FIA= Focal Impaired Awareness, F-BTC= Focal to Bilateral Tonic Clonic, Temp=Temporal, Par=Parietal, NC= Not Clear) . . . 38
4.2 SeizeIT2: An overview of the seizure types, origins and hemispheres (n=Number of patients, FA= Focal Aware, FIA= Focal Impaired Awareness, F-BTC= Focal to Bilateral Tonic Clonic, Temp=Temporal, Par=Parietal) 40
4.3 Freiburg dataset: An overview of the seizure types, origins and hemispheres (n=Number of seizures, FA= Focal Aware, FIA= Focal Impaired Awareness, F-BTC= Focal to Bilateral Tonic Clonic, Temp=Temporal, Par=Parietal, Occ=Occipital, NC= Not Clear) 43
4.4 Paris dataset: An overview of the seizure types, origins and hemispheres (n=Number of seizures, FA= Focal Aware, FIA= Focal Impaired Awareness, F-BTC= Focal to Bilateral Tonic Clonic, Temp=Temporal, Par=Parietal, Occ=Occipital, NC= Not Clear) 43
4.5 TUSZ dataset: An overview of the seizure types [n= Number of seizures, FN= Focal Non-Specific, GN=Generalized Non-Specific, FA=Simple Partial, FIA= Focal Impaired Awareness, AB=Absence, TN=Tonic, CN=Clonic, TC=Tonic Clonic, AT=Atonic, MY=Myloclonic]. 44

6.1 An overview of the dataset RD = Recording Duration, SD = Seizure Duration 60
6.2 Seizure performance: the sensitivities (Se), false positives per hour (FP/h) and positive predictive value (PPV) are shown with the patient average (Pat.-av.) and total average (Tot.-av.). . . 64

7.1 Extracted features [HF, high-frequency] 76
7.2 Results of visual seizure recognition (Sens and Spec) and automated seizure detection I with aim of detecting all seizures annotated on video-EEG and automated seizure detection II with aim of detecting only seizures recognized by the neurologist on behind-the-ear EEG for PS and PI models (number of patients and seizures, Sens, false detection rate, PPV, detection delay, and F1-score) [EEG, electroencephalography; FP, false positive; PI, patient-independent model; PPV, positive predictive value; PS, patient-specific model; Sens, sensitivity; Spec, specificity] . 79

8.1 A. False Alarm Rate (FAR) [FP/hour] and Sensitivity (Sens) [%] for the unimodal EEG and ECG at a FAR of 1 FP/hour for the different databases. B. False Alarm Rate and Sensitivity (%) of the multimodal (at a threshold generating 1FP/h for the unimodal modalities) and EEG-based detectors at the same FAR for the different databases. Mean [95% confidence interval] / median [min max] are shown in the table. 94

A.1 SeizeIT1 seizure detection results: three channels versus two channels 108
A.2 SeizeIT2 seizure detection results: hospital equipment versus sensor dot [Abbreviations: FIA= Focal Impaired Aware, FA= Focal Aware, Temp= Temporal, Par= Parietal, Front= Frontal] 108

B.1 Seizure detection results: comparison of different filtering techniques 112

D.1 Feature selection PPG 134
D.2 Feature selection ACC 134
D.3 Feature selection ALL 135
D.4 Classification performance 136
D.5 Comparison with literature [Rec.=Recording, Acc=Accuracy, Se=Sensitivity, Sp=Specificity, Results are in %]. 138

Chapter 1

Introduction

1.1 Problem statement

Epilepsy is one of the most common neurological disorders, which affects almost 1% of the population worldwide. Anti-epileptic drugs provide adequate treatment for about 70% of epilepsy patients [80]. The remaining 30% of the patients continue to have seizures, which drastically affects their quality of life. In order to obtain efficacy measures of therapeutic interventions for these patients, an objective way to count and document seizures is needed [69]. The frequency of seizure occurrence is important to quantify the success of therapeutic interventions, f.e. new type of medication. However, in an outpatient setting, one of the major problems is that seizure diaries kept by patients are unreliable [25, 75, 103, 195, 236]. It was shown that adult patients with focal epilepsies undergoing video-electroencephalographic monitoring, failed to document 55.5% of all recorded seizures and 73.2% of focal impaired awareness seizures [103].

Automated seizure detection systems could help to objectively quantify seizures. Those detection systems are typically based on full scalp Electroencephalography (EEG). In an outpatient setting, full scalp EEG is of limited use because patients will not tolerate wearing a full EEG cap for long time periods in daily life [12]. There is a need for seizure detection systems based on signals, recorded with wearables outside the hospital. Those wearable devices could provide a more reliable seizure documentation in a home environment. On one hand, epileptic seizure detection devices should provide high sensitivity with a false detection rate as low as possible. On the other hand, those devices should be comfortable,

unobtrusive and non-stigmatizing to wear in a daily life setting.

Most existing wearable devices are developed for seizures with strong muscle and motor components. Accelerometry and electromyography are excellent modalities since they can be measured with a smartwatch. Nowadays, those smartwatches are highly accepted to wear in a daily life environment. Algorithms using accelerometry could be developed with high sensitivity and low false alarms. In this thesis, the focus lies on focal seizures without typical motor activation. For this group, there are no existing effective solutions for seizure detection in a daily life environment.

The main goal of this thesis is to prove the usefulnes of signals, which can be recorded with a wearable device, for focal seizure detection. In addition, offline seizure detection algorithms based on those signals were developed to construct automatically a seizure diary. The investigated signals are ECG, PPG and behind-the-ear EEG.

1.2 Outline of the thesis

The overall structure of this manuscript takes the form over 8 main chapters. Chapters 2, 3, 4 explain the physiological background, machine learning methods and the used datasets. Chapter 5 gives an overview of the state-of-the-art algorithms. Chapters 6, 7 and 8 are the original contributions of this PhD. Chapter 9 concludes the research by summarizing the main contributions and listing future research perspectives.

More specifically, Chapter 2 provides an overview of the physiological background in epilepsy. An introduction to the physiology and anatomy of the brain and the autonomic nervous system is given. Different aspects of epilepsy and the modalities to monitor seizures are explained. Chapter 3 is concerned with the machine learning methods. The used classifiers, normalization techniques, strategies for handling unbalanced datasets, cross-validation and the performance metrics are depicted. Chapter 4 gives an overview of the data used in this thesis. Chapter 5 gives an overview of the state-of-the-art algorithms and introduces the contributions and collaborations of this thesis. The algorithms based on EEG, ECG, PPG and multimodal systems are discussed.

Chapter 6 contains the content of the publication by K. Vandecasteele et al. [255]. This study investigates the use of a wrist-worn PPG device for seizure detection in focal patients. The performance of two wearable devices, based on ECG and PPG, are compared with the ECG, recorded in the hospital.

Chapter 7 contains the content of the publication by K. Vandecasteele et al. [254]. First, we determined whether the recognition of ictal patterns using only behind-the-ear EEG channels is possible. Second, an automated seizure detection algorithm was developed using only those behind-the-ear channels.

Chapter 8 contains the content of the manuscript submitted to Epilepsia [253]. The aim of this study was the development of an automated multimodal seizure detection algorithm using behind-the-ear EEG and ECG. The added value of ECG was investigated in this framework.

Chapter 9 concludes this thesis.

1.3 Collaborations

This PhD research was conducted in the research group (BIOMED), Stadius Center for Dynamical Systems, Signal Processing, and Data Analytics, Department of Electrical Engineering (ESAT) at the KU Leuven under the supervision of Prof. Sabine Van Huffel, Prof. Borbála Hunyadi and Prof. Wim Van Paesschen.

This research was part of an ICON project SeizeIT (HBC.2016.0167), a two year project from 2016 until 2018. The aim of the project was the development of a discreet wearable seizure detection device. One of the strenghts was a strong multidisciplinary team with the partners: Byteflies, UCB, Pilipili and UZ Leuven. Byteflies is a start-up company specialized in the development of wearable health applications and was responsible for the specific hardware prototyping. UCB is a well-known biopharmaceutical company and took care of the project management, business modeling and strategy. Pilipili is specialized in design and was responsible for the user centered design of the SeizeIT prototype. UZ Leuven was responsible for the medical input and data collection.

A follow-up project EIT HEALTH (19263: SeizeIT2), funded by the European Union, entitled "Discreet Personalized Epileptic Seizure Detection Device", was granted to continue the efforts during the ICON project SeizeIT1. The team of partners was extended with Helpilepsy and other clinical partners for data collection, King's College London, Oxford University, University of Aachen, Karolinska Institute, Freiburg University Medical Center and Coimbra University Hospital.

In addition, the Flanders AI Research Program, sponsored by the Flemish government, has officially started on July 1, 2019 [1]. This big project focuses on three main pillars: strategic basic research, technology transfer & industrial applications, and supporting activities (awareness, training, ethics...). The

strategic basic research program consists of 4 main challenges. Challenge 1, steered by Stadius and IDLab, deals with 'Making complex decisions through data science', which consists in total of 8 work packages. Work package 7 contains 5 use case studies in health. One of the use cases is 'Clinical Decision Support: Epilepsy monitoring', organized by Stadius. Three main objectives are defined: improved quantification of biomedical signals for seizure detection, improved (multimodal) classification, improved personalization of seizure detection algorithms. For this use case, the SeizeIT1 dataset, explained in Chapter 4 and the Pulderbos dataset [249] were shared. In this context, the Neureka Challenge research [171, 36] and collaborations with researchers from different universities in Flanders, for example Thijs Becker [13], explained in Chapter 5, took place. The chapters 7 and 8 are contributions to this program.

Chapter 2

Epilepsy and monitoring solutions

Understanding the physiological background of epilepsy is important to develop an epileptic seizure detection system, f.e. to select suitable modalities. The first section explains the physiology and anatomy of the brain. The second section gives an introduction of the autonomic nervous system. The third section explains different aspects of epilepsy. The following section depicts interesting modalities to monitor seizures. As last, the most important existing wearable seizure detection devices are briefly described.

2.1 The brain: physiology and anatomy

The brain deserves our attention since epilepsy is a disorder of the brain. The elementary building blocks of the brain are neurons or brain cells, shown in Figure 2.1. Those neurons are specialized for the rapid transmission of signals. Each neuron consists of a cell body, dendrites, an axon ending in synaptic or axon terminals. The dendrites receive information from other cells, the axon conducts this information from the cell body to the synaptic terminals. To allow a rapid electrical information conduction, the axons are surrounded by myelin sheaths to insulate them. The synaptic terminals transmit this information to other neighboring cells. The flow of information between the neurons is achieved by electrical and chemical activity. In the neurons, information propagates in the form of electrical action potentials along the axon. In the synapses, communication between dendrites and synaptic terminals of other neurons is a

chemical process, shown in Figure 2.2. An action potential in a synaptic terminal causes a release of chemical neurotransmitters. Those neurotransmitters will bind to the receptors of the dendrites, which will open the ion channels allowing an ion flux across the membrane. When ions are flowing in or out the neuron cell, the membrane potential is altered. The membrane potential will deviate from its resting equilibrium state. If the membrane potential exceeds a certain threshold, an electrical action potential is fired and propagates along the axon [187].

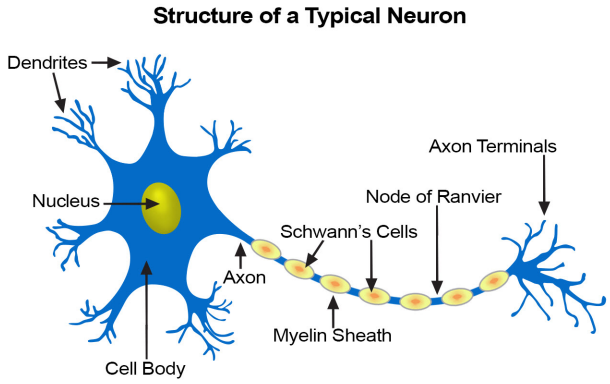


Figure 2.1: Digram of a neuron. Taken from [109]

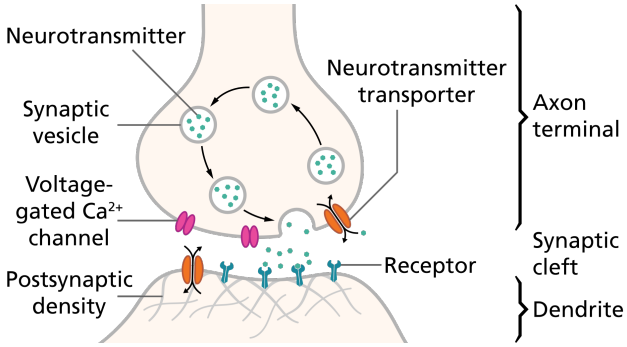


Figure 2.2: Synaptic transmission. Taken from Wikipedia.org

The macroscopic structure of the brain is shown in Figure 2.3. The brain consists of the cranium, cerebellum, brainstem and cerebrum. The cranium is forming a bony protection for the soft structures inside the brain. The

cerebellum lies at the back of the head and is responsible for voluntary muscle movements, fine motor skills and maintaining balance, posture and equilibrium. The brainstem is located in front of the cerebellum and is the main control center of the body. The cerebellum, cerebrum and spinal court are connected with each other by the brainstem. The cerebrum is the largest part of the brain and consists of the right and left cerebral hemispheres, which are connected by the corpus callosum. In general, the right cerebral hemisphere controls the left side of the body, and the left cerebral hemisphere controls the right side. The outer matter of the cerebral hemisphere forms the cortex, which has a gray color due to numerous cell bodies and relatively few myelinated axons. The inner white matter contains relatively few cell bodies and a large amount of few myelinated axons. The cerebral hemispheres are divided into lobes, shown in Figure 2.4: frontal, occipital, parietal and temporal lobes. Each lobe is fulfilling certain functions. The frontal lobe takes care of cognitive functions and controls the voluntary motion. The parietal lobe is involved with sensation, processes information about temperature, taste, touch and movement. The occipital lobe is responsible for vision, whereas the temporal lobe is responsible for language, speech and memory [187, 196].

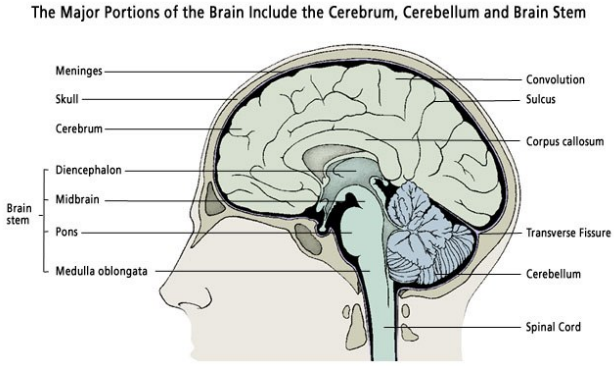


Figure 2.3: Brain anatomy. Taken from [196]

2.2 The autonomic nervous system

The autonomic nervous system (ANS) is a component of the peripheral nervous system that regulates involuntary physiological processes such as respiration, heart rate, sweat production, digestion and sexual arousal. The ANS is regulated by autonomic reflexes, where sensory information is transmitted to homeostatic control centers, particularly, those located in the hypothalamus and brainstem.

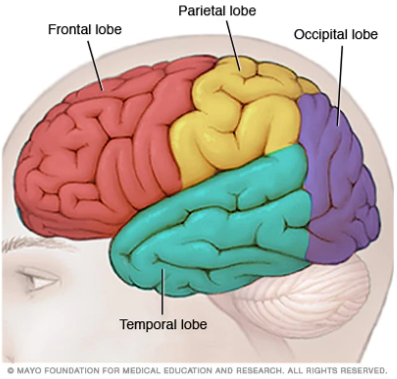


Figure 2.4: Different lobes of the brain. Taken from [159]

It is composed of two anatomically and functionally distinct divisions, the sympathetic and parasympathetic system, shown in Figure 2.5. Both systems are active all the time, but one of them is dominant under certain conditions. The sympathetic system is dominant during emergency 'fight-or-flight' reactions and during exercise. The body is prepared for physical activity, more specifically, the blood flow which is well-oxygenated and rich in nutrients is increased in muscle tissues. In addition, heart rate is increased, the airways are dilated to make breathing easier, sweat production is increased. It slows body processes like digestion and urination. The parasympathetic system is dominant during a quiet and resting condition. The overall effect is to conserve and store energy and regulate basic body functions such as digestion and urination [160, 187, 152].

2.3 Epilepsy

2.3.1 Definition and diagnosis

Epilepsy is one of the most common neurological disorders, which affects almost 1% of the population worldwide [79]. Epilepsy is characterized by sudden abnormal excessive and synchronous neural activities in the brain. These discharges, which are called epileptic seizures, can cause for example an uncontrolled jerking movement or a momentary loss of awareness. Usually, those seizures are unpredictable and happen without any warning. This unpredictability together with the consequences of such a seizure reduces the quality of life for patients and their caregivers. Epilepsy is clinically diagnosed

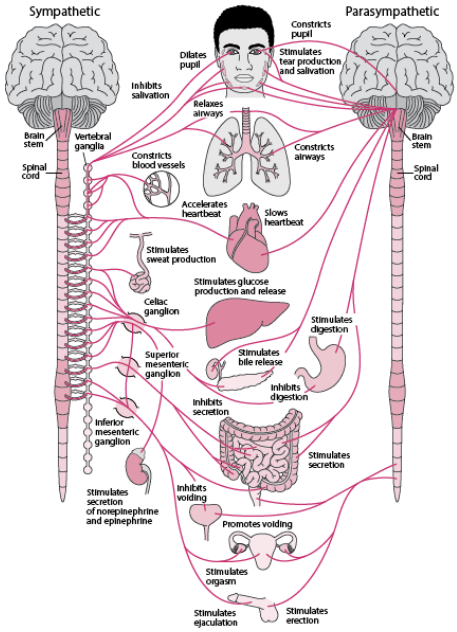


Figure 2.5: The autonomic nervous system. Taken from [152]

when there is a repetition of seizures, effectively having two unprovoked seizures more than 24 hours apart [74].

The prevalence of epilepsy has a bimodal distribution with peaks in infancy and older age (65+). There are many different causes for epilepsy, congenital or developed during life. Common congenital reasons are brain malformations, metabolism malfunctions or other genetic defects. Infections, trauma or stroke can trigger the development of epilepsy during life [63].

Video-electroencephalography (vEEG) is the gold standard for diagnosing epilepsy. The patient visits the hospital and is observed with video and EEG is recorded along. Not only the EEG during seizures is important, the EEG in between seizures can also have interictal epileptiform discharges. Those discharges are pathological patterns in the EEG activity, produced by groups of neurons that are pathologically connected due to epilepsy [8]. More information on the EEG is given in section 2.4. On top of this information, brain imaging techniques, for example MRI can provide information about brain abnormalities. Laboratory testing, such as complete blood counts, blood glucose, and electrolyte panels (particularly sodium) may be helpful for the diagnosis of epilepsy [127].

2.3.2 Seizure classification

Different types of seizures exist. In Figure 2.6 the current classification of seizures is shown. This classification begins with the determination of the initial seizure manifestations or onset. If the onset is in one specific part of the brain, it is called a focal onset seizure. If the onset is widely spread across the whole brain, it is called a generalized onset seizure. The onset may be missed or obscured, in which the seizure is of unknown onset.

For focal seizures, the level of awareness is an important feature of a seizure. A focal aware (FA) seizure means that the person is aware of himself and the environment during the seizure. If awareness is impaired at any point during the seizure, the seizure is a focal impaired awareness (FIA) seizure. A FA or FIA seizure optionally may be further characterized by one of the motor-onset or nonmotor-onset symptoms. The seizure type 'focal to bilateral tonic-clonic (F-BTC)' is a special seizure type, which is a seizure that has a focal onset but propagates to a generalized seizure, involving the whole brain. Generalized seizures are further divided into motor and non-motor (absence) seizures [76]. Generalized motor seizures includes Generalized Tonic Clonic (GTC) or Grand mal seizures, which involve an initial contraction or stiffening of the muscles (tonic phase) followed by rhythmic muscle contractions causing rhythmic motions (clonic phase). Seizures having only a Tonic or a Clonic phase are called Generalized Tonic (GT) or Generalized Clonic (GC) seizures.

The focus of this thesis is focal epilepsy with nonmotor-onset symptoms.

For focal seizures, the particular onset region can have an influence on the clinical symptoms during a seizure. Depending on the lobe of this onset region, different clinical symptoms are observed. Seizures arising from the frontal lobes are usually involved with muscle and motor components like twitching, jerking or stiffening of muscles. Occipital lobe seizures typically affect a person's visual capabilities. Parietal seizures often involve strange sensations or feelings. Typical symptoms of temporal lobe seizures are changes in the autonomic nervous system [71].

2.3.3 Treatment

There are various ways to treat epilepsy. The optimal treatment depends on the type of seizure.

Medication is the most used treatment, i.e. Anti-epileptic drugs (AEDs). 70% of the patients can be controlled with the use of AEDs. A variety of AEDs are available to adjust the medication to the individual patient needs. A

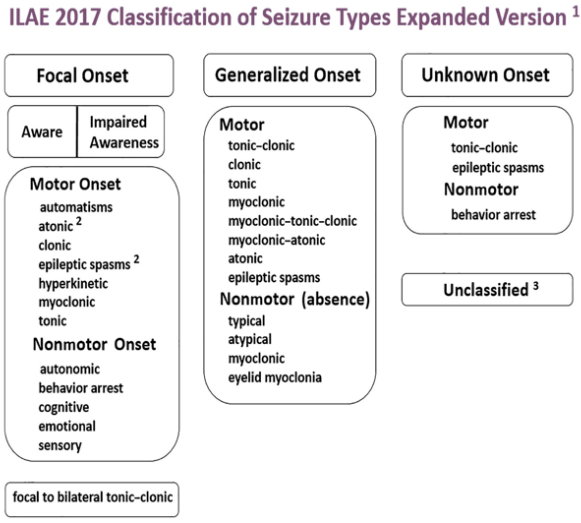


Figure 2.6: ILEA Classification of Seizure Types. Taken from [76]

monotherapy (use of 1 AED) as the first-line treatment is recommended. In case of failure, an alternative monotherapy is tried. If this therapy also fails, polytherapy, which is a combination of different AEDs, can be applied. By choosing the optimal medication, the clinician should take into account the side effects. The goal is to select an AED or a combination of AEDs that provides optimum control of seizures with an acceptable level of side effects. When a person has failed to become (and stay) seizure free with adequate trials of AEDs, the patient suffers from refractory epilepsy, which is about 30% of the epilepsy patients [63].

If patients are diagnosed with refractory epilepsy, it should be investigated whether the patient would benefit from a surgical treatment. With the use of medical imaging together with the ictal semiology, the epileptic zone should be determined. This epileptic zone is the part of the brain responsible for the seizure onset. Surgical resection of the epileptic zone may render the patient possibly seizure-free. However, not all patients are possible candidates for such a surgical treatment. The epileptic zone should be small enough and not interfering with vital functions of the brain [34].

Another treatment to epilepsy is a ketogenic diet, mainly used as a treatment for drug-resistant childhood epilepsy. The basics of the diet are the high fat and restricted carbohydrate content, which is thought to mimic the biochemical response to starvation. During starvation, ketone bodies become the main

fuel for the brain's energy demands. These ketone bodies often suppress the occurrence of seizures, however, the exact mechanism is still unknown. An observational study has shown that this diet in more than half of the children led to a decrease of more than 50% of their seizures [174].

A relatively new treatment to epilepsy is Vagus-Nerve Stimulation (VNS). Peripheral stimulation of the vagus nerve can affect the brain and cause changes in electroencephalographic patterns. VNS lowers or inhibits the frequency of spiking activity. The exact mechanism is yet unknown. Current information suggests that VNS activates neuronal networks in the thalamus and other limbic structures and that norepinephrine, a neurotransmitter, may mediate the antiseizure activity of VNS. It should be taken into account that improvement is not immediate but increases over 18–24 months of treatment [16].

In addition to VNS, Deep Brain Stimulation (DBS) is a technique where electrical stimulation can modulate or interrupt seizures. DBS sends pulses directly to the brain, whereas VNS stimulates the vagus nerve, leading to the brain as well. The benefit of stimulation tends to increase over time, with maximal effect seen typically 1-2 years after implantation. Typical reductions of seizure frequency are approximately 40% at the start of stimulation, and 50-69% after several years. The stimulation parameters and whether deep brain stimulation for epilepsy must be continuously applied or only when a seizure occurs are a matter of debate [121, 77].

2.3.4 Mortality risk for patients with epilepsy

The mortality risk for patients with epilepsy is increased with a factor two or three. Epilepsy related deaths are due to four main reasons. Firstly, epilepsy patients can die due to the underlying cause of epilepsy, for example a brain tumor or lesion. Secondly, the patient can experience an accident caused directly by the epileptic seizure attack for example a traffic, drowning or burning accident or the patient can experience a status epilepticus, when the seizure is long-lasting possibly causing brain damage. Thirdly, deaths are caused by co-morbidities, including depression leading to suicide, co-existent neurological diseases and respiratory tract infection or pneumonia. Fourthly, deaths of unknown causes appear, called sudden unexpected death in epilepsy (SUDEP) [30, 86, 231].

2.3.5 Seizure monitoring

Anti-epileptic drugs provide only adequate treatment for about 70% of epilepsy patients [80]. The remaining 30% of the patients continues to have seizures,

which drastically affects the quality of life. The unpredictability of the seizures causes stress not only to the patients, but also to the parents or caregivers. Parents for example are constantly afraid their child will experience a seizure and want to be there to reassure the child. Monitoring those seizures with automated seizure detection devices could potentially increase the quality of life. Depending on the patient preferences and type of seizures, the needs or goals for automated seizure devices are different. Some patients could be helped with a seizure warning system, that gives an alarm when a seizure is occurring. Other patients want to keep track of their seizures with a logging system. Another application is seizure prediction, where the patient or caregiver will be warned even before the seizure.

Seizure warning

The most investigated application is a seizure warning system, which provides the user a real-time alarm when a seizure is occurring. This seizure warning system is mostly needed for generalized tonic-clonic seizures (GTCS) including focal-to-bilateral tonic-clonic seizures since these seizure types are associated with the highest risk for morbidity and mortality [18]. Patients with GTCS can experience serious accidental injuries related to the seizure [209]. Furthermore the rist of sudden expected death in epilepsy (SUDEP) is increased [232]. An important aspect is the performance of the detection system. The number of seizures detected should be as high as possible (a high sensitivity), the false alarms should be as low as possible and the detection should occur as fast as possible after the seizure start with a minimum delay. On the other hand, the device measuring the biomedical signals, should be comfortable and non-stigmatizing. Otherwise the patient will be reluctant to wear this device. Furthermore, the device should have the desired computational power and battery capacity to allow real-time processing and alarming.

A seizure warning system is mostly desired for patients experiencing strong seizures involving heavy motor components (for example Generalized Tonic-Clonic seizures). In this case, the caregiver can decrease injuries and the patient can be reassured after his seizure.

Seizure logging

In case of a seizure logging system, the aim is to track the seizure occurrences. After diagnosis in the hospital, one needs a follow-up of the disease and evaluation of the treatment. This follow-up requires a seizure logging system that is functional in a daily life environment outside the hospital, such as a seizure

diary. A seizure diary, kept by patients or their families, is unfortunately unreliable [75]. With a seizure logging system, an electronic diary can be generated. The requirements are the same as in the case of a seizure warning system. Only the detection delay is not of interest since no alarm will be generated. Also the computational requirements become more flexible since computation can occur offline afterwards on another machine.

Seizure prediction

The majority of patients with epilepsy regard the unpredictability as a major issue. This issue could be resolved with a seizure prediction system. After a seizure prediction alarm, the patient can put himself in a safe position or warn a caregiver. Another application is the stimulation of the brain or vagus nerve, explained in 2.3.3. Typically (intracranial) Electroencephalogram (EEG) is used for this task [131]. Seizure prediction based on heart rate analysis is investigated [169].

This thesis focuses on automated seizure detection with the aim of seizure logging in a home environment.

2.4 Modalities for automated seizure detection

2.4.1 Electroencephalography (EEG)

Electroencephalography (EEG) is an electrophysiological technique for recording electrical activity in the brain. This electrical brain activity is generated by neurons propagating information in the form of action potentials. Those action potentials create voltage differences between electrodes placed on the scalp. The electrical activity detectable by EEG is the summation of the excitatory and inhibitory postsynaptic potentials of relatively large groups of neurons firing synchronously. EEG recorded at the scalp is unable to register the local field potentials arising from a few neuronal action potentials. Since, epilepsy is characterized by large groups of neurons synchronously firing, EEG is a very interesting modality to monitor electrical activity in the brain [31].

EEG electrodes are placed on the scalp on standardized positions. In a 10-20 system, typically used in standard EEG measurements, the electrode positions were based on 20% and 10% of standardized measurements from anatomical landmarks on the skull [216]. In Figure 2.7 the electrode positions of the 10-20 system are shown in a lateral view, frontal view and from the top. The electrode

names consist of letters and numbers. The letters indicate the lobe or region (F: frontal, T: temporal, P: parietal and O: occipital, C: central, Fp: Fronto-polar electrodes). Odd numbers are on the left side, and even numbers on the right side. In Figure 2.8 a focal impaired awareness seizure with the onset in the temporal lobe is visualized using the full EEG set-up (with EDFbrowser). In addition to the standard electrodes, behind-the-ear electrodes, which will be explained in the next subsection, and sphenoidal electrodes [129] were shown. The data was filtered with a bandpass filter between 0.5 and 30 Hz. The reference channel is Fz, which is a flatline in the plot. The seizure pattern becomes really clear at 3:29:31, a rhythmic pattern with increased amplitude is observed around 5 Hz.

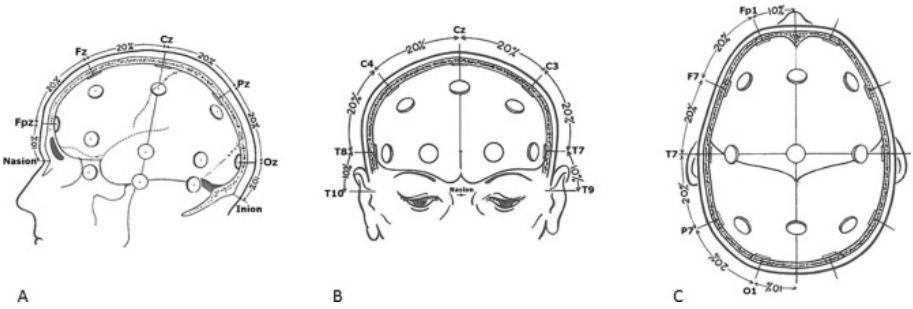


Figure 2.7: Placement of the standard electrodes of the 10-20 system (A: lateral view, B: frontal view, C: from the top, taken from [216]

2.4.2 Behind-the-ear EEG

In an outpatient setting, full scalp EEG is of limited use because patients will not tolerate wearing a full EEG cap for long time periods during everyday life. Researchers evaluated and compared reduced electrode montages with full scalp EEG for different tasks. Recordings with a wireless 14-channel EEG system were done outdoors on university campus [57]. Different studies present evidence that reliable EEG data can be recorded around/behind-the-ears in different tasks such as auditory oddball testing, the auditory steady-state response (ASSR) and steady-state visually-evoked potentials (SSVEP) [56, 93, 151, 24].

Wearable devices are being developed measuring only a few channels of EEG. In the SeizeIT project, we are developing a wearable recording EEG channel behind the ears. The position of the electrodes is depicted in Figure 2.9. The same seizure as in Figure 2.8 with full channel EEG is shown in Figure 2.10 with the bipolar behind-the-ear channel derivations. On the crosshead channels,

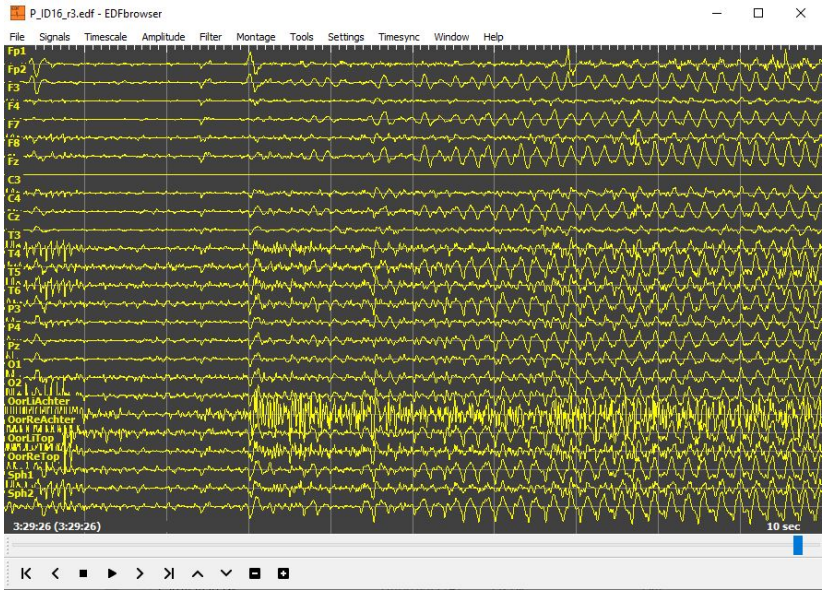


Figure 2.8: Example of Focal Impaired Awareness (FIA) seizure with the onset in the temporal lobe, right hemisphere with the full EEG set-up. The EEG is plotted in a window of 10s with the seizure onset at the start (3:29:26).

the pattern is the clearest, especially the OorLiTop - OorReTop channel (4rd channel). The channel OorLiAchter - OorReAchter channel (3rd channel) is less clear, there are small artifacts present in the channel OorLiAchter, as seen in Figure 2.8.

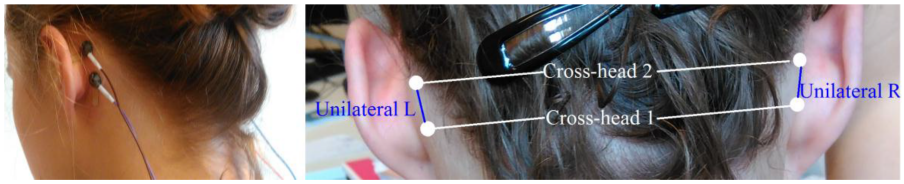


Figure 2.9: Behind-the-ear electroencephalographic setup. Left panel shows extra behind-the-ear electrodes glued to the skin. Right panel shows bipolar channel derivations.

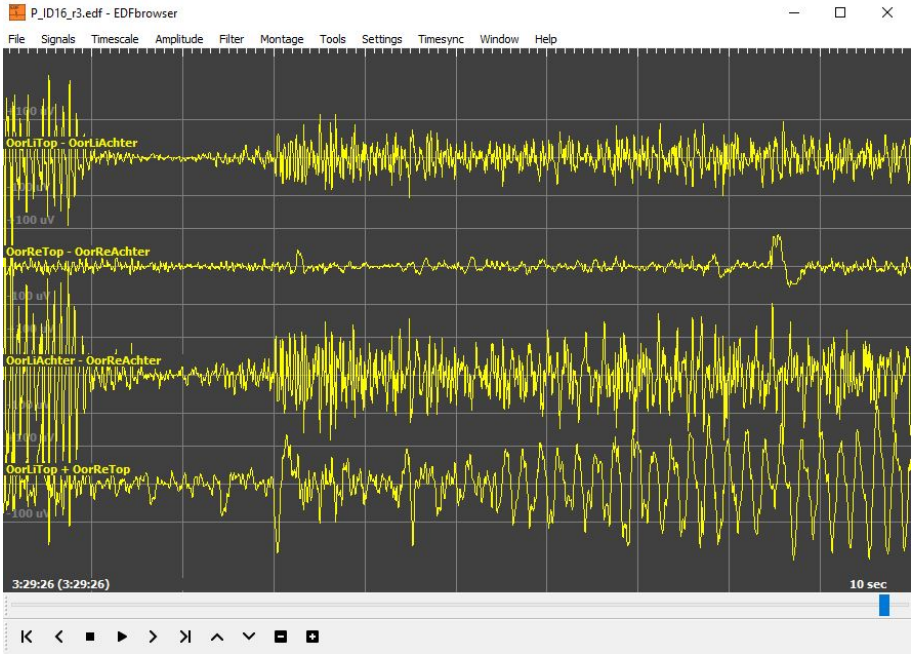


Figure 2.10: Example of Focal Impaired Awareness (FIA) seizure with the onset in the temporal lobe, right hemisphere with the behind-the-ear EEG set-up. Unilateral L: OorLiTop - OorLiAchter, Unilateral R: OorReTop - OorReAchter, CrossheadOorLiTop - OorReTop, Crosshead 1: OorLiAchter - OorReAchter, Crosshead 2: OorLiTop - OorReTop

2.4.3 Electrocardiography (ECG)

Not only the EEG can be used for seizure detection. Epileptic activity in the brain, consisting of neurons synchronously firing, can propagate to the control centers of the autonomic nervous system. As a result, the autonomic nervous system is affected, leading to the activation of the sympathetic or parasympathetic system. Other biomedical signals, affected by the autonomic nervous system, will show changes when a seizure is happening. Those changes can be used to detect epileptic seizures. The most suitable biomedical signals or combination of signals depends on the type, onset or clinical manifestation of the seizure [111, 248].

Temporal lobe epilepsy (TLE) seizures do affect the autonomic nervous system, in particular the cardiovascular system. It was previously shown that temporal lobe seizures are often accompanied with a strong ictal heart rate (HR) increase

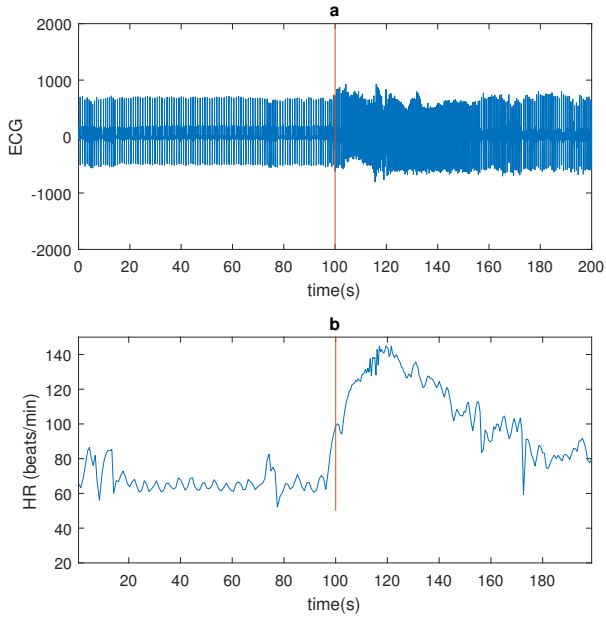


Figure 2.11: The effect of a seizure on ECG: (**a**) Electrocardiography (ECG) signal (bandpass filtered 1–40 Hz). (**b**) Heart rate (HR; red line indicates seizure onset as annotated by a clinician on the basis of electroencephalography (EEG)).

[111, 53, 277, 62]. One way to measure the HR is by Electrocardiography (ECG). Figure 2.11 shows the ECG signal and the extracted HR during a seizure.

The electrocardiogram (ECG) is a graphical representation of the electrical activity of the heart. The heart's electrical waveform can be detected by electrodes placed on the surface of the chest. Current ECGs are composed of 12 leads, including spatial information of the heart. The electrode placement for a 12-lead ECG is shown in Figure 2.12. A lead is defined as the signal found by evaluating the potential difference between two electrodes. For some topics, sufficient information can be derived from one lead, often lead II (LL-RA), shown in Figure 2.12. In the case of monitoring of epilepsy patients, typically lead II is measured together with the EEG.

An example of an ECG segment is shown in Figure 2.13. The ECG records three electrical cardiac events: (1) atrial depolarization, (2) ventricular depolarization, and (3) ventricular repolarization. The electrocardiographic correlates of these events are called the P wave, the QRS complex, and the T wave.

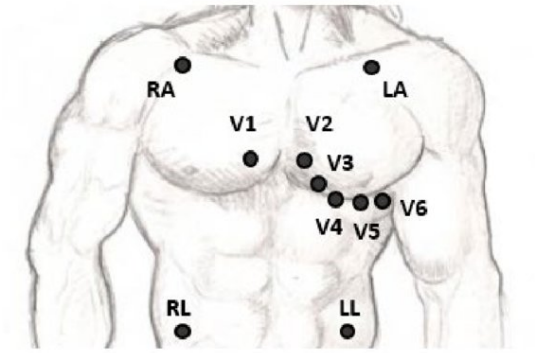


Figure 2.12: Electrode placement for a 12-lead ECG configuration, with electrodes on right arn (RA), left arm (LA), left leg (LL), Right leg (RL) and chest electrodes V1 to V6. Taken from [88]

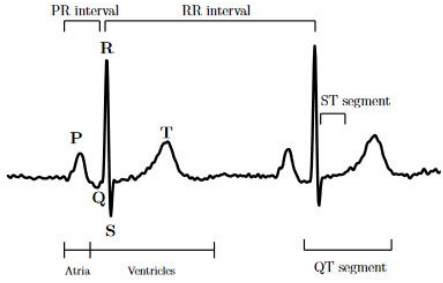


Figure 2.13: Characteristic waves and segments of a normal electrocardiogram. Two heart cycles are indicated. Taken from [258]

Each contraction of the heart gives rise to this cycle consisting of the three electrical cardiac events [190]. The heart rate can be extracted from the ECG by calculating the difference between two consecutive RR intervals with the following formula:

$$HR = 60/RR \tag{2.1}$$

with the HR in beats per min and the RR intervals in seconds.

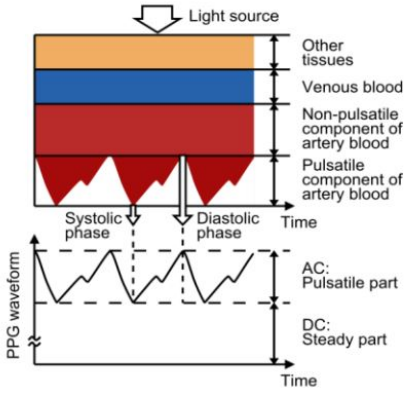


Figure 2.14: The basic principle of PPG measurements. Taken from [234]

2.4.4 Photoplethysmography (PPG)

Recording ECG always includes two electrodes placed close to the heart. Electrodes glued on the chest can be uncomfortable for long-term usage. An alternative is measuring photoplethysmography (PPG). The basic principle of measuring PPG is the change of light transmission or reflectance caused by a changing blood flow. In Figure 2.14 the basic principle is demonstrated. A light source, typically a red, infrared or green Light Emitting Diode (LED) is emitted through the skin. The light is absorbed by different layers: other tissues, venous blood, a non-pulsatile component of artery blood and a pulsatile component of artery blood. The first three layers are constant in time and are responsible for the DC part. The last one fluctuates due to the fluctuating blood volume. During the systolic phase, the heart contracts and blood is pumped through the body. The arteries will therefore contain a larger blood volume than during the diastolic phase when the heart chambers are filling again.

There are two different modes: a transmission and a reflective mode. In the transmission mode, the source is placed on one side of the tissue, whereas the light detector (LD) is placed on the other side, demonstrated in Figure 2.14. When the tissue is too thick, for example for an arm or a leg, the reflective mode can be used. Here the source is placed on the same side of the LD, which is the commenly used mode for wristbands measuring PPG [234].

2.4.5 Quality of PPG measured at different places on the body

PPG can be measured at different places on the body. The location of the LED and LD is an important design issue that affects the signal quality. However, the measurement site should be comfortable for recording PPG during daily life. PPG sensors are commonly worn on the fingers due to the high signal amplitude. However, this measurement site is not suitable during daily life since most daily activities involve the use of the fingers. Recently, different measurements sites of PPG are explored: the ring finger, wrist, brachia, earlobe, external ear cartilage, and the superior auricular region [234]. Maeda et al. [154] studied the influence of motion artifact with respect to light source and anatomical site. PPG was measured at the upper arm, forearm, wrist and finger with green and infrared light. The highest quality was observed at the upper arm with green light. Vanherck et al. [257], studied the quality of PPG measurements recorded at different places on the body during daily motions (typing, walking, stair climbing and running). The PPG data was recorded with the Byteflies sensor dots. The PPG recorded at the forehead clearly had a better quality than the PPG measurements at the upper arm, behind the ear, the wrist and the upper chest. During rest, 8% of the head PPG data was artifacted, behind the ear this was 37%, on the upper arm 62%. On the wrist and chest more than 95% of the PPG was artifacted, indicating that the wrist and the chest are no good positions to measure PPG with the sensor dot or that the predefined light frequency or light intensity were not suitable. The original idea of the SeizeIT device was measuring PPG behind the ear. However in the study of Anke Vanherck, 37% of the PPG data at rest was artifacted. During all the daily activities more than 85% of the data was artifacted, suggesting that the quality of the PPG measured behind the ear is currently not good enough for continuous monitoring during the day.

2.4.6 Others

Surface electromyography (sEMG)

Surface electromyography (sEMG) measures muscle response or electrical activity in response to a nerve's stimulation of the muscle on the surface of the skin. sEMG is useful to detected muscle stiffening as in Tonic(-Clonic) seizures.

Accelerometry (ACC)

Accelerometers measure the acceleration in three directions. These signals are suitable for detecting seizures having a strong and atypical motor component, for example (tonic-)clonic seizures.

Electrodermal activity

Electrodermal activity (EDA) measures the conductance of the skin, which increases when a person is sweating. The conductance of the skin is affected during GTCS and FBTC seizures [179].

2.5 Existing wearable seizure detection devices

There has been progress in the field of wearable seizure detection devices. Recently, wearable seizure detection devices were developed and available on the market. Verdru et al. [261] provides an overview and comparison between different wearable seizure detection devices. In order to compare those devices newly proposed standards for testing and clinical validation were taken into account [20]. There were four key features identified for determining the validation phase of such devices: subjects, recordings, data analysis and alarms, and reference standard. The devices in phase 3 and 4 are summarized in this thesis. Phase 3 requires at least 20 patients with seizures and 30 seizures in the validation study, continuous recordings should be made with the dedicated device and data should be recorded in multiple centers. Analysis and seizure detection need to be prospective and real time and algorithms should be predefined or trained on an independent dataset. Phase 4 requires at least 50 patients with seizures and in total more than 75 seizures. In addition to the requirement of phase 3 studies, phase 4 consists of in-field studies of seizure detection devices in the home environment of the patients, addressing aspects related to usability.

2.5.1 Epi-Care

Epi-Care (phase 3 and 4 studies) is a wearable wrist-worn ACC device suitable for detecting GTC seizures and F-BTC seizures. For this group of patients, a sensitivity of 90% with 0.1 - 0.2 false alarms per 24 hours was observed. Patients and caregivers were overall satisfied with the device (median = 5.5 on the 7-point Likert scale). The technical aspects were considered satisfactory and the device was considered comfortable and efficient [19, 162].

2.5.2 Empatica

The Empatica wristband (phase 3 and 4 studies) is a wearable device measuring multiple signals including ACC, EDA, temperature and PPG. Multiple publications show the validation of this wearable device: inpatient as well as outpatient studies. Patients having GTC seizures from multiple centers were studied. Overall, the sensitivity was ranging between 92% and 100% with 0.5 false alarms per 24 hours [205].

2.5.3 Nightwatch

The nightwatch (phase 3 study) is a wearable multimodal device measuring ACC and PPG, worn on the upper arm to detect (nocturnal) GT, GTC and focal hyperkinetic seizures longer than 30 seconds. The device gave a sensitivity of 86% with 0.25 false alarms per night. Combining heart rate and movement resulted in reliable detection of a broad range of nocturnal seizures. The caregivers had an increased sense of freedom and it ensured a more rapid response by the caregivers [10].

2.5.4 Brain Sentinel

SPEAC, the Brain Sentinel monitor and Alerting System (phase 3 study) is a wearable device measuring sEMG on the arm over the biceps muscle. 199 patients where included in the study with 24 patients having at least one GTC seizure. In total there were 29 GTC seizures recorded when the device was placed over the midline of the biceps muscle. For this group, the sensitivity was 100% with 1.44 false alarms per 24 hours [97].

2.5.5 EDDI

EDDI (phase 3 study) is a wearable sEMG detection device worn on the upper arm. 71 subjects were included in the study with 23 patients having seizures during the recordings. In total 32 GTC seizures were recorded. A sensitivity of 93.80% was obtained with 0.67 false alarms per 24 hours. The false positives were mostly due to physiological muscle activation during exercise. Other causes were device malfunction and detached electrodes [17].

2.5.6 Devices for focal seizures

Existing seizure detection devices are on the market for real-time detection of heavy motor seizures like GTC seizures. However, there is only one automated seizure detection device, UNEEG medical [65], for the detection of focal seizures. This device is a minimally invasive, subscalp, implantable EEG system allowing ultra-long-term seizure monitoring. No non-invasive devices are yet developed for focal seizures without considerable motor components. This thesis will focus on the detection of focal seizures using behind-the-ear EEG, ECG and PPG.

Chapter 3

Machine Learning Methods

Understanding the concept of various machine learning techniques is important in order to apply those techniques to epileptic seizure detection. In the first section, feature-based machine learning techniques such as Support Vector Machines and Random Forest are explained, which are used in the main contributions of the thesis. The second section summarized the concepts of deep learning. Those concepts are only briefly explained since they are not used in the main contributions of the thesis but they are intended as background for Chapter 5, which is a literature overview of automated algorithms. The third section depicts the strategies for training models with unbalanced data sets. The fourth section explains a normalization method: Median decaying memory. Next, cross-validation schemes are explained. Lastly, the performance metrics are depicted.

3.1 Machine Learning techniques: feature-based models

Machine learning can be defined as computation methods using experience to perform certain tasks, such as classification, regression, ranking and clustering. The experience is previously collected information available for the learner. The main task in this thesis is a classification task, classifying a data segment in two categories: seizure or non-seizure. The information available for the learner takes the form of previously recorded data of epilepsy patients with seizure annotations. Different machine learning scenarios exist, which differ in the type of training data available for the learner, such as supervised learning,

unsupervised learning and semi-supervised learning. In supervised learning, which is the scenario in this thesis, the learner receives labeled data examples for training. In unsupervised learning the learner receives unlabeled training data and in semi-supervised learning a mixture of labeled and unlabeled data is available [166].

Different machine learning techniques for supervised classification problems are described in the literature such as Linear Classifiers, Support Vector Machines (SVM), Decision Trees, Random Forests (RF), k-nearest neighbor and Neural Networks. Seen the previous promising results using SVM and RF for epileptic seizure detection [47], those machine learning techniques were used in this thesis and are explained here.

3.1.1 Support Vector Machines

Consider a given training set $\{\mathbf{x}_k, y_k\}_{k=1}^{N}$ with input data $\mathbf{x}_k \in \mathbb{R}^n$ and output data $y_k \in \{-1, +1\}$, which are the class labels. Non-linear SVMs make use of a kernel function $\varphi(\cdot) = \mathbb{R}^n \rightarrow \mathbb{R}^{n_h}$. This kernel function projects the n-dimensional input to the n_h-dimensional feature space. Then the hyperplane, which is the boundary between the two classes, is defined as $\mathbf{w}^T\varphi(\mathbf{x}) + b = 0$, where $\mathbf{w} \in \mathbb{R}^{n_h}$ is a weighting factor and $b \in \mathbb{R}$ a constant. The output of the classifier is defined as

$$y(\mathbf{x}) = sign[\mathbf{w}^T\varphi(\mathbf{x}) + b], \tag{3.1}$$

$\mathbf{w}^T\varphi(\mathbf{x}) + b$ is the continuous output of the classifier. It is the classification score or latent variable, which is the distance from the decision boundary. If this value is large, it is more certain that the input data belongs to that class. The sign of this function gives the corresponding class.

In the case where perfect separation is not possible, the resulting optimization problem becomes

$$\begin{aligned} \min_{\mathbf{w},b,\epsilon} \mathcal{J}_P(\mathbf{w}, \xi) &= \frac{1}{2}\mathbf{w}^T\mathbf{w} + C\sum_{k=1}^{N}\xi_k \\ \text{such that } y_k[\mathbf{w}^T\varphi(x_k) + b] &\geq 1 - \xi_k, k = 1, ..., N \\ \xi_k &\geq 0, k = 1, ..., N. \end{aligned} \tag{3.2}$$

ξ_k are the slack variables, which are added in order to tolerate some misclassifications. The parameter C is a positive regularization constant, which

is a trade-off between margin size and classification error. This parameter controls the risk of overfitting.

This optimization problem with constraints is solved by constructing the Lagrangian:

$$\mathcal{L}(\mathbf{w}, b, \xi; \alpha, \nu) = \mathcal{J}(\mathbf{w}, \xi) - \sum_{k=1}^{N} \alpha_k (y_k [\mathbf{w}^T \varphi(x_k) + b] - 1 + \xi_k) - \sum_{k=1}^{N} \nu_k \xi_k \quad (3.3)$$

with Lagrange multipliers $\alpha_k \geq 0$, $\nu_k \geq 0$ for k=1, ..., N. The solution is given by the saddle point of the Lagrangian:

$$\max_{\alpha,\nu} \min_{\mathbf{w},b,\xi} \mathcal{L}(\mathbf{w}, b, \xi; \alpha, \nu). \quad (3.4)$$

With the use of the Kernel trick $K(\mathbf{x}_k, \mathbf{x}_l) = \varphi(\mathbf{x}_k)^T \varphi(\mathbf{x}_l)$ for k, l = 1, ..., N, the quadratic programming problem in the dual space becomes

$$\begin{aligned} \max_{\alpha} \mathcal{J}_D(\alpha) = \frac{-1}{2} \sum_{k,l=1}^{N} y_k y_l K(x_k, y_l) \alpha_k \alpha_l + \sum_{k=1}^{N} \alpha_k \\ \text{such that} \sum_{k=1}^{N} \alpha_k y_k = 0 \\ 0 \leq \alpha_k \leq c, k = 1, ..., N. \end{aligned} \quad (3.5)$$

Finally, equation (3.1) can be written as

$$y(\mathbf{x}) = sign[\sum_{k=1}^{\#SV} \alpha_k y_k K(\mathbf{x}, \mathbf{x}_k) + b] \quad (3.6)$$

with $\#SV$ the number of support vectors. which is the number of non-zero α_k values.

In this thesis an RBF kernel is used:

$$K(\mathbf{x}, \mathbf{x_k}) = exp(\frac{-||\mathbf{x} - \mathbf{x}_k||_2^2}{\sigma^2}) \quad (3.7)$$

with σ the width of the RBF kernel.

3.1.2 Random Forest

A Random Forest classifier consists of a large number of individual decision tree models that operate as an ensemble, shown in Figure 3.1. An individual decision tree model is a tree where each internal node is labeled with a feature. Depending on the feature value, a leaf is selected. This leaf leads to a next node until the end of the tree is reached, which gives you the prediction class. Each individual tree in the random forest gives a class prediction and the class with the most votes becomes the model prediction of the random forest [22].

Data sampling/selection is needed to create different independent learners (in our case the different decision trees). Ideally, classifier outputs should be independent. Diversity in ensembles can be achieved through several strategies of selecting different subsets to train the individual learners. In our ECG-based algorithm in Chapter 8, the RUSBoost algorithm is used because it is suitable for data with class imbalance [194].

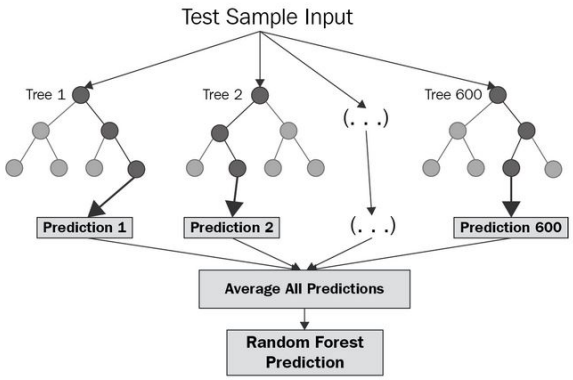


Figure 3.1: Example of a Random Forest classifier. Taken from [110]

3.2 Machine Learning techniques: Deep Learning models

My own contributions do not make use of deep learning models, only the collaborations mentioned in Chapter 5. Therefore, the concepts of deep learning are briefly summarized.

Deep Learning is a part of machine learning methods, which do not need human defined features. Those methods can learn the features themselves and use as input the raw or filtered data. Those models are based on artifical neural networks. Those artificial neural networks are a collection of nodes or neurons, connected to other neurons in different layers. A simple neural network with input and output with one hidder layer in shown in Figure 3.2. In deep learning, mutliple layers are present in the model. Each neuron, which are the building blocks of the neural networks, receives a set of input values. The neuron multiplies each input value x with its corresponding weight w and sums them up together with a bias b, shown in Figure 3.3. In order to allow non-linear interactions, a non-linear function f can be applied on this sum.

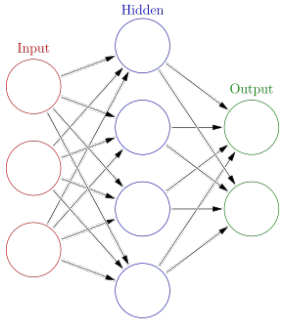


Figure 3.2: Artificial neural network. Taken from wikipedia.com

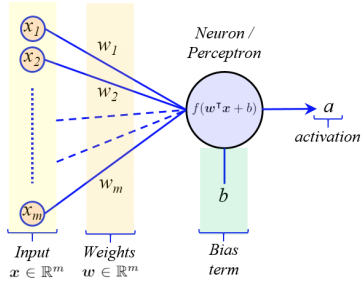


Figure 3.3: Illustration of a neuron. Taken from [7]

3.2.1 Convolutional Neural Networks (CNN)

Those artifacial neural networks are very powerful. However, deep architectures, which are needed for certain taks, have a very large number of training

parameters. This leads to high computational complexity for training such models. To solve this problem, a new type of network was introduced: Convolutional Neural Network (CNN). The CNN architecture consists of multiple stacked layers transforming an input to a certain feature representation, which serves as an input of the classification. A typical architecture of a CNN is shown in Figure 3.4. The feature learning consists of convolutional layers and pooling layers. Those convolutional layers apply spatial filters on the input and the pooling layers reduce the size of the input data. The classification consists of a fully connected layer.

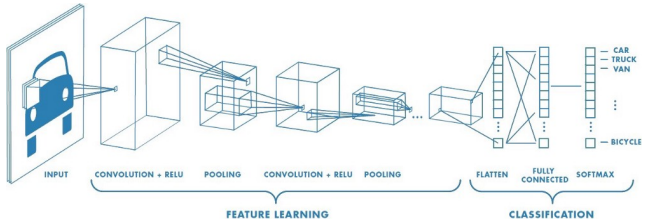


Figure 3.4: Architecture of a CNN. Taken from [242]

3.2.2 Recurrent Neural Networks (RNN)

Those artificial neural networks or CNN architectures do not take into account temporal information. Recurrent neural networks do not only look at the current input but also the previous input. Figure 3.5 shows a representation of a recurrent neural network. At time stamp Xn, there is an additional input from the previous time stamp. This way the neural network takes into account the past information. Different variants of RNN architectures exist, such as Long short-tem memory (LSTM) or Gated recurrent unit (GRUs).

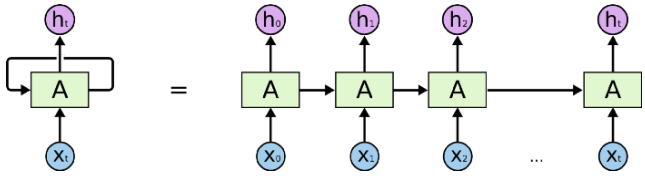


Figure 3.5: A recurrent neural netork. Taken from [161]

3.3 Imbalanced data set

Since seizures are very rare events, many more non-seizure data points compared to seizure points are present in the data set, creating an imbalanced data set. It is a good practice to create a more balanced data set for training the model. This is to avoid the risk of only detecting the majority class with the trained model. The strategies used to balance the data set are similar as described in [47].

In order to decrease the number of non-seizure points, a simple classification rule is applied for both the HR- and EEG-based seizure detection. In case of the HR-based seizure detection system, data segments without any heart rate increase, are assumed to be non-seizure data points and are not included in the training set. In case of the EEG-based seizure detection system, data segments having a root mean square amplitude lower than a certain value (13 μV) for all the channels are also excluded from the training set. For both modalities, this reduces already significantly the imbalance between the two classes. However, the data set remains still unbalanced. For the EEG-based seizure detection algorithm the non-seizure data points are further reduced with a random undersampling.

As a second strategy, Weighted SVM, which is a modification to the standard SVM formulation (formula 3.2) to remove the class imbalance from the data set [4], is applied:

$$\begin{aligned} & \min_{w,b,\xi} \frac{1}{2}||w||^2 + C\sum_{i=1}^{N} c_i\xi_i \\ s.t. \quad & \begin{cases} y_i(w^T\varphi(x_i)+b) \geq 1-\xi_i \\ \xi_i \geq 0 \end{cases} \quad ,\forall i \in [1,N] \end{aligned} \quad , \tag{3.8}$$

with ξ_i the error of the model on x_i and C a positive regularization constant. The values of c_i are defined as

$$c_i = \begin{cases} \gamma\frac{(N^+ + N^-)}{2N^-} & : y_i = -1 \\ \frac{N^+ + N^-}{2N^+} & : y_i = +1 \end{cases} . \tag{3.9}$$

The parameter γ gives more importance to the correct classification of seizure samples ($y_i = -1$) compared to non-seizure samples ($y_i = +1$) during classifier training.

3.4 Normalization method: Median decaying memory

Because differences in the EEG amplitude were present between individuals, and amplitude variations occurred over time, normalization of the features is crucial. Furthermore, when neurologists annotate seizures, possible seizure segments are compared with the background EEG before the seizure onset. A very important feature of focal seizures is the evolution of the ictal EEG pattern over time. One option to exploit the change of features over time in the seizure detection system, is to normalize each feature value with an average of a few past EEG segments. However, this is not robust for artifacts. The median decaying memory method [150] is used instead and the normalization factor z(k) is calculated as follows:

$$z(k) = (1 - \lambda) median(F(k-1)...F(k-236)) + \lambda z(k-1) \tag{3.10}$$

with $\lambda = 0.99$. The feature value F(k) is divided by z(k). The λ provides additional memory beyond the 236 segments. If k<236, s(k) is calculated as follows:

$$z(k) = (1 - \lambda) median(F(k-1)...F(1)) + \lambda z(k-1) \tag{3.11}$$

with $\lambda = 0.92$.

The number of segments was originally set to 118. Since artifacts can be longer than 118 seconds, the number of segments was doubled in this analysis. Although, the effect on the performance was negligible.

3.5 Cross-validation

Data driven algorithms, as used in the contributions of this thesis, need data to learn from, which is called the training data. This training data should be different than the test data, to allow the classifier to make predictions on unseen data.

The training data can be data from different patients, leading to a patient-independent model. No data of the specific test patient is needed for training, making those algorithms practical in daily life. However, patterns on the biomedical signals differ between patients. As a result, patient-independent models lead in general to lower performances.

The training data can be data from the same patient, leading to a patient-specific model. Data of the specific patient is needed to train the model as well as expert annotations, for supervised models.

In order to include all the data as test data once, cross-validation was applied. For patient-independent models, leave-one-patient (LOPO) was applied as cross-validation scheme, illustrated in Figure 3.6. The models were trained using the data of all patients, except the test patient. This was done N times with N the number of patients such that each patient is used once for testing. This was applied in Chapters 7 and 8 for the SeizeIT1 dataset. In chapter 6 and 8 for the Epilepsiae databases, the models were trained using another database.

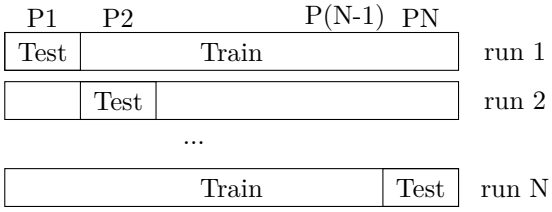


Figure 3.6: Leave-one-patient-out (LOPO) cross-validation

For the patient-specific models, leave-one-seizure-out (LOSO) was applied as cross-validation scheme. The patient-specifc data was split in different parts or folds. The splits between those folds were set exactly in the middle of the nonseizure data between two seizures. Each fold was used once as test data whereas the other folds were used to train the model. This was applied in Chapters 7 and 8 for all the patient-specific models.

3.6 Performance metrics

Objective performance metrics are needed to evaluate seizure detection systems. In literature, the most popular basic metrics are the sensitivity and false alarm rate. The exact definition of sensitivity and false alarm rate varies in the literature [278]. The cause of this variation is that the recorded data are sequential time series and the reference annotations are defined as fixed points in time (seizure start and seizure end). Multiple solutions can be found to quantify the match between those fixed reference annotation time points and a sequential output of the algorithm. For example, Figure 3.7 depicts the reference annotation and the output of the seizure detection system, the hypothesis. The sensitivity can be defined as the percentage of data segments correctly detected, which leads to a sensitivity of 50% in this case. Or the seizure can be assumed

to be detected if at least 1 detection is made between the seizure start and seizure end, which leads to a sensitivity of 100% in this case.

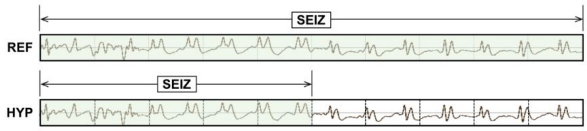


Figure 3.7: Example of a seizure reference annotation and an hypothesis [Taken from [278]]

How you define the sensitivity depends on the user requirements of the seizure detection system. For generating automatically a seizure diary, the most important question is how many seizures has occurred, less importance is given to the exact seizure start and seizure end.

In this thesis, the sensitivity and false alarm rate are defined as follows:

1. Detection sensitivity: TP/(TP + FN), where TP = true positive and FN = false negative. In Chapter 6 a seizure was detected correctly (TP) if the detection occurred between 30s before and 90s after the seizure onset. This rule was set since heart rate increases can precede or exceed seizure onsets. In Chapter 7 and 8 a seizure was detected correctly (TP) if the detection occurred between the EEG onset and offset of the seizure.
2. False positive (FP) detection rate per 24 hours: FPs/recording length; FPs within 10 or 60 seconds of each other were counted as one FP. In Chapter 6 the FPs are clustered within 60 seconds, whereas in Chapter 7 and 8 the FPs are clustered within 10 seconds.

In addition, extra metrics can be calculated as follows:

1. Detection delay: the time interval between the EEG seizure onset and detection by the algorithm. This delay should be as short as possible, in order to warn the parent or caregiver as soon as possible. This is an important requirement for real-time seizure detection systems.
2. Positive predictive value (PPV): TP/(TP + FP). The positive predictive value or precision is the ratio of correctly detected seizures and total detected seizures, which are the correctly detected seizures and wrongly detected seizures or false alarms. This PPV should be as high as possible.
3. F1-score: 2 * (PPV * Recall)/(PPV + Recall) with Recall = TP/(TP + FN). The F1-score is the harmonic mean of the PPV and recall or

sensitivity. Seizure detection systems require a high PPV and sensitivity, making the F1-score a suitable metric to combine them. The F1-score is an excellent measure to compare seizure detection performances between different studies or algorithms.

Chapter 4

Data description

This chapter gives an overview of the datasets used in this thesis. The first section describes the SeizeIT1 dataset, recorded during the ICON project SeizeIT at UZ Leuven. The SeizeIT2 dataset, described in section 2, is currently being recorded within the EIT Health (SeizeIT2) project. Section 3 details the European Epilepsiae Dataset, currently the largest European epilepsy dataset publicly available. As last, the Temple University Seizure Corpus (TUSZ) dataset is briefly explained, used in the Neureka challenge [171].

4.1 SeizeIT1

4.1.1 Data description

The SeizeIT1 dataset contains recordings from patients with refractory epilepsy who underwent presurgical evaluation at the University Hospital Leuven (UZ Leuven), Leuven, Belgium. The patients were recorded continuously mostly during three or four days. In total, 82 patients were recorded between January 23, 2017 and October 26, 2018. From those patients, 65 were recorded with the extra behind-the-ear electrodes. This thesis aims to detect focal seizures with a length of at least 10 seconds. Therefore, seven patients (11%) without ictal EEG correlates, two patients (3%) with generalized seizures that were too short, and two patients (3%) with unreadable ictal EEG due to muscle artifacts were excluded from this study. Twelve (18%) patients did not have seizures during the recordings, but were used to evaluate the false detection rate.

Table 4.1: SeizeIT1: An overview of the seizure types, origins and hemispheres (n=Number of seizures, FA= Focal Aware, FIA= Focal Impaired Awareness, F-BTC= Focal to Bilateral Tonic Clonic, Temp=Temporal, Par=Parietal, NC= Not Clear)

			Seizure type			
	FA	FIA	F-BTC			
N	18	162	2			
			Origin			
	Temp	Fronto-temp	Fronto-par	Occipito-temp	Par	NC
N	138	27	2	9	3	3
			Hemisphere			
	Left	Right	Bihemispheric	NC		
N	71	94	14	3		

The remaining dataset consisted of 54 patients with 5284 hours of data and 182 seizures, recorded in 42 patients. The number of seizures per patient ranged from 1 to 22, with a median of three seizures per patient. The duration of the seizures, the time difference of seizure EEG onset and end, varied between 11 and 695 seconds with a median of 50 seconds. Eighty-nine percent of the seizures were focal impaired awareness seizures. Ninety-one percent of the seizures originated from the (fronto-)temporal lobe. More information about the type, localization, and lateralization can be found in Table 4.1.

4.1.2 Experimental setup

The experimental setup of this study is shown in Figure 4.1. The patients were recorded with traditional 10-20 scalp EEG with 1 bipolar ECG channel having a sampling frequency of 250 Hz. The two ECG electrodes were placed supraclavicularly left and right. Four additional electrodes were glued to the skin behind the ears (two at each side) and were connected to the same EEG amplifier. Using these additional electrodes, four behind-the-ear bipolar channels (two crosshead, one left, and one right bipolar channel) were derived by taking the potential difference between these electrodes. Figure 4.2 displays a seizure recorded with the behind-the-ear EEG setup together with the seizure onset.

Additionally to the standard clinical equipment, recordings were made with a wearable ECG device, the 180° eMotion Faros [23], and a wrist-worn PPG device, the Empatica E4 smartwatch [70]. The Faros device was used in a one-channel configuration. The positive electrode was placed on the left side of the torso, medial-supraclavicularly; the negative electrode was placed on the left

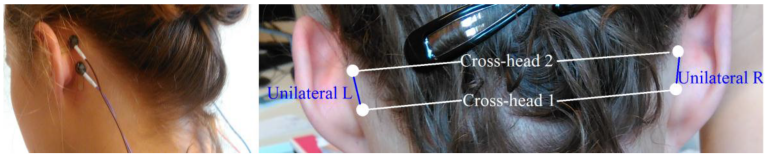


Figure 4.1: Behind-the-ear electroencephalographic setup. Left panel shows extra behind-the-ear electrodes glued to the skin. Right panel shows bipolar channel derivations. Reproduced with permission from Gu et al. [96]

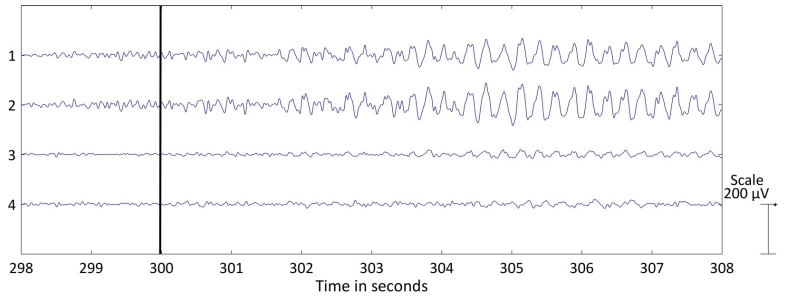


Figure 4.2: Left temporal lobe seizure recorded with behind-the-ear electroencephalographic (EEG) setup. The four bipolar EEG channels are shown over a period of 10 seconds: (1) crosshead 1, (2) crosshead 2, (3) unilateral left, (4) unilateral right. The bipolar EEG channels were filtered with a bandpass filter (1-25 Hz). The black horizontal line at 300 seconds depicts the seizure onset

side, laterally under the rib cage. The Empatica E4 measures reflective PPG using a green and a red light-emitting diode (LED) on the wrist. The device returns a single channel, which is obtained by combining the green and the red channels using Empatica's proprietary algorithm. The intravenous insertion, which is a needle inserted into a peripheral vein, used for administering fluids or medication, is mostly placed at the dominant wrist. As a result, the Empatica watch was worn on the other wrist. The respective sampling rates of the hospital ECG, Faros ECG and Empatica PPG signals were 250, 500 and 64 Hz. The data was managed using the Byteflies' cloud. This system allowed for the integration of the data from the wearable devices with the hospital's recording setup.

A clinical expert annotated the seizure onsets and ends with the use of video-EEG data (full channel EEG), validated afterward by a neurologist-epileptologist (W.V.P.). The ethical committee of UZ Leuven approved the study. All patients signed an informed consent form for their participation in this study.

Table 4.2: SeizeIT2: An overview of the seizure types, origins and hemispheres (n=Number of patients, FA= Focal Aware, FIA= Focal Impaired Awareness, F-BTC= Focal to Bilateral Tonic Clonic, Temp=Temporal, Par=Parietal)

	Seizure type		
	FA	FIA	F-BTC
N	2	7	2
	Origin		
	Temp	Frontal	Par
N	8	2	3
	Hemisphere		
	Left	Right	
N	6	3	

The SeizeIT1 dataset is used in Chapters 6, 7 and 8. In chapter 6 only the first part of the dataset is included, since this dataset was currently being recorded, whereas Chapters 7 and 8 used the complete dataset. In addition, Gu et al. [96] and Becker et al [13] did research using this dataset.

4.2 SeizeIT2

4.2.1 Data description

The SeizeIT2 dataset is a multicenter dataset, currently being recorded. Adult and pediatric patients with multiple types of epilepsy (focal and generalized seizure types) are measured in different clinical centers: University Hospital Leuven (UZ Leuven), King's College London, Oxford University, University of Aachen, Karolinska Institute, Freiburg University Medical Center and Coimbra University Hospital. The patients were recorded continuously during 1-4 days. Currently (January 2021) 125 patients were recorded in the University Hospital Leuven (65 pediatric and 60 adult patients) and 4 patients in the Freiburg University Medical Center. Between 24/1/2020 and 27/10/2020, 76 patients with focal epilepsy were recorded. From those, 9 patients were analyzed. The remaining patients were not analyzed due to the following reasons: 34 patients were not yet annotated, 20 patients experienced no seizures during the recordings, the recordings of 13 patients have technical problems. More information about the type, localization, and lateralization can be found in Table 4.2. Note that the seizure types, origins and hemispheres are given per patient. One patient can have seizures with different origins or origins.

4.2.2 Experimental setup

Similarly to the SeizeIT1 dataset, patients were recorded with traditional 10-20 scalp EEG with 1 bipolar ECG channel. Four behind-the-ear electrodes (two behind each ear) were connected to the hospital EEG amplifier. The electrode positions are shown in Figure 4.3, which are exactly the same as in the SeizeIT1 dataset. In contrast to SeizeIT1, two behind-the-ear EEG channels and 1 ECG channel were also recorded with wearable devices, the Byteflies Sensor Dots, shown in Figure 4.4. One Sensor Dot measures two behind-the-ear channels. Those channels include one crosshead channel and one local channel, left or right depending on the seizure onset zone. To record simultaneously the behind-the-ear EEG channels with the hospital equipment and Byteflies Sensor Dot, splitter cables were used to send the electrical signal to both devices, illustrated in Figure 4.5. The other Sensor Dot measures ECG. In addition, both Sensor Dots contain acceleration in the X,Y and Z-axis.

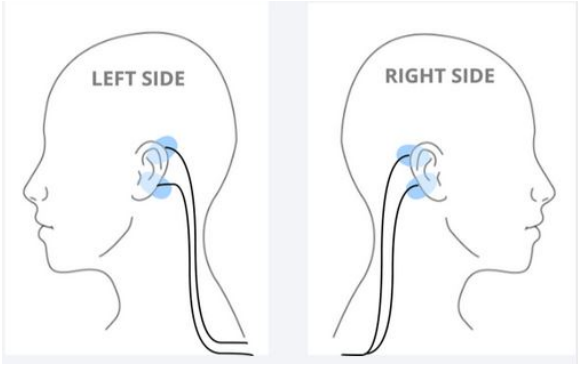


Figure 4.3: SeizeIT2: position of the behind-the-ear electrodes. Reproduced from the SeizeIT2 - EIT Health Consortium RedCap website [104]



Figure 4.4: Byteflies Sensor Dots. Reproduced from the Byteflies website [32]

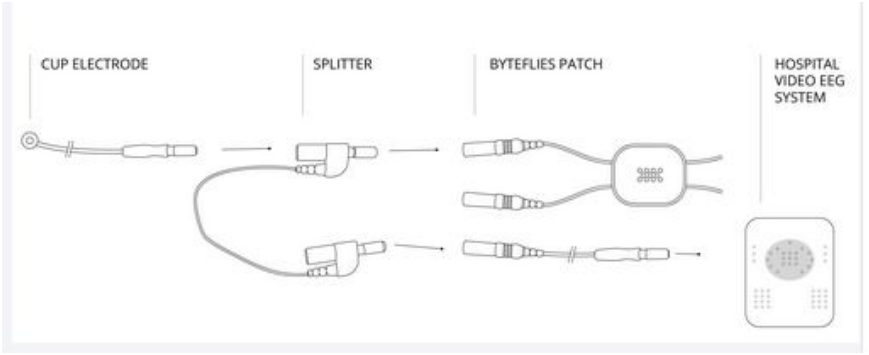


Figure 4.5: SeizeIT2: splitter configuration. Reproduced from the SeizeIT2 - EIT Health Consortium RedCap website [104]

There are no published studies yet using this dataset, but a preliminary analysis in described in Appendix A.

4.3 European Epilepsiae Dataset

4.3.1 Data description

The European Epilepsiae dataset, which was made publicly available in 2012, provides long-term EEG recordings of 275 patients [126, 108]. Those patients were recorded in multiple centers: the University Hospital Freiburg (Germany), the University Hospital of Coimbra (Portugal), the Hopital de la Pitier-Salpetriere in Paris (France). This dataset comprises surface recordings from 217 patients as well as invasive EEG recordings from 58 patients. The patients were recorded continuously during multiple days. In this thesis, only the patients having surface recordings from the centers in Freiburg ad Paris were analyzed. The Freiburg dataset consisted of 30 patients having in total 275 seizures, whereas the Paris dataset contained 63 patients having in total 400 seizures. Most of the seizures were FIA seizures originating in the (fronto-) temporal lobe with a duration between 60 and 120 seconds for both datasets. The overview of seizure types, localization, lateralization is provided in Table 4.3 and 4.4. In the Freiburg dataset, 243 (88%) seizures had ictal EEG changes, whereas all the seizures from the Paris dataset were associated with ictal EEG changes. From the Freiburg/Paris dataset, 196 (71%)/278 (70%) seizures had temporal lobe involvement.

Table 4.3: Freiburg dataset: An overview of the seizure types, origins and hemispheres (n=Number of seizures, FA= Focal Aware, FIA= Focal Impaired Awareness, F-BTC= Focal to Bilateral Tonic Clonic, Temp=Temporal, Par=Parietal, Occ=Occipital, NC= Not Clear)

			Seizure type		
	FA	FIA	F-BTC	NC	
N	49	139	22	65	
			Origin		
	(Fronto-)Temp	Frontal	(Fronto/Temporo-)Par	Occ	NC
N	135	25	29	8	78
			Hemisphere		
	Left	Right	Bihemispheric	NC	
N	117	81	29	48	

Table 4.4: Paris dataset: An overview of the seizure types, origins and hemispheres (n=Number of seizures, FA= Focal Aware, FIA= Focal Impaired Awareness, F-BTC= Focal to Bilateral Tonic Clonic, Temp=Temporal, Par=Parietal, Occ=Occipital, NC= Not Clear)

			Seizure type		
	FA	FIA	F-BTC	NC	
N	52	200	27	121	
			Origin		
	(Fronto-)Temp	Frontal	(Fronto/Temporo-)Par	Occ	NC
N	276	49	10	1	64
			Hemisphere		
	Left	Right	Bihemispheric	NC	
N	178	141	54	27	

4.3.2 Experimental setup

The patients were recorded with a standard set-up consisting of 10-20 scalp EEG with one or two bipolar leads ECG and one or two EMG channels. No behind-the-ear channels or wearable data were recorded.

The Epilepsiae dataset is used in Chapter 8.

Table 4.5: TUSZ dataset: An overview of the seizure types [n= Number of seizures, FN= Focal Non-Specific, GN=Generalized Non-Specific, FA=Simple Partial, FIA= Focal Impaired Awareness, AB=Absence, TN=Tonic, CN=Clonic, TC=Tonic Clonic, AT=Atonic, MY=Myloclonic].

	Seizure type									
	FN	GN	FA	FIA	AB	TN	CN	TC	AT	MY
N	1834	585	52	361	99	68	0	53	0	3

4.4 Temple University Seizure Corpus (TUSZ)

This dataset consists of routine EEG recordings performed on 692 patients. Multiple short recordings, mostly around 20-30 minutes per patient were recorded. In total 3055 seizures were recorded. Table 4.5 gives an overview of the different seizure types. The recordings in the dataset come in different EEG montages and with different sampling frequencies.

This dataset was used for the Neureka challenge [171].

Chapter 5

Automated algorithms

This chapter is a literature overview of algorithms for the three modalities discussed in this thesis: EEG, ECG and PPG and a combination of those modalities. For each modality, the first subsection describes the state-of-the-art seizure detection algorithms. In case of the EEG, algorithms based on full scalp EEG and reduced montages are discussed in two different subsections. Next, personalization approaches are described. On one hand, patient-independent or general models have low performance due to the patient-specific ictal patterns. On the other hand, only a limited amount of seizures per patients are recorded making the training of fully patient-specific algorithms challenging. Personalization of patient-independent models could be a way of tackling this problem. Lastly, artifact removal and artifact detection or quality assessment of the signal is discussed. In addition, all the contributions of my thesis and collaborations are depicted in bold in the text. With a footnote, explanation is given about those collaborations.

5.1 Electroencephalography (EEG)

5.1.1 Seizure detection based on Full scalp EEG

Most seizure detection research is based on full channel EEG. Baumgartner et al. [12] and Shoeibi et al. [220] provided good overviews of the important seizure detection algorithms in the field. Here an overview is given of state-of-the-art algorithms with respect to the following categorization below:

1. Heuristic rule based algorithms: Classification is based on empirically defined thresholds on the feature values.
2. Classical machine learning algorithms: Machine learning techniques are used for classification.
3. Deep Learning algorithms: End-to-end learning or deep learning solutions, where the input of the network are not extracted features, but the raw or filtered data.

Here, the methods of state-of-the-art studies are briefly described for those 3 categories.

Heuristic rule based algorithms

A typical pipeline of heuristic rule based algorithms consists of a preprocessing step, feature extraction and a rule based classification. The preprocessing step mostly contains filtering of the EEG data with or without an artifact reconstruction or rejection step. Features are extracted which are discriminative between seizure and non-seizure data. Based on those feature values, heuristic rules with thresholds are defined.

Gotman [92] presented the first paper on automated seizure detection. The EEG was decomposed into half-waves. The characteristics of those half-waves in each 2 second epoch were compared to the background (16 second segment). One of the classification rules was that the average amplitude of the half-waves in the epoch had to be at least 3 times higher than in the background. Pauri et al. [185] extended the method of Gotman by two extra features: the average duration of the half-waves as a measure of frequency and the coefficient of variation of half-wave duration expressing the degree of rhythmicity. Gabor et al. [85, 84] filtered the data first using weighted wavelet transform. The EEG was decomposed into 10 wavelet scales. Each of those wavelets were multiplied by a weighting factor (0-1) and were combined resulting in filtered time-series. Those time-series were transformed into a spectrogram, based on a self-organizing map neural network, features were extracted. Rules were set based on the time-series (3) and self-organizing map neural network features(4). Wilson et al. [266] developed a seizure detection algorithm [Persyst-Reveal], based on Matching Persuit decompositions to identify rhythmic activity. Connected-object clustering is applied to cluster background and seizure segments. Kelly et al. [123] developed an automated scalp- EEG–based seizure detection system (IdentEvent) processing multichannel scalp-EEG signals and translating them into 3 main EEG descriptors, namely pattern-match regularity statistic (PMRS as a measure of signal complexity), local maximum frequency (LMF), and

amplitude variation. The last two were used for artifact rejection. Different rules were defined for uni- and bi-lateral seizures. Hopfengärtner et al. [102, 101] developed a method based on power spectral analysis techniques. Hartmann et al. [98] developed a seizure detection system [EpiScan] based on periodic waveform analysis. The periodic waveforms were analyzed in three frequency bands. After normalizing, fixed thresholds were set for classification. Fürbass et al. [83] compared EpiScan with Persyst on a large multicentered dataset.

Classical machine learning algorithms

The pipeline of classical machine learning algorithms is similar to the heuristic rule based algorithms, only the classification step is different. Instead of defining a rule, machine learning techniques were used. Saab et al. [208] applied the 5-level wavelet transform. From the wavelet coefficients, three characterizing features were derived. Those features were required for the Bayesian formulation used in training and testing. Kuhlmann et al. [130] extended the analysis of Saab et al. by adding addditional features. Meier et al. [201] extracted seven features: Total signal energy of the wavelet transform of two different scales, mean sliding variance, mean cross correlation coefficient, power after smoothing the signal with a Savitzky-Golay filter, zero-crossings and zero-crossings after applying a Savitzky-Golay filter. Each sample of a feature vector was separately replaced with a measure for its change over the recent past. Classification was performed with a Support Vector Machine. Boonyakitanont et al. [29] summarizes and compares feature descriptions and their interpretations.

Deep Learning algorithms

The previous two classes need the extraction of desirable features. Those features require domain knowledge and are human defined, whereas Deep Learning (DL) methods learn feature representations from the raw or filtered data. DL methods, currently used to solve a plethora of other machine learning problems, have seen a more limited use in EEG-based epileptic seizure detection due to a lack of large annotated datasets [207]. However, recent public availability of large EEG seizure datasets such as the TUH EEG corpus [177] has led to a renewed focus in the development of DL methods for solving the seizure detection problem [90].

Currently, convolutional neural networks (CNNs) seem to be the most popular approach in the category of deep learning algorithms. [238, 274, 243, 3, 9]. Recurrent neural networks (RNN) such as Long Short Term Memory (LSTM) or Gated Recurrent Unit (GRU) have also been used [90, 238, 188, 91, 107].

In order to boost the development of seizure detection algorithms, the 2020 Epilepsy Challenge [171] was launched, which is a month-long challenge on seizure detection using the TUH EEG Seizure dataset [219]. The goal of the challenge was to have the best performance across subjects (with a minimal number of false detections) while using as few channels as possible. **Chatzichristos et al.[1][36] developed a seizure detection algorithm via fusion of multi-view attention-gated U-net deep neural networks. Their submission to the challenge was awarded the first place among 15 submissions from all over the world [171].**

The pipeline of the algorithm is shown in Figure 5.1. The input data was first rereferenced and bandpass filtered. The data was further preprocessed with three different methods, called the different views of the data. A first view is the data filtered using a set of multi-channel subspace filters. The second view is the data filtered with the use of the ICLabel toolbox provided by EEGlab [192]. The ICLabel toolbox filters the data with the use of Independent Component Analysis (ICA). The components containing artifacts are automatically detected. After removing the artifacted components, the EEG data is reconstructed. The last view is the rereferenced and bandpass filtered data. Those different views were individually fed to an attention-gated U-net neural network. U-net is a DL architecture originally developed for image segmentation [206]. The U-net is a convolutional autoencoder with skip connections to recover the local spatial information lost during compression. In the current work, we used a modified U-net architecture with attention gating [214]. This attention mechanism allows the network to focus on the specific channels that contain the most relevant information for the classification task. The output of the U-net is a prediction for each sample of the EEG input. The predictions of the three different views of the data were merged with an LSTM architecture. After preprocessing, the performance was calculated with the event Scoring (TAES) metric [278].

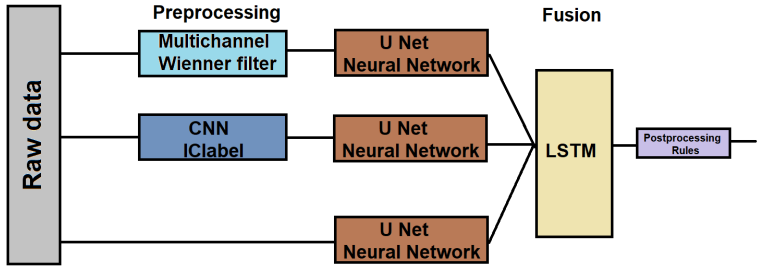


Figure 5.1: Neureka challenge: pipeline of the algorithm

[1] A collaboration of colleagues in Biomed-Stadius within the Flanders AI Research Program.

5.1.2 Seizure detection based on reduced EEG channels

Reduced electrode montages have been shown useful for seizure detection and documentation for several epilepsy types [21, 82, 227, 125, 269, 96]. Bennis et al. [21] investigated the usefulness of single-channel scalp EEG placed behind the earlobe for seizure identification. Fürbass et al. [82] investigates a reduced number of EEG electrodes. Two different montages were investigated: a 8 electrode forehead montage including frontal and temporal electrodes as well as ECG electrodes (FP1, F7, T7, FP2, F8, T8, FZ, ECG) and a 7 electrode montage including temporal and occipital as well as ECG electrodes (T7, P7, O1, T8, P8, O2, ECG). Sopic et al. [227] proposed a wearable system using 4 electrodes for the detection of epileptic seizures. The performance of the system was tested using the Physionet.org CHB-MIT Scalp EEG database for children. Kjaer et al. [125] developed a wearable absence seizure detection system for children using 3 electrodes placed near Fp1 (Ref), F7 and TP7. A very recent paper [269] presented an automatic seizure detection algorithm with a generative adversarial network (GAN) trained by unsupervised learning and evaluated it with behind-the-ear EEG for 6 patients. Our proof-of-concept study [96] showed that behind-the-ear EEG is useful for focal seizure detection.

It has been shown that EEG recorded with a small device in the ear can detect temporal lobe seizures [275] and generalized tonic-clonic seizures [276]. A similar visual seizure recognition study for temporal lobe seizures resulted in comparable performances [275]. Those results suggest that also the in-the-ear EEG signals could be used to detect temporal lobe seizures. An advantage of the in-the-ear EEG is the discreteness, but disadvantages are the possible hearing loss, discomfort, and need for individualized design.

Chapter 7, published in [254], describes a study on seizure detection using the behind-the-ear EEG channels. Firstly, a visual annotation study was done, where the neurologist was asked to annotate behind-the-ear EEG segments containing selected seizure and nonseizure fragments. Secondly, an automated data-driven seizure detection algorithm was developed. However, the sensitivity of this fully automated detection algorithm are slightly too low to be directly applied in clinical practice. **Thijs Becker et al.[2][13] investigated the performance of the classifier in case that the EEG segments for which the classifier is the least confident are deferred to a human annotator.** Furthermore, he found that filtering out untrustworthy segments could improve the final performance. Since predictions of several short segments are combined to obtain a final prediction, the predictions of untrustworthy segments could be ignored while relying on the predictions of the neighboring segments.

[2] A collaboration within the Flanders AI Research Program.

Callaerts et al.[3][33] has investigated deep learning techniques using the behind-the-ear data of the SeizeIT1 database. Since the number of seizures in the SeizeIT1 data is rather small and deep learning algorithm are data hungry, he investigated the possible use of transfer learning. In transfer learning, a model is trained on a certain dataset to solve a particular problem. This trained network is adapted using another dataset to solve another problem, instead of training the network from scratch. Hereby, the assumption is made that the problems and the datasets are similar. The used model is VGG (Visual Geometry Group) [223], which is a top-performing model for image recognition and related computer vision tasks. One difficulty is that the VGG model was trained on RGB (Red, Green, Blue) images, whereas the SeizeIT1 dataset contains of behind-the-ear EEG signals. To solve this problem, those EEG time-series were converted into images. Different possible transformations were investigated from which the Short-Time Fourier Transform (STFT) performed the best. This approach outperformed the results of the SVM-based approach, explained in Chapter 7 on a testset of 8 patients.

Application to wearable data recorded with the Byteflies Sensor Dots

The SeizeIT1 dataset contains only EEG channels recorded with the hospital equipment. In the SeizeIT2 dataset, we go one step further and record also EEG data with a wearable device, the Byteflies Sensor Dot. A description of the dataset is provided in Chapter 4. One difference between the collected wearable SeizeIT2 data and the SeizeIT1 data is the number of channels. The Byteflies Sensor Dot (SeizeIT2) measures only two channels, whereas the SeizeIT1 dataset consisted of 3 behind-the-ear EEG channels. **The algorithm was adapted for the usage of an input of two channels, described in Appendix A.** A slightly decreased sensitivity and increased false alarm rate was observed in most cases.

In Appendix A, the seizure detection performances of the hospital behind-the-ear EEG channels were compared with the Byteflies Sensor Dot EEG channels using a patient-independent algorithm.

5.1.3 Personalization of seizure detection algorithms

In the field of EEG signal analysis, transfer learning is widely applied to transfer the knowledge learnt in one domain into a different but related domain [264]. The applications include personalization. Only a few examples were found in

[3]Jasper Callaerts was a master student guided by Amir Hossein Ansari and Kaat Vandecasteele, 2019-2020

the domain of epilepsy. Jiang et al. [117] used transfer learning to reduce the discrepancy in data distribution between the training data and test data consisting of different patients. Semi-supervised learning based on the Takagi-Sugeno-Kang (TSK) fuzzy system [233] was employed to use the unlabeled testing data to remedy the shortage of training data. Page et al. [183] utilizes max-pooling convolutional neural networks (MPCNN). The MPCNN was first trained using no patient-specific data. This general model was fine-tuned with patient-specific data. The last 1-2 fully connected layers' weights were adjusted.

5.1.4 Motion and muscle artifact removal

The filtering of the EEG signals in the seizure detection algorithm described in Chapter 7, is a bandpass filter (1-25 Hz). However, a bandpass filter does not filter out the motion and muscle artifacts effectively since those artifacts have components between 1 and 25 Hz. This reduces the performance of the algorithm and many of the false alarms contain artifacts. Blind Source Separation (BSS) techniques are successfully applied to remove the artifacts in multichannel EEG recordings. Independent Component Analysis (ICA) has been applied to decompose EEG signals into maximally independent components. The components containing artifactual sources can be removed and the scalp EEG can be reconstructed [141]. For removing muscle artifacts, Canonical Correlation Analysis (CCA) outperformed ICA [46, 262]. However those BSS techniques extract components from a set of recorded signals and the number of electrodes (channels) is typically larger than or equal to the number of sources. However, this assumption is no longer valid for recordings with 4 behind-the-ear electrodes, resulting in 3 independent channels. Source separation techniques using single-channel recordings were investigated by first decomposing the single channel EEG into different spectral modes using wavelet transform or empirical mode decomposition [163]. **These techniques were applied to the SeizeIT1 dataset in a simulation study and applied in the automated seizure detection algorithm, described in appendix B**. However, no improvements were observed compared to a bandpass filter.

5.2 Electrocardiography (ECG)

5.2.1 Seizure detection algorithms based on ECG

A good overview of the different state-of-the-art seizure detection algorithms using ECG can be found in Van Westrhenen et al. [252] and [47]. 21 studies

were included in this review paper. Most of the studies (n=15) focused on ictal cardiac changes, including HRV (n=10), HR (n=4) and changes in QRS morphology (n=1). The other six studies reported multimodal algorithms. De Cooman et al. [53] did a comparison between different state-of-the-art patient-independent seizure detection algorithms [244, 181, 250] on the same dataset.

Most of the published articles about cardiac changes in epilepsy use two wired ECG electrodes, recorded together with the EEG [277, 250, 53, 48, 140, 181, 27]. However a wearable solution is preferred. In [158, 244] wearable ECG devices are used for seizure detection. These studies focused on nocturnal epileptic seizures only, and in only a few patients, three and five respectively. **Chapter 6, published in [255], presents a study that compares the seizure detection performance of a wearable ECG device with the standard wired electrodes in a hospital setting during day and night.**

5.2.2 Personalization of seizure detection algorithms

Most ECG-based seizure detection systems from the literature are based on patient-independent models [53, 181, 244, 158]. For this type of models, no patient-specific data is required, making them directly usable in practice. However, due to large inter-patient differences in heart rate characteristics, performance is too low for practical use.

In order to increase the performance, models can be adapted to the patient heart rate characteristics [251, 50, 55]. Different options are possible. A first option is the manual setting of some parameter thresholds per patient [251, 28]. This requires manual screening of previous patient data, and it only works well if the parameters are easily understandable. Simple thresholding approaches are however too simple to grasp the large complexity of the problem. Automated personalization is therefore advised, but it normally requires a lot of patient-specific data in order to find a robust algorithm for a specific patient [43]. Often, only a limited amount of annotated patient-specific data is available, hence a lot of complex approaches are not useful for making fully patient-specific classifiers. Heuristic automated algorithms allow a low-complex and fast personalization, but might lead to suboptimal results [50, 55]. **De Cooman T. and Vandecasteele K. et al.[4][52] presented a patient-specific heart-based seizure detection model trained through transfer learning.**

[4] A collaboration within Biomed-Stadius leading to a joint publication.

5.2.3 Artifact detection and quality assessment of ECG

Similar to EEG, ECG signals can be contaminated with artifacts or noise. Noise can originate from a variety of sources, such as power line, muscle activity or electrode movement. Assessing the quality of the ECG signal is important. Satija et al. [211] present a review paper on signal processing techniques for ecg signal quality assessment. Heuristic rule based methods using ECG waveform morphological and heartbeat interval features were developed [180, 199, 200, 119, 235, 268, 245, 265, 100, 149, 99, 35, 118]. Various papers were published using those features with a Machine Learning classification [145, 204, 41, 173, 15, 14, 133, 165]. Other researchers developed methods using time-domain, frequency-domain, time-frequency domain, statistical, and information theoretic features and heuristic classification rules [273, 155, 157, 153, 176, 167, 39, 135, 2, 72, 267, 138, 178] or machine learning classification rules [240, 168, 215, 41, 272, 271]. Some of the quality assessment methods were based on filtering techniques [175, 148, 146, 58, 221, 112, 113, 203]. Algorithms based on Deep Learning are under development in this research area. Within the AI in Flanders research program, Seeuws et al. [217] is developing an unsupervised deep learning algorithm, a data-driven model without the need of expert labels. A model of clean data is constructed and based on error measures on input data and reconstructions, anomalies in the data can be quantified. Those anomalies represent the artifacted data in this case.

5.3 Photoplethysmography (PPG)

5.3.1 Seizure detection algorithms based on PPG

The first paper on seizure detection using PPG is presented in [246]. Only two seizures were analyzed in this study. **Chapter 6, published in [255], presents a study that compares the seizure detection performance of a wearable PPG device with a wearable ECG device in a hospital setting during day and night.** The seizure detection performance of the PPG device was considerably lower compared with the wearable ECG. This lower performance lower is due to motion artifacts. A recent study [68] analyzed PPG data using a wearable sensor placed on the wrist or ankle of children having FIASs. Multiple PPG features were extracted and were used to identify preictal, ictal, postictal changes or seizure-free periods. However, the PPG segments affected by motion artifacts were not included in the analysis and no classification step was performed.

5.3.2 Personalization of seizure detection algorithms

No publications are found on personalization of PPG-based seizure detection algorithms. However, all the ECG-based personalization techniques based on HRV and HR measures explained in Subsection 5.2.2 could also be applied to the HRV and HR extracted from PPG recordings.

5.3.3 Artifact detection and quality assessment of PPG

It is well known that motion and noise artifacts (MNA) can distort the signal of PPG signals [189]. Those MNA are caused by 1) the movement of venous blood as well as other non-pulsatile components 2) variations in the optical coupling between the sensor and the skin [11, 239]. The MNA can be particularly challenging when computing derived features from the PPG waveform such as HR. Various design approaches to reduce MNA have been proposed [143]. With these improvements, MNA are still present. Therefore, algorithm-based MNA reduction methods were proposed [241, 134, 81, 184, 241, 270, 202, 137, 237, 241, 124]. These MNA reduction algorithms operate also on clean parts of the signal, which is unnecessary computation and can cause distortion of the signal. Therefore an algorithm which can distinguish clean parts from MNA is desired. MNA detection algorithms are designed with the use of waveform morphologies [230, 144, 147, 73] or filtered output [172, 122]. Statistical measures, such as skewness, kurtosis, shannon entropy and Renyi's entropy have been shown useful for automatic detection of MNA [218, 128]. Another approach, using Hjorth parameters was proposed [89]. Other methods were published, which perform classification with a support vector machine (SVM) with time-domain features [38] or time-frequency spectrum analysis [44]. **Appendix D, published in [256], proposes an automated computer-based method for the detection of MNA in PPG signals, recorded with a wrist watch.** The method is validated on 24-hour data recordings. The classification is performed with a LS-SVM model using previously published features [218, 89, 38], together with new features. Additionally, most smart watches also record the accelerometry (ACM). Therefore, it is investigated whether the ACM improves the MNA detection method.

Current literature focuses on classifiers to distinguish these artifacts [230, 144, 147, 73, 172, 122, 218, 128, 89, 256]. This binary classification neglects the fact that the needed level of quality might depend on the study objective. Furthermore, it is useful to know how strongly contaminated a segment is.

Vanherck et al.[5] **[257] proposed a continuous quality indicator based on posterior probabilities of the classifiers.** This quality index was validated using two different approaches. In the first approach, motion artefacts are added to clean PPG signal segments in known SNR's. The signal quality indices of these contaminated segments are computed and compared to their SNR's. In the second approach, all test segments are divided into groups based on the difference between the mean detected PPG pulse interval and the mean R-peak interval. The signal quality index significantly decreases ($p<0.05$) with more contaminated signals in both cases.

5.4 Multimodal seizure detection

Leijten et al. [139] presented a review of multimodal seizure detection. In those studies, the main focus is on accelerometry and the detection of tonic-clonic seizures. Poh et al [193] and Regalia et al. [205] described systems that uses simultaneous data from accelerometry and electrodermal activity. Milosevic et al [164] presented an algorithm based on accelerometry combined with EMG. Van Andel et al [247] combined the modalities accelerometry and heart rate. De Cooman et al. [54] compared and combined accelerometry, EMG and heart rate. A few multimodal algorithms were developed as well for focal patients combining EEG with ECG [82, 197, 42], but the question whether the inclusion of ECG increases the performance of an EEG-based seizure detection remains unanswered. **In Chapter 8, the added value of ECG in comparison with behind-the-ear-EEG-based seizure detection was investigated.**

[5]Anke Vanherck was a master student guided by John Fredy Morales Tellez Kaat Vandecasteele, 2018-2019

Chapter 6

Seizure detection based on wearable ECG/PPG

The content of this chapter is taken from the publication Vandecasteele et al. [255].

6.1 Abstract

Electrocardiography has added value to automatically detect seizures in temporal lobe epilepsy (TLE) patients. The wired hospital system is not suited for a long-term seizure detection system at home. To address this need, the performance of two wearable devices, based on electrocardiography (ECG) and photoplethysmography (PPG), are compared with hospital ECG using an existing seizure detection algorithm. This algorithm classifies the seizures on the basis of heart rate features, extracted from the heart rate increase. The algorithm was applied to recordings of 11 patients in a hospital setting with 701 h capturing 47 (fronto-)temporal lobe seizures. The sensitivities of the hospital system, the wearable ECG device and the wearable PPG device were respectively 57%, 70% and 32%, with corresponding false alarms per hour of 1.92, 2.11 and 1.80. Whereas seizure detection performance using the wrist-worn PPG device was considerably lower, the performance using the wearable ECG is proven to be similar to that of the hospital ECG.

6.2 Introduction

Epilepsy is one of the most common neurological disorders, and it affects almost 1% of the population worldwide [79]. Anti-epileptic drugs provide only adequate treatment for about 70% of epilepsy patients [80]. After diagnosis in the hospital, one needs a follow-up of the disease and evaluation of the treatment. This follow-up requires a seizure logging system that is functional in a daily life environment outside the hospital, such as a seizure diary. A seizure diary, kept by patients or their families, is unfortunately not reliable [75].

To log seizures in an objective way, there is a need for an automatic seizure detection device, which records biomedical signals of the patient during daily life. On the basis of these signals, a computer-based algorithm using signal processing and machine learning can be used to automatically detect the seizures. With this information, an electronic diary can be generated. Ideally, the device will be worn continuously day and night, so it is important that the device is wearable and comfortable. Furthermore, it should be as concealable as possible to reduce stigmatization. However, it is important to have high data quality in order to have a reliable seizure detection. This trade-off between patients' comfort and data quality should be investigated for different wearable devices.

Nowadays, the golden standard for recording epileptic seizures in the hospital is based on video-electroencephalography (EEG). This type of EEG recording requires wet electrodes on the scalp, which is uncomfortable for the patient, and a trained nurse is needed to position them. Furthermore, the detection is based on manual human assessment. As a result, a trained EEG analyst is needed to analyze the EEG, which is time consuming. Therefore, EEG is currently not suitable for an automated wearable long-term seizure detection system at home [248].

Other biomedical signals used to detect epileptic seizures include accelerometry (ACC), electromyography (EMG), galvanic skin response and electrocardiography (ECG). The most suitable modality or combination of modalities depends on the type of the seizure. ACC and EMG modalities are of added value and therefore are often used for the detection of tonic, clonic, tonic–clonic and hypermotor seizures, because substantial muscle activity and/or motion is present [248].

Temporal lobe epilepsy (TLE) seizures do not often have a motor component worth mentioning. They do however affect the autonomic nervous system, in particular the cardiovascular system. It was previously shown that temporal lobe seizures are often accompanied with a strong ictal heart rate (HR) increase [111, 53, 277, 62].

Most of the published articles about cardiac changes in epilepsy use two wired ECG electrodes, recorded together with the EEG [277, 250, 53, 48, 140, 181, 27]. However a wearable solution is preferred. In [158, 244] wearable ECG devices are used for seizure detection. These studies focused on nocturnal epileptic seizures only, and in only a few patients, three and five respectively. To the best of our knowledge, this is the first study that compares the seizure detection performance of a wearable ECG device with the standard wired electrodes in a hospital setting during day and night.

ECG electrodes can be uncomfortable and can cause skin irritation after a few days. Another way to measure HR is by using the photoplethysmography (PPG) sensor in a smartwatch. PPG makes use of reflected light to measure changes in light absorption, caused by changes in the blood volume due to heart beats [6]. In [246], a PPG device is used, tested on two seizures only. To the best of our knowledge, no other publications exist for which the performance of a PPG device is evaluated on a multipatient dataset.

The aim of this study is to compare the performance of a wearable ECG and PPG device with the standard wired ECG. The testing was performed in a hospital setting in order to compare with the standard wired ECG and to obtain accurate seizure annotations on the basis of video-EEG. The seizure detection performances are evaluated on the same clinical database of TLE patients using an existing computer-based, automated algorithm. In a later study, the wearables, which are performing as accurately as the hospital ECG, will be tested in a real-world scenario.

6.3 Data Acquisition

The epilepsy patients were recorded with 10–20 scalp EEG with 1 bipolar ECG channel in the hospital. The two ECG electrodes were placed supraclavicularly left and right. Additionally to the standard clinical equipment, recordings were made with a wearable ECG device, the 180° eMotion Faros [23], and a wrist-worn PPG device, the Empatica E4 smartwatch [70]. The Faros device was used in a one-channel configuration. The positive electrode was placed on the left side of the torso, medial-supraclavicularly; the negative electrode was placed on the left side, laterally under the rib cage. The Empatica E4 measures reflective PPG using a green and a red light-emitting diode (LED) on the wrist. The device returns a single channel, which is obtained by combining the green and the red channels using Empatica's proprietary algorithm. The intravenous insertion, which is a needle inserted into a peripheral vein, used for administering fluids or medication, is mostly placed at the dominant wrist.

Table 6.1: An overview of the dataset RD = Recording Duration, SD = Seizure Duration

Patient	Seizures	RD (h)	Hemisphere	Origin	Age	Gender	Mean SD (s)	Range SD (s)
1	6	20	Left	Temp	28	M	28.7	[26 31]
2	3	72	Left	Temp	49	F	51	[24 68]
3	1	72	Bihemi	Temp	67	F	26	[26 26]
4	7	73	Right	Fronto-temp	24	F	47.5	[33 85]
5	8	95	Right	Temp	32	M	46	[25 61]
6	2	23	Left	Temp	19	F	83	[83 83]
7	1	43	Left	Temp	64	M	55	[55 55]
8	10	71	EEG not readable		49	M	17	[8 30]
9	2	91	Right	Temp	61	M	250	[34 466]
10	5	71	Left	Temp	45	M	63.8	[11 95]
11	2	70	Left	temp	32	F	43.5	[20 67]
Total	47	701						

As a result, the Empatica watch was worn on the other wrist. The respective sampling rates of the hospital ECG, Faros ECG and Empatica PPG signals were 250, 500 and 64 Hz. The data was managed using the Byteflies' cloud. This system allowed for the integration of the data from the wearable devices with the hospital's recording setup.

The dataset contains a part of the SeizeIT1 dataset, described in Chapter 4. All the patients with complex partial seizures, which were already recorded at the moment of this analysis were included. In total, 11 patients with 47 seizures were recorded during 701 h of data. All the seizures originated from the (fronto-)temporal lobe. However, the ictal EEG of patient 8 was unreadable due to muscle artifacts. Consequently, the type and origin could not be determined for that patient. The patients were recorded over 3, 4 or 5 days. Occasionally, due to practical or technical reasons, interruptions were present in the dataset; for example, when the patient needed to go to a scanner or when technical errors occurred. If one of the recordings was interrupted, the data of that specific time period was not analyzed. In this way, the three recording systems were evaluated exactly on the same data. A clinical expert annotated the seizure onsets and ends on the basis of the video-EEG data, without considering the ECG changes. Afterwards, the annotations were validated by a medical doctor. Table 6.1 gives a detailed overview of the seizure dataset. For every patient, the number of occurring seizures, the recording duration (RD), the hemisphere and origin of the epileptic focus, the age, the gender, and the mean and range of the seizure duration (SD) are given. During some seizures, the end of the seizure could not be determined, which was the case for patients 13, 17 and 23 for one seizure and for patient 6 in three seizures. The study was approved by the ethical commission of the University Hospital, Leuven. All patients gave informed consent for their participation in this study.

6.4 Methodology

The recorded datasets were analyzed using an automated algorithm implemented in Matlab. The algorithm consists of two steps: the heart/pulse rate variability (HRV/PRV) calculation and a seizure detection algorithm. The HRV quantifies the beat-to-beat variation in the HR, whereas the PRV quantifies the beat-to-beat variation in blood pulsation. Lastly, the evaluation criteria are explained.

6.4.1 HRV/PRV Extraction from ECG/PPG

ECG

In order to extract the HRV from the ECG, a method developed in [260] was used. In the first step, the ECG signal is segmented into epochs of 60 s. Thereafter, the power line interference at 50 Hz is removed by a notch-filter, and the mean of the signal is removed. An adapted Pan-Tompkins algorithm is used to find the R-peak locations. Instead of the classical filtering steps (bandpass, derivative, and integrator), the upper (U_{ecg}) and lower (L_{ecg}) ECG envelopes are calculated. A flattened version of the ECG is defined as $F_{ecg} = U_{ecg} - L_{ecg}$, which is used to find the possible locations of the R-peaks. The HRV is calculated from the differences between the locations of the R-peaks.

PPG

In order to extract the PRV from the PPG, a method developed in [136] was used. This algorithm consists of two phases: a linear filtering transformation and an adaptive thresholding operation. The filtering step consists of a linear-phase finite impulse response (FIR) low-pass-differentiator filter, which is used to accentuate the abrupt upslopes of the PPG pulses. The abrupt upslopes correspond to peaks in the filtered signal, which are detected by an adaptive thresholding operation. Once the peaks in the filtered signal are found, the maximum point in the original PPG signal is found. For the calculation of the PRV, the medium-amplitude point, defined as that in which the amplitude has reached 50% of its maximum, is calculated. This medium-amplitude point is shown to result in the most precise PRV. The PRV is calculated from the differences between the locations of the medium-amplitude points.

6.4.2 Seizure Detection Algorithm

In order to perform seizure detection, an algorithm developed in [53] was used. The algorithm uses the HRV or PRV as input. After filtering, the algorithm looks online for a HR increase. If this HR increase satisfies the preimposed rules [53], features are extracted and classification is performed. Three features are extracted for classification: HR_{peak}, $\overline{HR}_{base}$ and the $STDHR_{base}$. HR_{peak} is the peak HR at the end of the HR increase. $\overline{HR}_{base}$ is the average HR over the 60 s before the start of the HR increase. $STDHR_{base}$ is the standard deviation of the HR over the 60 s before the start of the HR increase. The classification is performed with a support vector machine (SVM) classifier with a Gaussian kernel. The SVM model was trained with an independent dataset consisting of 17 TLE patients previously recorded at UZ Gasthuisberg [53].

6.4.3 Evaluation Criteria

Four metrics were used to describe the seizure detection performance. The sensitivity (Se) and false positives per hour (FP/h) were calculated. Seizures were detected when an alarm was given between 30 s before and 90 s after the seizure onset. False alarms within 1 min of each other were counted as one alarm. Additionally, the positive predictive value (PPV) was calculated. Average measures over the entire dataset can be expressed as a patient-average performance (Pat.-av.) (the average of the performance of each patient) or an overall performance (Tot.-av.) (computed on the total number of seizures or recording duration). The latter was used, unless specifically mentioned. Lastly, the sensitivity and false alarm rate were calculated for different thresholds, similarly to a receiver operating characteristic (ROC) curve. In this context, it is more meaningful to plot sensitivity against FA/h instead of the classical true positive rate against the false positive rate. It is informative to know how the sensitivity is affected by the seizure duration. Therefore the seizure sensitivity is calculated as a function of the seizure duration, which is calculated using the start and end of the EEG seizure pattern, annotated by a medical doctor.

6.4.4 Evaluation of Sensitivity and False Alarms

In order to compare the different modalities in detail, the underlying cause of missed seizures and false alarms should be investigated. The reasons for the missed seizures and false alarms may be physiological or related to the data quality of the recording system. A first possible physiological reason is that no HR changes are observed during the seizure. Second, the HR increase may be

too small (lower than 20 beats per minute) to be detected by the algorithm. Third, a HR decrease may be observed during a seizure. Quality-related reasons in this dataset were motion artifacts and interference. A physiological reason for false alarms is the occurrence of a HR increase during a non-ictal period, for example, during light physical exercise. Similarly to the missed seizures, a quality-related reason is the presence of motion artifacts. Furthermore, it is interesting to know if these false alarms of the different modalities occur at the same time. For every patient, the percentage of coincidences of the FPs were calculated for the different modalities.

6.5 Results

Table 6.2 gives an overview of the results. The highest sensitivity (70%) was obtained with the wearable ECG, whereas the sensitivity of the hospital ECG was 57%. With the wearable PPG, a sensitivity of only 32% was obtained. The FP/h values are comparable for the three recording systems: 1.92, 2.11 and 1.80 for the hospital ECG, the wearable ECG and the wearable PPG, respectively. In Figure 6.1, the sensitivity and false alarm rate for different thresholds of the SVM classifier are plotted. This curve shows that for the same FP/h value, the wearable ECG achieved a higher sensitivity than the hospital ECG, whereas the wearable PPG had a lower sensitivity. Additionally, sensitivity was calculated for seizures of different durations, namely, 0–20, 20–40, 40–60, and >60 s. In Figure 6.2 the sensitivity is plotted for the hospital ECG, the wearable ECG and the wearable PPG for the different seizure durations. The seizures with an unknown seizure duration were neglected by this analysis. Unfortunately, the number of seizures in each of the seizure length categories (9, 9, 3 and 10) were too small to draw conclusions.

6.5.1 Sensitivity

The number of missed seizures for the hospital ECG, the wearable ECG and the wearable PPG were 20, 14 and 32, respectively. In Figure 6.3, the number of and reason for missed seizures are shown for the three different recording systems.

6.5.2 False Alarms

The obtained false alarm rates were in accordance with previously published results [53]. The average (± standard deviation) FP coinciding from the wearable

Table 6.2: Seizure performance: the sensitivities (Se), false positives per hour (FP/h) and positive predictive value (PPV) are shown with the patient average (Pat.-av.) and total average (Tot.-av.).

Patient	Hospital ECG			Wearable ECG			Wearable PPG		
	Se (%)	FP/h	PPV (%)	Se (%)	FP/h	PPV (%)	Se (%)	FP/h	PPV (%)
1	33	3.98	2.50	33	3.98	2.44	33	1.77	5.26
2	0	1.55	0.00	33	2.06	0.67	33	1.49	0.92
3	100	1.55	0.89	100	2.09	0.65	0	2.27	0.00
4	71	2.27	2.94	100	2.89	3.23	43	1.91	2.11
5	88	2.30	3.10	88	1.96	3.61	38	1.55	1.99
6	50	2.91	1.02	50	4.24	0.99	100	2.41	3.39
7	100	0.45	5.00	100	1.03	2.22	0	1.64	0.00
8	50	3.44	2.02	90	2.64	4.62	20	2.53	1.09
9	0	0.40	0.00	0	0.62	0.00	0	1.08	0.00
10	80	1.03	6.56	75	1.53	3.54	0	2.06	0.00
11	50	2.73	0.34	50	2.78	0.36	100	1.94	1.04
Pat.-av.	57	2.05	2.22	64	2.35	2.03	33	1.88	1.43
Tot.-av.	57	1.92	1.93	70	2.11	2.15	32	1.80	1.12

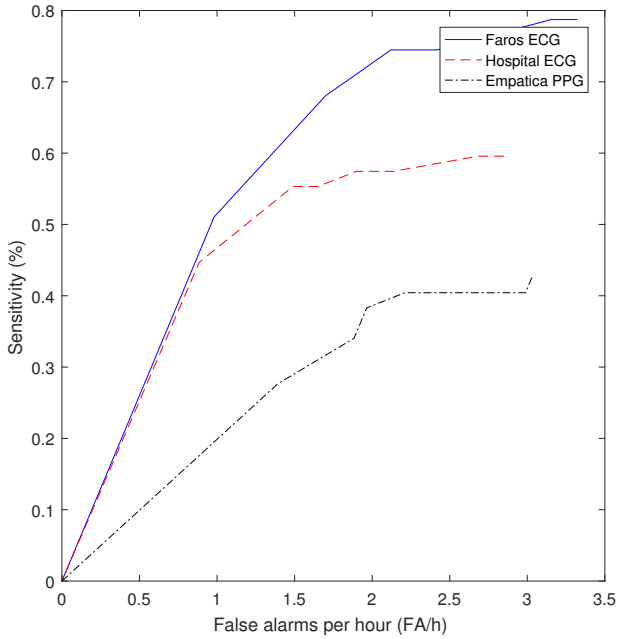


Figure 6.1: The sensitivity and false alarm rate for different thresholds of the support vector machine (SVM) classifier.

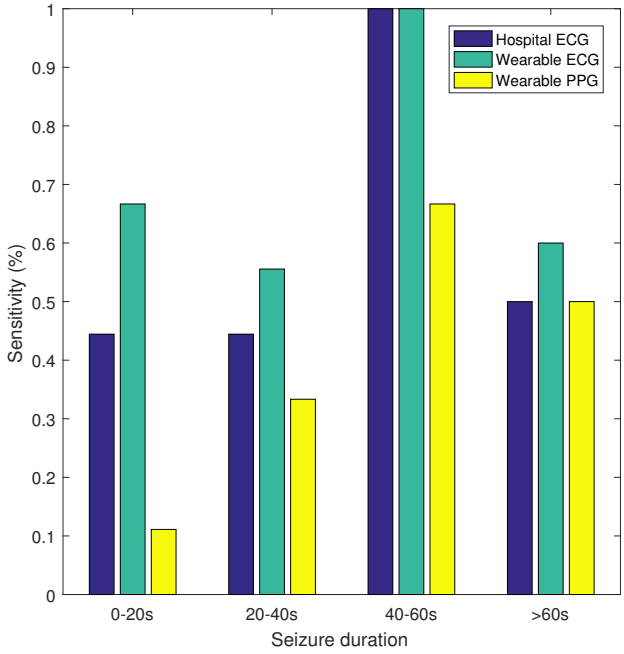


Figure 6.2: Sensitivity versus seizure duration.

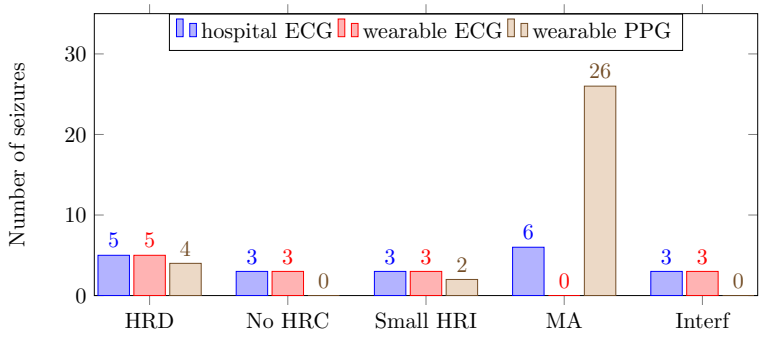


Figure 6.3: Number of and reason for missed seizures (HRD: heart rate decrease; No HRC: no heart rate change; Small HRI: small heart rate increase: MA: notion artifacts; Interf: interference).

ECG and wearable PPG with respect to the hospital ECG were respectively $63\% \pm 20\%$ and $35\% \pm 16\%$. The FP coincidence of the wearable ECG with respect to wearable PPG was $36\% \pm 14\%$.

6.6 Discussion

In order to have a good seizure detection performance, the sensitivity should be as high as possible, whereas the false alarm rate should be as low as possible. A statistical evaluation of the seizure detection performance is very important [170, 213]. It has been proven previously [53] that the applied seizure detection algorithm performs better than chance. Here, using wearable ECG, we obtained a comparable seizure detection performance to that of [53]. Below, we discuss in detail the reasons for missed seizures and false alarms.

6.6.1 Sensitivity

In the dataset, 11 seizures could not be detected because of physiological reasons: HR decrease (5), no HR changes (3) and a small HR increase (3). Logically, these seizures appeared as missed seizures, with the exception of PPG signals, for which five of the seizures were detected because of motion artifacts. In other words, in this dataset, 77% of the seizures were accompanied with a HR increase. In previous research, 88% and 92% of the temporal lobe seizures were accompanied with a HR increase [140, 62]. Furthermore, the same seizure detection algorithm obtained a sensitivity of 82% for another dataset of temporal lobe seizures [53]. Adding HR-based information is only suitable for patients who have a change in cardiac activity during a seizure. For this dataset, patients 1, 2 and 9 did not show a strong HR increase. In order to increase sensitivity, a prescreening is useful to determine if ECG is a suitable modality for the patient.

Both for the hospital ECG and the wearable ECG, three missed seizures were due to the presence of interference, which was around 12 Hz. This interference was difficult to remove because the R-peaks of the ECG signals contained that particular frequency. Fortunately, this was only present during one day of recording, for patients 8 and 10. In the rest of the dataset, this was not observed. It is likely that there was an electronic device present close to the ECG equipment. Because the PPG does not pick up an electrical signal, no interferences were observed in the PPG.

The number of missed seizures, as a result of motion artifacts, differred greatly for the three recording systems. For the hospital ECG, the wearable ECG and the

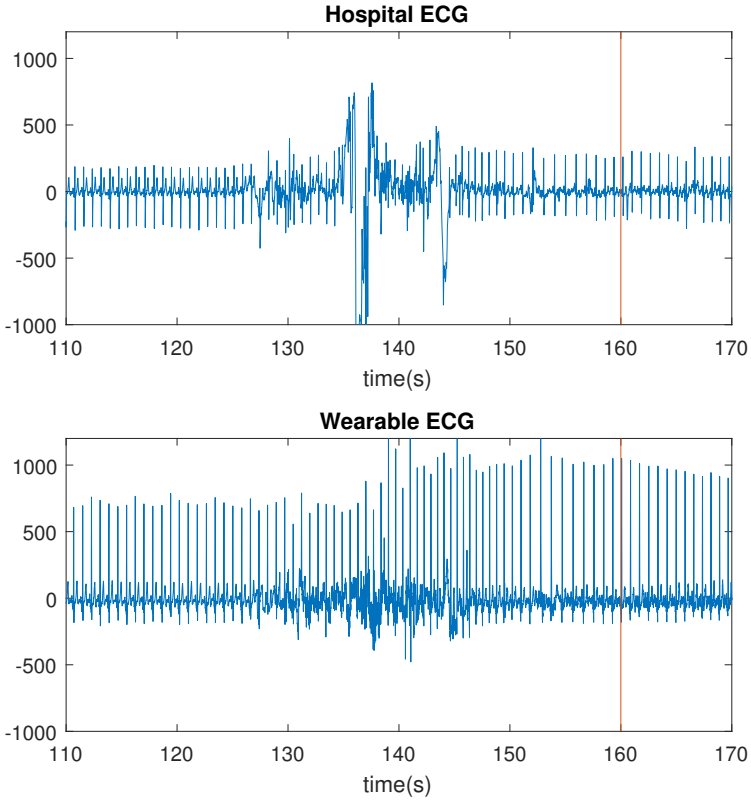


Figure 6.4: Comparison of motion artifacts: hospital electrocardiography (ECG) and wearable ECG (red line indicates annotated seizure start).

wearable PPG, the numbers were respectively 6, 0 and 26. The wearable ECG performed better than the hospital ECG because of the lack of wires. Motion affects the wires of the hospital ECG, thereby including small displacements of the electrodes, resulting in motion artifacts in the signals. In Figure 6.4, the HR increase, corresponding to a seizure of patient 2, is shown. For this seizure, the HR increase occurred before the seizure onset. Both ECG signals were bandpass filtered between 1 and 40 Hz with a butterworth filter.

The PPG signal was drastically affected by the motion artifacts; 55% of the seizures could not be detected because of motion artifacts, which is unacceptably high. These motion artifacts are caused by (1) the movement of venous blood as well as other non-pulsatile components, and (2) variations in the optical coupling between the sensor and the skin [11, 239]. As a result of these motion

artifacts, no reliable HR could be extracted by the algorithm. Furthermore, by visually inspecting the power spectra, the HR frequency was often no longer present in the signal.

The PPG wristband is mostly worn on the dominant hand, because the intravenous insertion is typically performed on the non-dominant hand. The dominant hand is expected to move even more compared to the non-dominant hand; therefore, in the home environment, placing the watch on the non-dominant hand may bring about some improvement. Alternatively, the smartwatch can be placed on the upper arm [246]. Further research is needed to investigate positions with which to measure the PPG.

6.6.2 False Alarms

The coincidences of FPs for the hospital and wearable ECG were substantially greater than for the wearable PPG. It is expected that the FPs with physiological causes will coincide. In contrast, the FPs due to quality are specific for each recording system. Therefore we speculate that the FPs of the wearable PPG are more often due to motion artifacts.

6.6.3 Limitations and Further Work

In this work, the quality of a wearable ECG and PPG device are compared against the hospital ECG. The comparison was performed by running the same seizure detection algorithm on different datasets. However, one can also compare the quality of the signals or the extracted HR, which is more direct. By doing so, one ignores the fact that the algorithm can cope with certain artifacts and wrong HR estimates. Yet, we chose this approach as we are also interested in how the seizure performance is affected by such artifacts.

Another limitation is that the seizure classifier is trained with the HR extracted from an ECG signal and not from a PPG signal. This might cause some bias, because the nature of artifacts is different and will have a different influence on the seizure classifier performance.

The recordings were taken in a hospital environment, where the patient was limited in their natural daily behaviour because of the wired hospital recording system. In a daily life or home environment, there may be even more artifacts present.

Noise removal algorithms should be tested on the PPG data to reconstruct the HRV information [210].

In this work, only data of (fronto-)TLE patients is analyzed. The seizure performance of other patient groups is not evaluated.

The false alarms rate per hour for the three detection systems were around 2 FP/h (Table 6.2), which is comparable with those in the literature [53]. A comparison between different state-of-the art HR-based independent detection algorithms is included in [53]. These algorithms have on average two false alarms per hour, which is not acceptable for practical use. In order to reduce false alarms, a patient-dependent or adaptive algorithm should be considered. An algorithm with tunable parameters and thresholds is provided in [244, 158]. In this case, medical data should be available for that patient. In [51], an online algorithm is developed, which starts from a patient-independent algorithm and adapts to the characteristics of the seizures of that specific patient. For this, no data of the patient is needed beforehand. Another way to reduce false alarms is the combination of multiple signals. Depending on the seizure characteristics, other biomedical signals can be integrated [248]. However the aim of this paper is to compare the performance of an ECG and a PPG wearable device with the ECG hospital system, not to outperform the state-of-the-art seizure detection systems.

6.7 Conclusions

The performances of two wearable devices (ECG and PPG) are compared with the hospital ECG using an existing automated algorithm based on cardiac activity. The algorithm was tested on a dataset of 11 patients in a hospital setting over 701 h and 47 (fronto-)temporal lobe seizures. Whereas seizure detection performance using the wrist-worn PPG device was considerably lower, the performance using the wearable ECG is proven to be similar to that of the hospital ECG. This suggests that the wearable ECG has potential to be used for long-term monitoring. Future work will further evaluate the signal quality and seizure detection performance in daily life outside the hospital.

Chapter 7

Seizure detection based on behind-the-ear EEG

The content of this chapter is taken from the publication Vandecasteele et al. [254].

7.1 Abstract

7.1.1 Objective

Seizure diaries kept by patients are unreliable. Automated electroencephalography (EEG)-based seizure detection systems are a useful support tool to objectively detect and register seizures during long-term video-EEG recording. However, this standard full scalp-EEG recording setup is of limited use outside the hospital, and a discreet, wearable device is needed for capturing seizures in the home setting. We are developing a wearable device that records EEG with behind-the-ear electrodes. In this study, we determined whether the recognition of ictal patterns using only behind-the-ear EEG channels is possible. Second, an automated seizure detection algorithm was developed using only those behind-the-ear EEG channels.

7.1.2 Methods

Fifty-four patients with a total of 182 seizures, mostly temporal lobe epilepsy (TLE), and 5284 hours of data, were recorded with a standard video-EEG at University Hospital Leuven. In addition, extra behind-the-ear EEG channels were recorded. First, a neurologist was asked to annotate behind-the-ear EEG segments containing selected seizure and nonseizure fragments. Second, a data-driven algorithm was developed using only behind-the-ear EEG. This algorithm was trained using data from other patients (patient-independent model) or from the same patient (patient-specific model).

7.1.3 Results

The visual recognition study resulted in 65.7% sensitivity and 94.4% specificity. By using those seizure annotations, the automated algorithm obtained 64.1% sensitivity and 2.8 false-positive detections (FPs)/24 hours with the patient-independent model. The patient-specific model achieved 69.1% sensitivity and 0.49 FPs/24 hours.

7.1.4 Significance

Visual recognition of ictal EEG patterns using only behind-the-ear EEG is possible in a significant number of patients with TLE. A patient-specific seizure detection algorithm using only behind-the-ear EEG was able to detect more seizures automatically than what patients typically report, with 0.49 FPs/24 hours. We conclude that a large number of refractory TLE patients can benefit from using this device.

7.2 Introduction

Epilepsy is one of the most common neurological disorders, affecting almost 1% of the population worldwide [79]. Anti-epileptic drugs provide adequate treatment for about 70% of patients with epilepsy [80]. The remaining 30% of patients continue to have seizures, drastically reducing their life quality. To obtain efficacy measures of therapeutic interventions for these patients, objective measures of seizure documentation and counting are needed [69]. However, in an outpatient setting, the unreliability of seizure documentation and counting by patients is a major problem [25, 75, 103, 195, 236]. Adult patients with focal

epilepsy undergoing video-electroencephalographic (EEG) monitoring failed to document around 55% of all recorded seizures and 73% of focal impaired awareness seizures [103].

Automated seizure detection systems could help to objectively quantify seizures. Those detection systems are typically based on full scalp EEG. In an outpatient setting, full scalp EEG is of limited use because patients will not tolerate wearing a full EEG cap for long time periods during everyday life [12].

First, research is needed on the recognition of epileptic seizure activity on limited channels, which can be recorded unobtrusively in a nonstigmatizing way. To prove the usefulness of limited channels for seizure detection, an ictal pattern should be visually present on the reduced channel configuration. Previously, the usefulness of single-channel scalp EEG placed behind the earlobe for seizure identification has been investigated [21]. The sensitivity and specificity for recognition of seizures was 86% and 95% for Reviewer 1, 79% and 99% for Reviewer 2. However, only 21 seizures and single-channel derivations were investigated.

Second, algorithms to detect seizures automatically need to be developed using only that limited amount of EEG channels. Previously, reduced electrode montages have been shown useful for seizure detection and documentation for several epilepsy types [82, 227, 125, 96]. Our proof-of-concept study showed that behind-the-ear EEG is useful for focal seizure detection [96]. However, the algorithm had false detection rates too high for clinical use.

In this paper, behind-the-ear EEG channels were used that can be recorded with a wearable device [26]. First, a visual analysis was done on 182 seizures by a neurologist to investigate the presence of ictal patterns on the behind-the-ear channels. Second, an algorithm was developed suitable for constructing a seizure diary offline due to the lower false alarm rate compared to the literature [96]. Two different models were evaluated. The first model was a patient-independent (PI) model, trained with data from different patients. For this PI model, no patient-specific data were needed to train the model, practical in daily life. However, this type of algorithm results in lower performance [12]. The second model was a patient-specific (PS) model, trained with data from the same patient.

This is a class 1 study according to the standards for testing seizure detection devices [20], because real seizure data from patients with epilepsy were included and gold standard annotations were used for validation. However, the analysis was done retrospectively and the data were not recorded with the dedicated device, but with extra electrodes using traditional scalp EEG.

7.3 Data Acquisition

The SeizeIT1 dataset was used in this study, described in Chapter 4.

7.4 Methodology

7.4.1 Visual seizure recognition

Behind-the-ear EEG segments containing seizures and nonseizures were shown to the neurologist-epileptologist (W.V.P.), who was blinded to patient information and recording time. The neurologist was asked to annotate all the segments.

Each 10-minute-long seizure segment contained one seizure with the onset in the middle of the segment. Each 10-minute-long nonseizure EEG segment contained a false detection, obtained with the algorithm described below, in the middle of the segment. The information regarding this onset timing was explained to the neurologist. The duration of 10 minutes was chosen to provide enough preictal and postictal EEG data. The number of nonseizure EEG segments per patient varied randomly between 0.5 and 1.5 times the number of seizure segments. The segments were shown to the neurologist clustered per patient. In total, 182 seizure and 172 nonseizure segments were annotated.

The segments were shown using MATLAB 2017a with EEGLAB graphic interface [59]. The data were shown in a scroll plot using a window of 10 seconds. The plotted data were filtered with a bandpass filter (1-25 Hz), which could be changed. Additionally, the data filtered with a 1 Hz high-pass filter and 50 Hz notch filter were shown. The data were visualized by default between - 200 and 200 μV, but this scale was adaptable.

To evaluate the performance, sensitivity and specificity were defined as the percentage of recognized and nonrecognized seizure and nonseizure segments, respectively. To summarize the performance measures across the dataset, average values with 95% confidence interval and median with range were calculated.

7.4.2 Autmodated seizure detection

The automated seizure detection algorithm was applied twice with two different aims. The aim of algorithm I was to detect all annotated seizures with ictal EEG correlate using video-EEG (full EEG). All those seizures were included in the training and test set. The aim of algorithm II was to detect only those

seizures that were recognized on the behind-the-ear EEG by the neurologist. Here, only those recognized seizures were included in the training and test set. The PI model was applied on all patients. However, the PS model could only be applied on patients with at least two seizures, because one seizure was needed to train the model and one seizure to test the model.

The different steps of the algorithm are explained: preprocessing, feature extraction, feature normalization, classification, cross-validation, and postprocessing with the algorithm evaluation criteria.

Preprocessing

As input, three bipolar behind-the-ear EEG channels were used: crosshead channel 2, and the unilateral left and right channels. Each bipolar channel was filtered with a bandpass filter (1-25 Hz). After filtering, the data were segmented in 2-second windows with 50% overlap. Windows with a root mean square amplitude greater than 150 µV or less than 13 µV were removed from the analysis, because those windows contained high-amplitude artifacts or contained only background EEG.

Feature extraction

Features, taken from literature, were extracted from each channel and each window, unless removed by the preprocessing. Time domain and frequency domain features were extracted [106]. Two extra frequency domain features were extracted, mean and normalized power in the high-frequency band between 40 and 80 Hz (before applying the bandpass filter) to discriminate between artifacts and seizure activity. Entropy-based features were also added [94, 226]. Finally, the power asymmetry at different frequency bands was calculated [105]. Here, the power asymmetry was calculated between the left and right channel. A list of all the features can be found in Table 7.1. Features 1-21 were calculated for all three channels, whereas features 22-25 resulted in one feature for each frequency band. This resulted in a total of 67 features.

Feature normalization

Because differences in the EEG amplitude were present between individuals, and amplitude variations occurred over time, normalization was crucial. The median decaying memory method was shown to be the best approach using line length features [150]. This normalization method was applied on all the

Table 7.1: Extracted features [HF, high-frequency]

Time domain	1-3. Number of zero crossings, maxima and minima [106] 4. Skewness [106] 5. Kurtosis [106] 6. Root mean square amplitude [106]
Frequency domain	7. Total power [106] 8. Peak frequency [106] 9-16. Mean (9-12) and normalized (13-16) power in frequency bands: delta (1-3 Hz), theta (4 - 8 Hz), alpha (9-13 Hz), beta (14 - 20 Hz) [106] 17-18. Mean (17) and normalized (18) power in HF band [40-80 Hz]
Entropy derived	19. Sample Entropy [226] 20. Shannon Entropy [94] 21. Spectral Entropy [94]
Asymmetry	22-25. The power asymmetry in frequency bands: delta (1-3 Hz), theta (4 - 8 Hz), alpha (9-13 Hz), beta (14 - 20 Hz) [105]

amplitude-dependent features, which were the root mean square amplitude, total power, and mean power in the different frequency bands (features 6, 7, 9-12, and 17 in Table 7.1). Additionally, log transformation was applied on features 5-7, 9-12, 14, 15, 17, 18, and 20, selected visually by comparing the distribution before and after log transformation. Features 1-21 were calculated for all three channels. For each feature, the left and right channel values were sorted largest to smallest [95], which removed information about the spatial seizure location. This step is important because both left and right seizures were present in the training and test sets.

Classification

To classify each 2-second window, support vector machine (SVM) with a radial basis function kernel was used. To account for the class imbalance from the dataset (ie, very few training examples in the seizure vs the nonseizure class), Weighted SVM [5, 53] was applied. To find the optimal classifier, the SVM minimizes the misclassification of training data points. To account for class imbalance, the cost given to each nonseizure data point is $(N^+ + N^-)/2 * N^2$, whereas the cost given to each seizure data point is $(N^+ + N^-)/2 * N^-$

with N^+ and N^- representing the number of data points belonging to the nonseizure and seizure class, respectively. The values of the hyperparameters were selected using a fivefold cross-validation using the training set for the PI model. The most frequently selected values for those parameters were used for the PS model, because not enough data were available to perform a cross-validation on the training set.

Nonseizure training data were selected from the first 24-hour EEG recording, as this period covers the different brain states [198]. To cover as many different EEG patterns as possible from the nonseizure vigilance states, 1-minute long segments, consisting of 30 nonoverlapping 2-second windows, recorded every 15 minutes, were selected [59]. From this selection, 100 and 150 nonseizure windows were randomly sampled per patient for training the PI and PS classifiers.

Seizure training segments of 10 seconds [96, 106], further split into 2-second windows, during each seizure were selected visually at the seizure onset by the first author. A length of 10 seconds was chosen to give each seizure, short or long, the same importance in the classifier, as the minimum seizure duration was 10 seconds. Visual selection by the first author was needed to include a typical ictal pattern in the training set and to avoid attenuation at the start of the seizure or artifacts.

Cross-validation

Only a single retrospective dataset was available for the study. However, different nonoverlapping folds of the dataset were used for training and testing purposes. The cross-validation for the PI model was leave-one-patient-out. The cross-validation for the PS model was leave-one-seizure-out. The fold splits were set exactly in the middle of the nonseizure data between two seizures. The test set, the fold left out for training, was a continuous tract that contained all the nonseizure/seizure data in that fold, that is, various vigilance states and the direct neighborhood of a seizure.

Postprocessing

To generate a seizure detection, eight of 10 consecutive 2-second overlapping windows should be classified as seizure by the model. Ten consecutive windows were chosen, because the minimal duration of a seizure was taken as 10 seconds. To allow for small artifacts during a seizure, only eight of the windows should be classified as seizure.

Algorithm evaluation

The following measures were applied to determine the performance of the seizure detection algorithm:

1. Detection sensitivity: TP/(TP + FN), where TP = true positive and FN = false negative. A seizure was detected correctly (TP) if the detection occurred between the EEG onset and end of the seizure.
2. False positive (FP) detection rate per 24 hours: FPs/recording length; FPs within 10 seconds of each other were counted as one FP.
3. Detection delay: the time interval between the EEG seizure onset and detection by the algorithm.
4. Positive predictive value (PPV): TP/(TP + FP).
5. F1-score: 2 * (PPV * Recall)/(PPV + Recall) with Recall = TP/(TP + FN).

To summarize the performance measures across the dataset, the averages including their 95% confidence intervals and medians with their range were calculated.

7.5 Results

7.5.1 Visual seizure recognition

The neurologist identified 114 of 182 seizure segments and 161 of 172 nonseizure segments in total. An average sensitivity of 65.7% and specificity of 94.4% was obtained, as shown in Table 7.2. In Table S2, the results per patient are shown.

Table 7.2: Results of visual seizure recognition (Sens and Spec) and automated seizure detection I with aim of detecting all seizures annotated on video-EEG and automated seizure detection II with aim of detecting only seizures recognized by the neurologist on behind-the-ear EEG for PS and PI models (number of patients and seizures, Sens, false detection rate, PPV, detection delay, and F1-score) [EEG, electroencephalography; FP, false positive; PI, patient-independent model; PPV, positive predictive value; PS, patient-specific model; Sens, sensitivity; Spec, specificity]

A. Average [95% confidence interval]

Visual seizure recognition

	Patients, n (seizures, n)	Sens [%]	Spec [%]			
	42 (182)	65.7 [54-77]	94 [89-99.9]			
Automated seizure detection I						
	Patients, n (seizures, n)	Sens [%]	FPs/24h [%]	PPV [%]	Delay [s]	F1-score
PI	54 (182)	72.7 [61-84]	34.2 [17-51]	11.5 [6-17]	22.4 [17-28]	0.16 [0.09-0.23]
PS	36 (176)	63.4 [51-76]	0.88 [0.4-1.4]	57.3 [43-71]	21.6 [18-26]	0.57 [0.45-0.70]
Automated seizure detection II						
	Patients, n (seizures, n)	Sens [%]	FPs/24h [%]	PPV [%]	Delay [s]	F1-score
PI	54 (114)	64.1 [50-79]	2.8 [1.3-4.3]	38.9 [25-52]	22.8 [18-28]	0.38 [0.26-0.50]
PS	24 (103)	69.1 [54-84]	0.49 [0.1-0.9]	65.4 [49-81]	20.2 [15-26]	0.62 [0.46-0.78]

B. Median [range]

Visual seizure recognition

	Patients, n (seizures, n)	Sens [%]	Spec [%]			
	42 (182)	70.8 [0-100]	100 [0-100]			
Automated seizure detection I						
	Patients, n (seizures, n)	Sens [%]	FPs/24h [%]	PPV [%]	Delay [s]	F1-score
PI	54 (182)	100 [0-100]	13.6 [0-384]	3.4 [0-100]	17 [3-77]	0.07 [0-1]
PS	36 (176)	67.4 [0-100]	0 [0- 4.2]	63 [0-100]	18 [10-56]	0.64 [0-1]
Automated seizure detection II						
	Patients, n (seizures, n)	Sens [%]	FPs/24h [%]	PPV [%]	Delay [s]	F1-score
PI	54 (114)	100 [0-100]	1.2 [0-31.5]	23 [0-100]	20 [3-56]	0.29 [0-1]
PS	24 (103)	83.3 [0-100]	0 [0-3.7]	72 [0-100]	16 [9-65]	0.72 [0-1]

Figure 7.1 shows the sensitivities for the different seizure types (A), localization (B), lateralization (C), and seizure duration (D). The sensitivities were calculated as percentage recognized seizures in that category over the whole database. Sensitivity for focal impaired awareness seizures was 59%, for focal aware (FA) seizures 89%, and for focal to bilateral tonic-clonic seizures 100%. The temporal, frontotemporal, and occipitotemporal lobe seizures had a sensitivity of 62%, 85%, and 22%, respectively. The frontoparietal and parietal seizures had 0% and 67% sensitivity. The bilateral group had lower sensitivities (43%) than the lateralized groups, left 58% and right 70%, respectively. The sensitivity increased with the seizure duration.

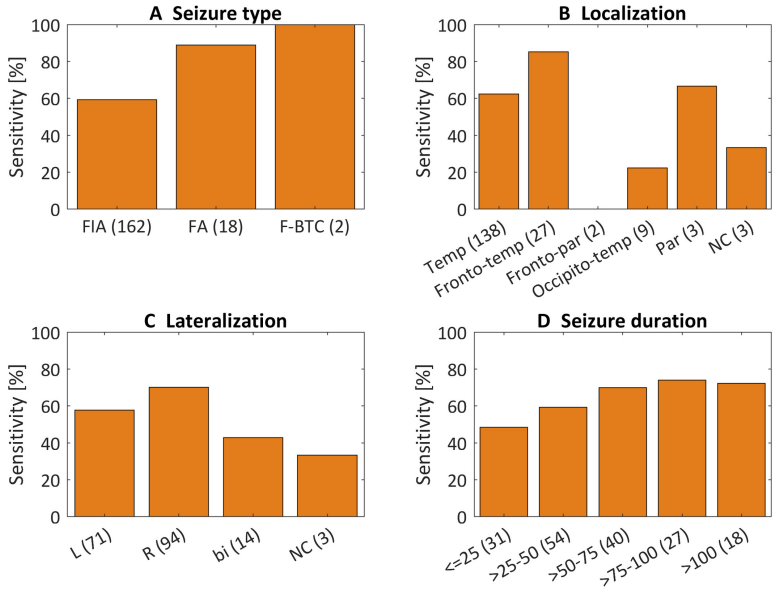


Figure 7.1: Sensitivities for the different seizure types (A), localizations (B), lateralizations (C) and seizure durations in seconds (D) are plotted for the patient-independent model with aim I and visual recognition study. The sensitivities were calculated as percentage recognized seizures in that category over whole the database. bi, bilateral; FA, focal aware; F-BTC, focal to bilateral tonic-clonic; FIA, focal impaired awareness; L, left; NC, not clear; par, parietal; R, right; temp, temporal

7.5.2 Automated seizure detection

An overview of the results of the PI and PS model with the two different aims, detecting all the seizures and detecting the seizures recognized on behind-the-ear EEG, are shown in Table 7.2. In Table S2, the results per patient are shown. The PI model resulted in an average sensitivity of 72.7% (aim I) and 64.1% (aim II), whereas the FP rate decreased from 34.2 FPs/24 hours (aim I) to 2.8 FPs/24 hours (aim II). The PS model resulted in a higher average sensitivity of 69.1% (aim II) compared to 63.4% (aim I), whereas the FPs/24 hours rate was 0.88 (aim I) and 0.49 (aim II). By analyzing the 24 patients tested with the PS model (aim II), the number of patients with a sensitivity $\geq 60\%$ and FPs/24 hours ≤ 1 was nine with the PI model and 15 with the PS model.

The PI model with aim II detected 14 extra seizures, from six patients, which the neurologist did not recognize. The PS model with aim II detected 4 extra

seizures, from four patients, which were not annotated on the full scalp EEG, but recognized with hindsight. Note that these seizures were not taken into account for calculating the sensitivity of aim II.

7.6 Discussion

7.6.1 Visual seizure recognition

Average sensitivity for visual recognition of seizures on behind-the-ear EEG was 65.7% (ie, 68 of 182 seizures were not recognized), which was lower than expected, because the database mostly consisted of temporal lobe seizures and the behind-the-ear electrodes were closely located to the temporal lobe. To explain these results, the neurologist inspected the behind-the-ear EEG again, together with the full EEG, and identified three main reasons for missed seizures in the behind-the-ear EEG. Most importantly, 63 seizures (93%) that were not recognized on behind-the-ear EEG contained artifacts, mainly muscle. In 11 seizures, a salt bridge was present in a channel that was crucial for seizure recognition. This salt bridge, which is the smearing of electrode paste between electrodes causing a very low impedance (short circuit), was recognized due to a lower frequency and amplitude content of one bipolar channel compared to the background [229]. Full scalp EEG of the same seizures contained the same artifacts at the location of the behind-the-ear electrodes, but the ictal patterns were visible in other channels. Second, 39 seizures (57%) had only subtle ictal EEG patterns on the full EEG. Those seizures were annotated taking the presence of a clinical seizure on video into account. This information was not available when reviewing behind-the-ear EEG blindly. Third, 29 seizures (43%) had a bilateral ictal pattern from the onset, which was more difficult to pick up with the crosshead channels, where the ictal discharges were less obvious due to differential amplification of the relatively symmetric signals. Typical lateralized recruiting theta patterns, as in Figure 4.2, were easily recognized. We conclude that a majority of temporal lobe seizures are recognized on behind-the-ear EEG, but the impact of artifacts in the recognition of seizures is higher when only a limited number of electrodes and channels are available as compared with a full EEG.

The neurologist annotated 11 of the 172 nonseizure segments as a seizure. With hindsight, four segments did contain a seizure on the full EEG and were actually correctly annotated on the behind-the-ear EEG. Those seizures were missed during the first annotation session of the video-EEG. Four segments contained artifacts, which the neurologist annotated as a seizure, which could have been avoided by looking at the unfiltered EEG. One segment did not seem

to contain an ictal pattern on second examination. Two segments contained the appearance of an occipital alpha rhythm, which was clear on the full EEG, but was interpreted as an ictal pattern on the behind-the-ear EEG. We conclude that with a conservative reading of behind-the-ear EEG, specificity is very high (around 96%).

The higher sensitivity for visual recognition on behind-the-ear EEG of FA seizures (89%) compared to the focal impaired awareness seizures (59%) was not expected, because only 15%-30% of FA seizures contain ictal EEG changes [61]. However, we included in this study only seizures with an ictal EEG correlate. Furthermore, the dataset contained 28 FA seizures in four different patients, who had respectively one (not detected), 14 (all detected), two (all detected), and one (not detected) seizures. By averaging the sensitivity across patients, an average sensitivity of 50% was obtained. A higher sensitivity for the temporal lobe group compared to the extratemporal lobe group was expected, because behind-the-ear electrodes are closer to the temporal lobe. However, it is interesting that we could pick up two of three parietal lobe seizures, which indicates that ictal discharges arising from extratemporal lobes propagate to the behind-the-ear electrodes. However, further testing needs to be done on seizures originating from other lobes to determine whether the seizures are visible on the behind-the-ear channels. The bilateral group (43%) had lower sensitivity than the left (58%) and right (70%) groups, because a bilateral ictal pattern was more difficult to pick up with the crosshead channels due to differential amplification of the relatively symmetric signals. The increased sensitivity with seizure length was expected, because longer seizures are often associated with stronger ictal discharges.

7.6.2 Automated seizure detection

The PI seizure detection algorithm had lower performance compared to the PS algorithm for both aims I and II; in particular, the FP rate of the PS algorithm was decreased and PPV was increased. This is in agreement with the literature, as ictal behavior is highly patient-specific [12].

The algorithm with aim II improved the results compared to aim I, because subtle ictal EEG patterns and seizures with artifacts, which were not recognized by the neurologist, were left out from the test set. Furthermore, leaving out these unclear and artifacted seizures also resulted in a better training set, which in turn led to a better classifier and a lower FP rate for aim II.

The PS algorithm aim II had in total 22 false detections. The reasons for those false detections were diverse: high-amplitude artifacts in two channels, probably due to a technical problem with one EEG behind-the-ear electrode

(n = 1); slightly higher amplitude and change in frequency power, which are characteristics of ictal EEG (n = 2); seizures that were missed while annotating the video-EEG (n = 4); chewing artifacts (n = 9); high-frequency artifacts, probably due to muscle activity (n = 5); and a technical artifact (flat line; n = 1). The reasons for the FPs of the PI algorithm aim II were similar, most frequently high-frequency artifacts.

Large differences were observed between the mean and average results, because outliers were present. Outliers for the PS algorithm (three patients had a sensitivity of 0%) were often due to the limited amount of training data, which caused overfitting of the model. This resulted in low sensitivity if the test seizures were different from the training seizures. Outliers for the PI algorithm, especially for aim I (two patients had a false alarm rate higher than six per hour), were caused by a combination of three main reasons: large power in the theta band, high-frequency artifacts, and a salt bridge in the right channel. This caused a lateralization, which is typical for unilateral seizures.

In this study, the EEG was measured behind the ears, as shown in Figure 4.1. However, recently it has been shown that EEG recorded with a small device in the ear can detect temporal lobe seizures [275] and generalized tonic-clonic seizures [276]. A similar visual seizure recognition study for temporal lobe seizures resulted in comparable performances [275]. Those results suggest that the signals of both behind-the-ear and in-the-ear EEG could be used to detect temporal lobe seizures. However, the design of the devices is different. An advantage of the in-the-ear EEG is the discreteness, but disadvantages are the possible hearing loss, discomfort, and need for individualized design.

7.6.3 Clinical use of algorithm

A PI algorithm is more suitable for clinical use, because one device with the same algorithm can be given to all patients and no ictal EEG data are required beforehand. In this study, 24 patients had a sensitivity $> 50\%$ with the PI algorithm, tested on 35 patients. Originally, 65 patients were recorded with the behind-the-ear electrodes, so 37% of the patients in this study could potentially benefit from a device with a PI algorithm. One hundred eighty-two seizures were recorded, 114 (63%) were identified by the doctor and 71 (39%) were detected with the algorithm. Those values might seem to be low, but they were better than self-reporting by patients. Only 27% of focal impaired awareness seizures were reported by patients [103]. However, the false detection rate of the PI algorithm was high (2.8 FPs/24 hours) and PPV was low (38.9%). Those could be improved by personalizing the algorithm. The PS algorithm had lower FPs/24 hours (0.49) and higher PPV (65.4%).

Although PS algorithms are in general impractical, they can be useful in certain scenarios. They could be used in patients with refractory temporal lobe epilepsy who have video-EEG recordings of their habitual seizures. Using this patient-specific ictal EEG data, the algorithm could be trained automatically with minimal time investment by the clinician. The neurologist only needs to provide the annotations for the start and end of the seizures, which is usually part of the clinical review of video-EEG recordings.

7.6.4 Future work

The ictal EEG data used in this study were recorded with the hospital system using Ag/AgCl electrodes. The recorded patients were hospitalized, which limits the movements and artifacts present in the data. We showed that artifacts may have an important impact in the correct interpretation of seizures recorded with behind-the-ear EEGs. The algorithm should be tested on behind-the-ear EEG data, recorded with a wearable device [26] in an outpatient setting as written in the standards for testing and clinical validation [20]. The preprocessing, more specifically the removal of artifacts, should be adapted to the wearable data.

Training and testing the algorithm was done using the same database, and a retrospective analysis was performed. To extend the research, separate databases need to be used for training and testing and prospective analysis needs to be performed [20].

In this work, SVMs were used as classifiers. Other classifiers, for example, random forest [156], should be implemented and tested.

Behind-the-ear EEG is not the only type of signal suitable for a wearable seizure detection system in an outpatient setting. Electrocardiography (ECG), which can be recorded in an outpatient setting, has added value to automatically detect seizures in temporal lobe epilepsy patients [53, 140, 66, 114, 255]. Previous studies investigated multimodal seizure detection algorithms [82]. A multimodal algorithm should be developed combining information from behind-the-ear EEG and ECG, recorded with wearable devices in an outpatient setting. We are currently validating our wearable device measuring behind-the-ear EEG, movement, and ECG in a multicenter study [67] (EIT Health: SeizeIT237).

Chapter 8

Multimodal seizure detection based on ECG and behind-the-ear EEG

The content of this chapter is submitted to the journal Epilepsia [253].

8.1 Abstract

8.1.1 Objective

Wearable seizure detection devices could provide a more reliable seizure documentation outside the hospital compared to seizure self-reporting by patients. In the SeizeIT1 project, we studied the possibility to detect seizures based on behind-the-ear EEG. However, the obtained sensitivities were too low for practical use since not all seizures are associated with typical ictal EEG patterns. Therefore, we aim to develop a multimodal automated seizure detection algorithm integrating behind-the-ear EEG and ECG to detect focal seizures. In this framework, we quantified the added value of ECG to behind-the-ear EEG.

8.1.2 Methods

This study analyzed three multicenter databases consisting of 135 patients having focal epilepsy and a total of 896 seizures. A patient-specific multimodal automated seizure detection algorithm was developed using behind-the-ear/temporal EEG and single-lead ECG. The results were shown as 'sensitivity in function of false alarm rate' graphs. Two readers were asked to annotate ECG segments containing seizure or non-seizure fragments.

8.1.3 Results

The multimodal algorithm outperformed the EEG-based algorithm in two of three databases with an increase of 11% and 8% in sensitivity for the same false alarm rate.

8.1.4 Significance

ECG can be of added value to an EEG-based seizure detection algorithm using only behind-the-ear/ temporal lobe electrodes for patients with focal epilepsy.

8.2 Introduction

Epilepsy is amongst the most common neurological disorders, affecting almost 1% of the population worldwide [79]. Anti-epileptic drugs provide adequate treatment for about 70% of patients [80]. The remaining 30% continue to have seizures, which drastically affect their quality of life. To optimize therapeutic interventions for these patients, objective measures of seizure documentation and counting are needed [69]. However, seizure self-reporting by patients is unreliable [25, 75, 103, 195, 236]. Wearable seizure detection devices could provide a more reliable seizure documentation. In the SeizeIT1 project, we studied the possibility to record behind-the-ear EEG. Consequently, algorithms were developed using only behind-the-ear EEG channels for patients with focal epilepsy [96, 254]. However, the obtained sensitivities were too low for practical use since not all seizures are associated with typical ictal EEG patterns. Sensitivity of full-scalp EEG to localize focal seizures has been reported to be around 21% in focal aware [61] and 50-70% in focal impaired awareness seizures [78, 263, 228]. Furthermore, from the seizures with EEG correlation on full scalp EEG, 62% could be annotated as a seizure by a neurologist using only the behind-the-ear EEG channels [254].

Ictal heart rate changes as measured with electrocardiography (ECG) have been shown useful for seizure detection in patients with focal epilepsy [186, 53, 116, 255], especially temporal lobe epilepsy. Ictal tachycardia was observed in 71 - 84% of the seizures [66, 277, 37]. Figure 8.1 shows the behind-the-ear EEG and ECG signals during a selected seizure.

Multimodal algorithms were developed combining ECG with full/reduced EEG montages [82, 197, 42]. Fürbass et al. [82] showed the added value of ECG to a 7/8 electrode EEG montage in terms of sensitivity. However, the question whether adding ECG can increase sensitivity while maintaining the same false alarm rate remains unanswered. Furthermore, the added value of ECG compared to behind-the-ear EEG remains uninvestigated. In this paper, a patient-specific multimodal seizure detection algorithm was developed using three channels EEG and single-lead ECG, with the focus on obtaining a high sensitivity. In total, data from 135 patients with focal epilepsy and 896 seizures were analyzed. The novelties of the paper are twofold. First, a novel ECG-based seizure detection algorithm was proposed. Second, the added value of ECG in comparison with behind-the-ear/temporal EEG-based seizure detection was investigated. Graphs were obtained with sensitivity in function of false alarms rate allowing to compare sensitivities of different modalities at the same false alarm rate. Furthermore, the dependence of seizure type and localization was investigated.

This is a class 1 study according to the proposed standards for testing seizure detection devices [20], because real seizure data from patients were included and gold standard annotations were used for validation. However, the data were not acquired with wearables.

8.3 Data Acquisition

The data used in this study consists of 3 different databases: SeizeIT1, Epilepsiae-Freiburg and Epilepsiae-Paris, explained in Chapter 4. The algorithm was developed using the SeizeIT1 database and was tested on Epilepsiae-Freiburg and Epilepsiae-Paris. The multimodal algorithm which was found to be optimal in one center (UZ Leuven) was still valid on completely independent datasets, recorded in other centers (Freiburg and Paris).

No behind-the-ear channels were recorded in the Epilepsiae-Freiburg and Epilepsiae-Paris dataset. In our study, we have used the closest electrodes to the behind-the-ear placements as surrogates: namely, the T7, T8, P7 and P8 electrodes [216].

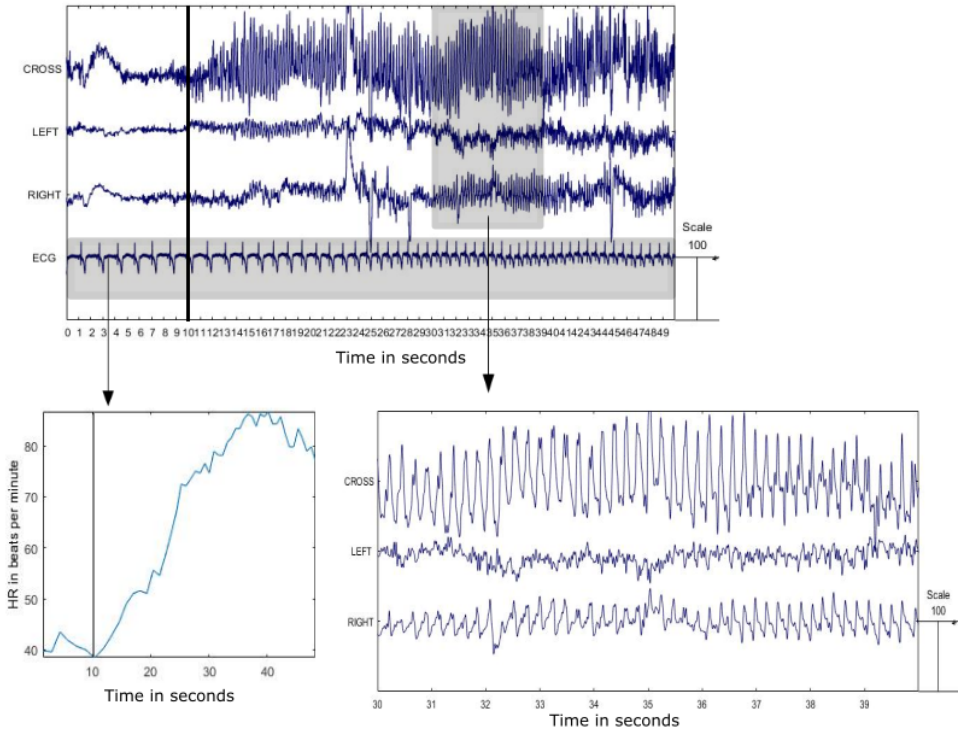


Figure 8.1: The behind-the-ear EEG and ECG are shown during a temporal focal impaired awareness seizures from the right hemisphere. The top figure contains 4 channels: crosshead (cross), left channel, right channel and ECG. The amplitude of the ECG signal is decreased with a factor 10. The seizure onset is depicted with a vertical black line at 10 seconds. The left bottom figure shows the extracted heart rate in beats per minute during the seizure. A heart rate increase from 40 to 80 beats per minute is observed. The right bottom figure shows a close-up of the behind-the-ear EEG channel during 20 – 30 seconds after the seizure onset.

8.4 Methodology

A schematic overview of the different steps of the automated seizure detection algorithm is shown in Figure 8.2.

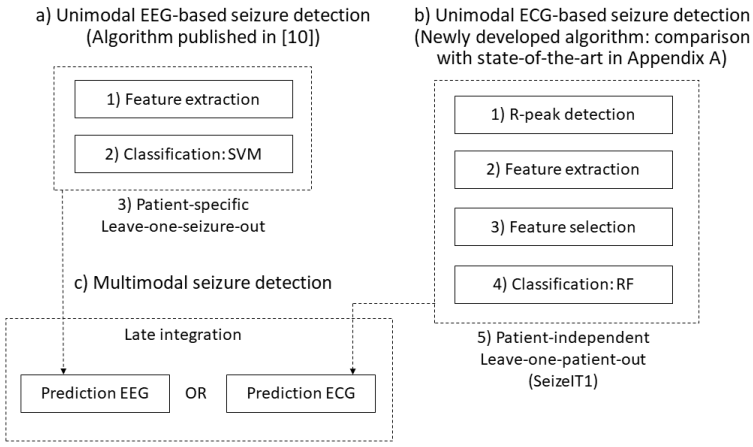


Figure 8.2: A schematic overview of the different steps in the automated seizure detection algorithm.

8.4.1 Unimodal EEG-based seizure detection algorithm using only behind-the-ear/temporal EEG electrodes

A patient-specific algorithm for offline seizure detection [254] was used as unimodal EEG-based seizure detection algorithm. For SeizeIT1, only the behind-the-ear EEG channels were used [254]. For the Epilepsiae databases, those specific EEG channels were not recorded and the mid-posterotemporal electrodes T7, T8, P7, and P8 were used instead.

1. Feature extraction: The data was segmented into 2-second windows with 1-second overlap. For each window, time domain, frequency domain, entropy derived and asymmetry features were extracted [254].

2. Classification: In order to classify those 2-second windows, a support vector machine (SVM) with a radial basis function kernel was applied. To train the SVM model for SeizeIT1, original seizure annotations (onset and end of seizure) from the neurologist were adapted by an engineer to exclude artifacts and non-typical EEG patterns [254]. For the Epilepsia datasets, the provided annotations were used to train the models. In order to obtain 'sensitivity in function of false alarm rate (FAR)' graphs, the continuous output of the SVM classifier was rescaled to a probability

between 0 (very low probability) and 1 (very high probability to be a seizure segment). By changing the cut-off value for this probability, ROC graphs were obtained with the sensitivity in function of FAR.

3. Cross-validation: A patient-specific seizure detection algorithm was applied in this work, meaning that we used data from the test patient to train the models. We have shown before that patient-specific algorithms achieve better performances than patient-independent ones [254]. The cross-validation scheme was leave-one-seizure-out.

8.4.2 Unimodal ECG-based seizure detection algorithm

A new patient-independent ECG algorithm was developed using the SeizeIT1 database. The performance of the algorithm was compared to two state-of-the-art algorithms in appendix C.1. The different steps of the algorithm are summarized.

1. R-peak detection: The method consists of an ensemble of three different R-peak detection algorithms. The first one is based on a wavelet decomposition [142], the second one extracts the R-peaks from the derivative signal with an adaptive threshold [53] and the last one uses an adapted version of the Pan-Tompkins algorithm. Upper and lower envelopes were extracted to obtain a clean signal [259]. The different R-peak detection algorithms generate three different R-peak series. These R-peak locations were combined with an ensemble method [49].

2. Feature extraction: The data was segmented in windows of 60 seconds with 10 seconds overlap. Compared to EEG (windows of 2 seconds), larger windows are needed to extract reliable ECG features. For each window 133 features were extracted (the detailed description of all the features is provided in Appendix C.2). The feature set consisted of different features both from the time domain Heart Rate Variability (HRV), frequency domain HRV and other features also applied in various (non-)epilepsy publications [53, 115, 64, 180, 120, 87, 40, 181, 182, 244].

3. Feature selection: In order to select discriminatory features, a random-forest based feature selection scheme [60] resulted in a subset of the six most discriminant features, namely: the modified cardiac sympathetic index based on Lorenz plot (CSI100) [115], circadian rhythm-based feature, duration of the Heart Rate (HR) increase, HR after tachycardia/ HR before tachycardia, Very Low Frequency (VLF) power and Low Frequency (LF) power.

4. Classification: In order to classify each 60-second window, a random-forest classifier was used. Following the rationale used in the EEG-algorithm, the continuous output of the random forest was converted to a probability and an ROC 'sensitivity versus FAR' graph was computed.

5. Cross-validation: A patient-independent seizure detection algorithm was developed. In an ideal case, the same patient-specific cross-validation scheme would be applied for ECG as for the EEG model. However, due to the lack of multiple available data points per patient this was not possible without overfitting the model. Indeed, in the case of EEG, multiple 2-second windows are available per seizure whereas for ECG, only one heart rate increase is present per seizure. The cross-validation scheme was leave-one-patient-out for SeizeIT1. The Epilepsiae databases were tested with a model trained on SeizeIT1.

8.4.3 Multimodal seizure detection algorithm

Different strategies to fuse multiple modalities exist; the main categories of such fusing strategies are the early and late fusion. In this work, we opted for a late integration strategy due to the difference in the cross-validation schemes used and the different alignment of the events in both modalities. More specifically, a patient-specific cross-validation scheme led to optimal results for the EEG-based model [254], while for ECG, the lack of available data points per patient did not allow the application of exactly the same patient-specific cross-validation scheme without overfitting the model. In the case of EEG, multiple 2 second windows are available per seizure whereas for ECG, only one heart rate increase is present per seizure. Secondly, the typical patterns of EEG and ECG do not occur exactly at the same time. The HR increase/decrease can follow or precede the EEG onset [277]. Hence, a late integration, 'OR' strategy, has been applied: a seizure should be detected by at least one of the modalities (EEG or ECG) in order to generate a seizure detection alarm, similarly to Fürbass et al. [82]. This choice was made since not all seizures have ictal ECG changes or EEG correlation and we aimed for a high sensitivity. For this multimodal algorithm, there are two varying thresholds (one for EEG and one for ECG). If we want to show all possibilities, the results would be a plane to be visualized in 3D. For simplicity, a threshold was selected for each modality leading to 0.2 FP/hour and those two thresholds were used to produce the multimodal results. This procedure was also done for an FAR/hour of 0.5 and 1.

8.4.4 Performance evaluation

The following measures were applied to determine the performance of the seizure detection algorithm:

1. Detection sensitivity: TP/ (TP+FN), where TP is a true positive and FN is a false negative. A seizure was detected correctly (TP) if a detection occurred between the EEG onset and offset of the seizure.
2. False alarm rate (FAR) per hour: False Positives (FPs)/recording length. FPs within 10 seconds of each other were counted as one FP. FPs happening 60 seconds before the seizure onset or 60 seconds after the seizure offset were not counted as false alarms since ictal tachycardia can precede EEG seizure onsets.

The 'sensitivity in function of FAR' graphs were constructed by changing the cut-off values of the probabilities both for the ECG- and EEG-based algorithms. For each patient a graph was constructed, and the graphs of all patients were averaged.

8.5 Results

8.5.1 Performance of the Unimodal models: EEG and ECG

In Figure 8.3 'sensitivity in function of FAR' graphs are shown for the unimodal algorithms: EEG and ECG. Table I.A shows the average sensitivities corresponding to a FAR of one FP/hour. For the EEG-based algorithm, Epilepsiae-Freiburg had the lowest sensitivity (77%), SeizeIT1 had a sensitivity of 79%, whereas Epilepsiae - Paris had the highest sensitivity (82%). For the ECG-based algorithm, Epilepsiae-Freiburg had the highest sensitivity (74%), SeizeIT1 had a sensitivity of 65%, whereas Epilepsiae-Paris had the lowest sensitivity (52%). For all the databases, the EEG-based seizure detection algorithm had the highest average and median sensitivities. By analyzing individual patients, 88 patients (65%) exhibited a higher sensitivity with EEG, 29 patients (21%) had equal sensitivity with EEG and ECG and 18 patients (13%) exhibited a higher sensitivity with ECG. In total, 463 seizures (52%) were detected with both EEG and ECG, 244 seizures (27%) were detected only with EEG, and 131 seizures (15%) were not detected either with EEG nor with ECG. It shall be noted that 58 seizures (6%), from 38 patients, were detected only with ECG. Appendix C.3 describes the percentage of detected seizures in function of seizure type and localization for the different modalities.

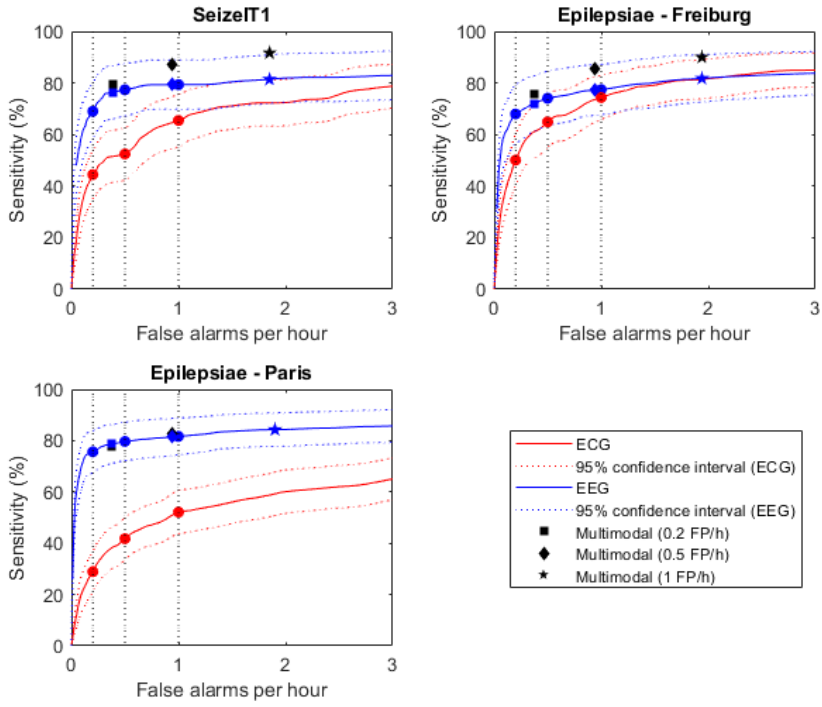


Figure 8.3: Sensitivity in function of FAR for the different datasets. The blue graph depicts the unimodal results of EEG, the red one the results of ECG. On those graphs, the sensitivities at a FAR at 0.2 FP/hour, 0.5 FP/hour and 1 FP/hour are depicted with circles. The black points are the results of the multimodal algorithm at three discrete thresholds (square: 0.2 FP/hour, diamond: 0.5 FP/hour and star: 1FP/hour). For comparison, the results on the EEG graph with the same FAR are indicated with blue marks.

8.5.2 Performance of the Multimodal model

In Figure 8.3, we present the results of the multimodal algorithm. The outcome of the two unimodal algorithms were combined with a late integration approach at three discrete thresholds: the thresholds leading to 0.2 FP/hour, 0.5 and 1 for both the EEG and ECG algorithm. Those three (sensitivity, FP/hour)-pairs were shown together with the corresponding sensitivities leading to the same FAR on the EEG graph. By analyzing those three pairs, the lowest increase in sensitivity was observed with the 0.2 FP/hour threshold and the highest with

Table 8.1: A. False Alarm Rate (FAR) [FP/hour] and Sensitivity (Sens) [%] for the unimodal EEG and ECG at a FAR of 1 FP/hour for the different databases. B. False Alarm Rate and Sensitivity (%) of the multimodal (at a threshold generating 1FP/h for the unimodal modalities) and EEG-based detectors at the same FAR for the different databases. Mean [95% confidence interval] / median [min max] are shown in the table.

A

	FAR (FP/hour)	Sens (Unimodal EEG) [%]	Sens (Unimodal ECG) [%]
SeizeIT1	1	79 [70 - 89] (100 [0 100])	65 [55 - 76] (67 [0 100])
Epilepsiae - Freiburg	1	77 [68 87] (85 [0 100])	74 [66 - 83] (79 [12 100])
Epilepsiae – Paris	1	82 [74 - 89] (100 [0 100])	52 [44 - 61] (50 [0 100])

B

	FAR (FP/hour)	Multimodal	Unimodal EEG
SeizeIT1	1.85	92 [87 - 96] (100 [50 100])	81 [72 - 91] (100 [0 100])
Epilepsiae - Freiburg	1.94	90 [85 - 95] (100 [50 100])	82 [73 - 91] (88 [6 100])
Epilepsiae – Paris	1.90	84 [77 - 91] (100 [0 100])	84 [78 - 91] (100 [0 100])

the 1 FP/hour threshold. In Table 8.1(B) the sensitivity of the multimodal algorithm (threshold leading to 1 FP/hour) is presented along with the outcome of the EEG-based detectors with the same FP/hour. For SeizeIT1, an increase was observed from 81% (EEG unimodal) to 92% (Multimodal). A similar increase was seen for Epilepsiae-Freiburg (from 82 % to 90%). No increase was observed for Epilepsiae-Paris (from 84% to 84%). In total, 31 (23%) patients had increased sensitivity (with the multimodal algorithm compared to the EEG unimodal), 88 (65%) patients had the same sensitivity and 16 (11%) patients had a decreased sensitivity.

8.6 Discussion

Mobile health and digital biomarkers involve the application of wearable sensors to obtain data pertinent to wellness and disease diagnosis, prevention and management [222]. Current non-invasive wearables in epilepsy are accelerometer- and EMG-based devices for online-automated detection of tonic-clonic seizures, mostly for generalized tonic-clonic seizures, the easiest group of seizures to detect. Those wearable devices generate an immediate alarm for caregivers and health care professionals. Accelerometry can be recorded unobtrusively with wristbands, which are commonly used in daily life nowadays. sEMG can be recorded with a wearable device placed on the upper arm. These devices have a sensitivity of around 90% and a PPV (Positive Predictive Value) of around 55%. The F1-score of these devices is around 0.68 [132, 261]. Focal non-motor seizures are typically not accompanied with such strong and typical movement

and/or muscle activity. For those focal seizures, the authors are aware of only 1 automated seizure detection device, UNEEG medical [65]. This device is a minimally invasive, subscalp, implantable EEG system allowing ultra-long-term seizure monitoring.

No non-invasive wearable devices are currently available for the detection of focal seizures. An important methodological problem is the diversity of focal epileptic seizures: there are three focal seizure types, namely focal aware, focal impaired awareness and focal to bilateral tonic clonic seizures, which can be generated from four different lobes, namely temporal, frontal, occipital and parietal lobe [212]. We observe that one single biosignal is not able to detect all types of focal seizures. Therefore, including multiple biosignals is recommended to achieve higher sensitivities. Variability in performances across datasets is high, multiple datasets were included in this study to derive general claims. In our study, a multicenter dataset of 135 patients with 896 seizures recorded during a presurgical evaluation was used. Behind-the-ear/temporal EEG plus ECG captured 52% of seizures, EEG-alone 27% and ECG-alone 6%. In those 6%, probable reasons why those seizures could not be picked up with EEG are listed in appendix C.4. Around 21% of the seizures remained difficult to detect with behind-the-ear EEG, which was due to unclear ictal EEG patterns, short seizures or artifacts on the restricted set of temporal lobe or behind-the-ear electrodes. These observations suggest that wearables to detect focal seizures should be multimodal, i.e. able to capture different biosignals. The neurologist should be aware of ictal EEG and ECG changes of an individual patient beforehand in order to select which biosignals to capture with the multimodal wearable device. This would also allow creating a personalized algorithm, i.e. trained with seizure data from the individual patient, as in our study.

Our 'sensitivity in function of FAR-graphs' showed that high sensitivity can be obtained at the cost of a higher number of false positive detections. In our view, the FAR is too high to use the algorithm for online/immediate seizure detection in daily practice. It would be very useful, however, to use the algorithm to reduce the amount of data to be reviewed. The neurologist has only to review the automatically flagged regions and decide whether it was a seizure or a false positive detection. Our multimodal algorithm had a high average sensitivity of 90% at 2 FP/hour. This would mean that two data points should be reviewed per hour, which would reduce the review time with probably more than 90%. A follow-up study will be conducted to measure the performances after visual analysis of a neurologist/EEG expert and the review time will be quantified. Furthermore, this study will investigate whether ECG can improve visual behind-the-ear EEG seizure recognition by a neurologist/EEG expert.

With our current algorithm, 15% of all seizures were not captured with EEG or ECG. The majority of those seizures had an unclear or fronto-temporal onset

zone. Seizures with an unclear origin often have motion and noise artifacts on the EEG, which complicates localization. Seizures from the fronto-temporal origin could have an onset zone in the frontal area. Those seizures are typically associated with motor and muscle components and could be picked up with electromyography (EMG). Adding EMG/motion to the analysis could potentially increase the sensitivity even more.

To integrate the EEG and ECG, a late integration approach with an 'OR' strategy was applied: the ECG or the EEG should give a seizure detection to generate a seizure detection alarm. Assigning the same contribution to the different modalities might be suboptimal. Different weights attributed to the different modalities can be trained in an additional second classification level. Alternatively, those weights can be assigned based on the level of noise on the raw signals and the certainties of detections (seizure/no seizure), different weights could be assigned to the output seizure probabilities of the two modalities. To quantify uncertainties, trust scores could be a good methodology [13].

In this work, the EEG model is patient-specific, trained on data from a specific patient. We have shown before that patient-specific algorithms are more sensitive than patient-independent ones [254]. However, limited seizure data from patients are available due to low seizure frequencies, possibly leading to overfitted models. Improvements can be made by starting with a patient-independent model and adapting this model to a particular patient with limited patient-specific data. Deep transfer learning approaches have shown to be successful for reduced EEG montages in other fields, like automatic sleep staging [191]. The ECG model in this work is patient-independent, using data from other patients to train the model. Patient-independent models achieved better performances than fully patient-specific ones [52]. This is due to limited patient-specific seizure data since only one heart rate increase per seizure is available. Transfer learning approaches could be helpful for the ECG modality as well [52].

When developing a wearable, good quality of signals will be vital to obtain reliable results. In the current study, a lower sensitivity for the ECG-based algorithm was observed for Epilepsiae-Paris. By inspecting the raw ECG data, an increased number of artifacts was observed. Those artifacts looked like motion artifacts with usually high frequency muscle activity on top. In the visual annotation study using ECG, therefore, the number of false alarms due to artifacts was higher in Epilepsiae-Paris (60%) compared with Epilepsiae - Freiburg (37%) and SeizeIT1 (23%).

The present work was part of the SeizeIT1 project, in which we used EEG and ECG data from standard hospital equipment. We are continuing this work in the SeizeIT2 project https://eithealth.eu/project/seizeit2/ (ClinicalTrials.gov: NCT04284072) with a multimodal wearable based on Byteflies's Sensor-Dot

(https://www.byteflies.com/) , measuring two channels EEG behind-the-ear, ECG, accelerometry and EMG of the left deltoid muscle. We are planning to determine F1 scores for typical absences, focal seizures and tonic-clonic seizures in a hospital-based and home-based international multicenter study. We are further developing new and improved electrode patches to measure EEG, ECG, EMG, respiration, oxygen saturation and skin temperature in the study of epileptic seizures (ClinicalTrials.gov: NCT04642105). We will study the prevalence of epileptic seizures and sleep-wake disturbances in Alzheimer's disease using this wearable (ClinicalTrials.gov: NCT03617497) and tonic, atonic and myoclonic seizures in childhood epilepsy (ClinicalTrials.gov: NCT04584385). Development of improved seizure detection algorithms based on artificial intelligence and machine learning will be an essential step to integrate this wearable into everyday clinical practice of the neurologist-epileptologist to improve management of patients with refractory focal epilepsy.

Chapter 9

Conclusions and future directions

The aim of this thesis was the development of an offline seizure detection algorithm for patients with focal epilepsy to construct automatically a seizure diary in a home environment . There were three major contributions: seizure detection based on wearable ECG/PPG, seizure detection based on behind-the-ear EEG channels and multimodal seizure detection based on behind-the-ear EEG and ECG. The conclusions from these three studies are drawn in the first section. Those studies serve as a proof-of-concept for wearable monitoring and are an important part of the research and development of the SeizeIT device. The second section discusses the future directions for the development of the SeizeIT device and the seizure detection algorithm.

9.1 Conclusions

9.1.1 Seizure detection based on wearable ECG/PPG

The performance of two wearable devices, based on electrocardiography (ECG) and photoplethysmography (PPG) recorded at the wrist, were compared with ECG recorded with the wired hospital equipment in Chapter 6. The simultaneous data collection of the wearable devices and the ECG recorded with the hospital equipment allowed a fair comparison between them. An existing algorithm using characteristics of the heart rate, which can be derived from

ECG as well as PPG, was applied and performances were compared. The wearable ECG device had very similar or even better performances, whereas the wearable PPG device had a decreased performance compared to the wired hospital equipment. Higher sensitivities for the wearable ECG device were observed due to the absence of wires. Those wires cause electrode displacements during motion. As a result, artifacts were more frequently present on the ECG recorded with the wired hospital equipment, especially during seizures involving motor activity. Lower sensitivities for the wearable PPG device were observed due to the presence of strong motion artifacts. During motion of the wrist, the heart rate could not be extracted. Artifact removal methods were investigated but during most motion artifacts, the frequency related to the heart rate was not present in the frequency spectrum.

Despite the improved seizure detection performance using wearable ECG, a patient-independent HR-based algorithm is not suitable for automatically constructing a seizure diary. Those algorithms based on the heart rate have typically a false alarm rate around 2 false detections per hour, leading to much more false alarms than true seizure alarms. Focal patients have typically only a few seizures per week.

9.1.2 Seizure detection based on behind-the-ear EEG

Visual seizure annotation and automated seizure detection using behind-the-ear EEG was investigated in Chapter 7. Firstly, we determined whether the recognition of ictal patterns using only behind-the-ear EEG channels was possible. Secondly, an automated seizure detection algorithm was developed using only those behind-the-ear EEG channels. The visual recognition of ictal EEG patterns using only behind-the-ear EEG resulted in a sensitivity of 65.7%. This value was lower than expected since the majority are temporal lobe seizures. The two most important reasons for unrecognized seizures were artifacts and subtle ictal patterns. Those artifacts were also present on full scalp EEG at temporal electrodes, but with the use of other channels the seizure could be recognized. The use of a reduced montage did not explain that the seizures with subtle ictal patterns were unrecognized, as the pattern was subtle on full EEG as well. Those seizures were annotated taking the presence of a clinical seizure on video into account.

An automated seizure detection algorithm was developed and tested in two scenarios. The aim of the first scenario was to detect all the seizures, also the seizures not recognized by the neurologist. In this case the training data included all seizures. The aim of the second scenario was to detect only the seizures visible for a neurologist. In this case the training data included only

the recognized seizures by the neurologist. Those two scenarios were tested in a patient-specific and patient-independent framework. The patient-specific model with the aim of detecting the recognized seizures by the neurologist, achieved a sensitivity of 69.1% and 0.49 FPs/24 hours. The obtained false alarms were very low, which is a crucial requirement for a fully automated algorithm. The sensitivity might seem to be low, but the number of detected seizures was higher than self-reporting by patients. Nevertheless, we aim for a higher sensitivity by including ECG, discussed in the next subsection.

9.1.3 Multimodal seizure detection based on behind-the-ear EEG and ECG

We aimed to develop an automated multimodal seizure detection algorithm integrating behind-the-ear EEG and ECG to detect focal seizures, explained in Chapter 8. In this framework, we quantified the added value of ECG to behind-the-ear EEG using three different databases. The multimodal algorithm outperformed the EEG-based seizure detection in two out of the three databases with an increase in sensitivity of 10% and 8% for the same false alarm rate. Lower quality of ECG signals was observed in the third database. In total, 6% of the seizures were only detected with the ECG modality. Those seizures remained difficult to detect with behind-the-ear EEG due to unclear ictal EEG patterns, short seizures or artifacts on the restricted set of temporal lobe or behind-the-ear electrodes.

9.2 Future directions

9.2.1 Future directions for the SeizeIT device

A continuation of efforts is needed to further develop the SeizeIT device. The wearable device should be a medical device under full supervision of the neurologist, who will prescribe the device to the patient. Other seizure detection devices on the market are sold to patients directly. Here under full supervision of the neurologist means that the device does not go to the patient directly, but goes to the neurologist. This is a big advantage compared to other devices or solutions, as the neurologist can contribute with expertise (which modality to use) and with data. Only patients having ictal heart rate changes need ECG to be recorded, only patients having visible ictal behind-the-ear EEG changes need EEG to be recorded. Also the algorithm should be personalized since ictal patterns differ largely between patients. Personalized

algorithms are less practical to apply since data of the patient itself is needed. In the case of traditional devices on the market, personalization of algorithms is impossible due to the lack of annotated patient specific data. However, the neurologist has access to full patient history including past seizure recordings. During presurgical analysis, video-EEG of their habitual seizures was recorded. Using this patient-specific ictal data, algorithms could be trained with minimal investment by the neurologist. After giving the device to the patient, he should be able to look at the raw data generating false alarms. Based on this reduced dataset, he can discriminate the real seizures from false alarms. This data can potentially be used for further updating the algorithm to achieve higher performances. Also the sensitivity of the algorithm should be adaptable.

In a first phase, this will be an offline seizure detection device, generating a seizure diary. In a later phase, this can be extended to an online alarming device. Based on the patient preferences, the intended goal of the device should be selected. Typically, focal patients do have more benefit from an offline seizure detection generating a seizure diary. When using the algorithm for an online purpose, redesigning the algorithm will be required. The current algorithm is computationally too expensive due to the complex computations to run on a small device with limited battery.

Within the EIT Health project, not only focal seizures are recorded. Also typical absences, tonic-clonic seizures are currently being recorded in different clinical centers. Recordings are not only done in a hospital environment, patients are also recorded at home. Efforts are already done and are ongoing to develop algorithms for different seizure types. The analysis will be extended for typical absences and tonic-clonic seizure types.

9.2.2 Future directions for algorithm development

Our research group did a comparison of seizure detection based on full scalp EEG versus behind-the-ear channels in 12 patients [96]. With scalp EEG, a median detection sensitivity of 100% and a false detection rate of 1.14 per hour was obtained, while behind-the-ear EEG achieved a sensitivity of 94.5% and a false detection rate of 0.52 per hour. Those results are very promising but the number of patients need to be extended to draw strong conclusions. 10 out of the 12 patients had temporal lobe epilepsy. More patients having different seizure onset zones should be investigated. We hypothesize that seizures having extratemporal lobe onset zone will be visible on the crosshead channel. Artifacts were removed for both recordings by applying a canonical correlation analysis for blind source separation using all the channels. Interesting would be to

investigate the impact on the behind-the-ear EEG performance in case the scalp EEG was not used for artifact removal.

With the current algorithm based on behind-the-ear EEG and ECG, 14% of the seizures were not detected by any of those modalities. The majority of those seizures had an unclear or fronto-temporal onset zone. Seizures with an unclear origin often have motion and noise artifacts on the EEG, which complicates localization. Seizures from the fronto-temporal origin could have an onset zone in the frontal area. Those seizures are typically associated with motor and muscle components and could be picked up with electromyography (EMG). Adding EMG/motion to the analysis could potentially increase the sensitivity even more.

All the analysis in this thesis was done with recordings made in the hospital, where the patients are limited in their activities. Artifacts will possibly cause a large increase in false alarms. Solutions need to be found to suppress or remove those artifacts. When this remains too challenging, artifact detection needs to be investigated to eliminate those alarms. This is a challenging task as well since seizure data contain artifacts and those true seizure alarms should not be eliminated. This could be potentially solved in a multimodal way. Based on the signals of the individual modalities, an automated artifact detection algorithm should give the level of quality. If the level of quality is high for that particular modality, more importance or weight should be given to that corresponding signal. Seizures having artifacts on the EEG/ECG channels typically have a motor component. So we should rely more on EMG and motion for those seizures.

A challenge in epileptic seizure detection is the large variability across patients and the low number of recorded seizures per patient. On one hand, patient-independent seizure detection systems give suboptimal performances since the ictal patterns both on EEG and ECG are different for each patient. A model trained on characteristics of other patients is not a good solution. On the other hand, patient-specific systems require a sufficient number of collected seizures of that particular patient. This is challenge in practice since seizure frequencies are very low. One way to solve this, is starting from a patient-independent algorithm and personalize this algorithm based on a limited amount of data. Personalization approaches were successfully applied on full channel EEG using CNN with transfer learning [183] and ECG using supervised SVM transfer learning [52]. Investigation is needed for limited channels of EEG. In other research disciplines, deep transfer learning approaches are investigated using limited channels. For example, Phan et al. [191] proposed deep transfer learning for automatic sleep staging. The networks were first trained using a large dataset and this network is adapted using a small dataset recorded with a different setup. This idea could also be applied on personalization of seizure algorithms. First

a network can be trained using all the patients, then this network is adapted using the patient specific data.

The growing datasets available in our research group opens the possibility to apply deep learning strategies, which need large datasets in the training process. An interesting algorithm is the multi-view attention-gated U-net deep neural network [36], which achieved the first place in the Neureka challenge. The preprocessing methods, multi-channel subspace filters and ICLabel, which is an artifact removal method based on blind source separation - independent component analysis (BSS-ICA), use multi-channel EEG as input. Therefore, they can not be directly applied to the behind-the-ear channels. However the U-net architecture could be applied on behind-the-ear EEG. This U-net architecture differs from classical deep learning approaches. Classical methods have first a segmentation step (for example 2 second data segments). One prediction (seizure/non-seizure) is made for each segment, whereas the U-net does not have such a segmentation step and uses whole the recording, which is more information, to make a prediction for every sample.

A challenge in the global research on epileptic seizure detection algorithms is the lack of open source datasets. Only a few datasets are open source and free to use, for example the TUH EEG seizure corpus. As a result, many seizure detection algorithms in the literature are validated using small datasets, often collected in one hospital. Furthermore, the performances can not be compared due to the use of different datasets. Between those datasets, large differences are present since protocols in the hospital and inclusion criteria differ and focal epileptic seizures are diverse. Furthermore, performance metrics (typically sensitivity and false alarm rate) are not always defined the same way, making the results even more difficult to compare. A joint effort is needed between different hospitals and epilepsy centers to compare the state-of-the-art algorithms on the same set of databases.

Since the set-up and hardware specifications can differ between datasets, applying a network trained on a large dataset A to another dataset B, can lead to lower accuracies. Retraining the model can be difficult due a smaller dataset B. A good example here is the SeizeIT2 analysis: a model was trained on the SeizeIT1 data using behind-the-ear EEG data since the SeizeIT2 dataset currently consists of a limited number of patients (9). By applying this model to the SeizeIT2 data recorded with the Byteflies sensor dot data, slightly lower sensitivity and higher false alarm rates were observed, possibly due to different hardware settings. Transfer learning can be applied to reduce the data discrepancy between dataset A and B [264].

The contributions of this thesis are proof-of-concepts for wearable seizure monitoring and are an important part of the research and development of the

SeizeIT device. I hope those contributions pave the way for a SeizeIT device available on the market and worn by patients, who experience an improved quality of life due to the device.

Appendix A

SeizeIT2 analysis

A.1 SeizeIT1: Analysis using two behind-the-ear channels

Since the Byteflies Sensor Dot (SeizeIT2) measures only two channels and the EEG-based seizure detection algorithm was designed for three channels, the algorithm was adapted and tested on the SeizeIT1 database. Features were only extracted from two bipolar channels: crosshead and a local channel, left or right depending on the seizure onset. The asymmetry features (features 22-25 in Table 7.1) were not calculated since those features represent the asymmetry between the left and right side. The patient-specific and patient-independent models (aim I) were compared and tested using only two channels. The average and median results are depicted in Table A.1.

A.2 SeizeIT2: Comparison between hospital equipment and Sensor Dot (SD)

The SeizeIT2 dataset contains 76 patients recorded with focal epilepsy. From those, 9 patients were analyzed. The remaining patients were not analyzed due to the following reasons: 34 patients were not yet annotated, 20 patients experienced no seizures during the recordings, the recordings of 13 patients have technical problems.

Table A.1: SeizeIT1 seizure detection results: three channels versus two channels

	Average results	
	Sensitivity (%)	FPs/24 hours
Patient-Specific (3 channels)	63.4	0.88
Patient-Specific (2 channels)	58.6	1.98
Patient-Independent (3 channels)	72.7	34.2
Patient-Independent (2 channels)	65.0	32.0
	Median results	
	Sensitivity (%)	FPs/24 hours
Patient-Specific (3 channels)	67.4	0
Patient-Specific (2 channels)	61.3	0.65
Patient-Independent (3 channels)	100	13.6
Patient-Independent (2 channels)	84.4	19.5

Table A.2: SeizeIT2 seizure detection results: hospital equipment versus sensor dot [Abbreviations: FIA= Focal Impaired Aware, FA= Focal Aware, Temp= Temporal, Par= Parietal, Front= Frontal]

					Hospital equipment		**Sensor dot**	
Subject	Seizure type	lobe	set-up	#seizures	Sens (%)	FP/h	Sens (%)	FP/h
SUBJ-1a-006	FIA, FBTC	Temp	Left	13	23.08	0.35	0.00	0.07
SUBJ-1a-025	FBTC	Temp	Right	1	100.00	3.20	100.00	3.71
SUBJ-1a-045	FIA, FBTC	Temp	Left	14	100.00	0.53	100.00	1.38
SUBJ-1a-046	FIA	Temp	Left	3	100.00	1.25	100.00	0.67
SUBJ-1a-054	FA, FIA	Front, Par	Left	12	100.00	2.25	90.00	5.26
SUBJ-1b-023	FIA	Front, Temp	Left	3	66.67	2.17	33.33	1.93
SUBJ-1b-042	FIA	Temp, Par	Right	2	100.00	1.98	100.00	4.05
SUBJ-1b-047	FIA	Temp, Par	Right	4	100.00	0.96	75.00	1.47
SUBJ-1b-057	FA, FIA	Temp	Left	1	100.00	2.39	100.00	10.71
AVERAGE					**87.75**	**1.68**	**77.59**	**3.25**
MEDIAN					**100**	**1.98**	**100**	**1.93**

The results of the SeizeIT2 analysis per patients are shown in Figure A.2 together with the seizure characteristics such as seizure type, lobe and the used set-up.

Appendix B

Motion and noise artifact removal using behind-the-ear EEG channels

This appendix describes the simulations on motion and noise artifact removal using the behind-the-ear EEG channels.

First, a simulation study was done where artifacts were added on clean EEG segments with different Signal to Noise Ratios (SNRs). The reconstructed signals were compared to the original clean signals. Afterwards, the two best artifact removal methods were applied to the current patient-specific seizure detection algorithm pipeline. The performances were compared to a bandpass filter.

B.1 Simulation study

B.1.1 Methods

Different single channel artifact removal methods were tested. First the behind-the-ear EEG cannels were decomposed using Empirical Mode Decomposition (EMD), Ensemble Empirical Mode Decomposition (EEMD) or Wavelet [163]. Each channel of the behind-the-ear electrodes was decomposed into 8 modes. All those modes were taken together and ICA/CCA was run. The sources containing

muscle activity were removed. Those muscle sources were identified as the sources having a power ratio $\frac{[3-15Hz]}{[25-50Hz]}$ lower than 1.5. The following techniques were applied: Empirical Mode Decomposition - Canonical Correlation Analysis (EMD-CCA), Empirical Mode Decomposition - Independent Component Analysis (EMD-ICA), Ensemble Empirical Mode Decomposition - Canonical Correlation Analysis (EEMD-CCA), Ensemble Empirical Mode Decomposition - Independent Component Analysis (EEMD-ICA), Wavelet-CCA and Wavelet-ICA. In addition, CCA was applied without decomposing the EEG channels. As last, a Multichannel Wiener Filter (MWF) [224] was applied with the provided toolbox [225]. The MWF filter was trained with 8 (10s) clean EEG segments and 5 (10s) artifacted segments. Temporal information was included up to a delay of 5 samples.

To evaluate the performance, the Relative Root Mean Squared Error (RRMSE) and the correlation was calculated between the reconstructed signal and the clean EEG signal. The RRMSE was calculated as follows:

$$RRMSE = \frac{RMS(a(t) - \hat{a}(t))}{RMS(a(t))} * 100\% \tag{B.1}$$

with a(t) the clean EEG signal and â(t) the reconstructed signal

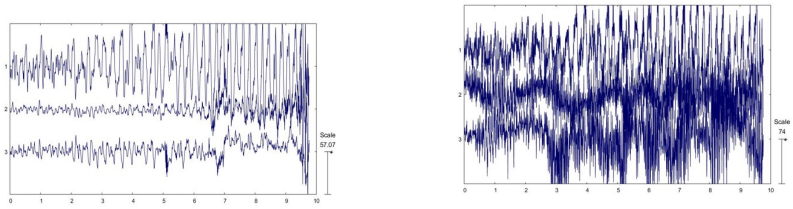
B.1.2 Simulated dataset

8 (10s) clean EEG segments were manually selected, 5 of them were background segments and 3 were seizure segments without artifacts. 5 muscle artifact segments were manually selected. In order to generate contaminated EEG segments, the clean EEG signals and muscle artifact segments were added $[X(\lambda) = A + \lambda * B]$ with different SNRs $[SNR(\lambda) = \frac{RMS(A)}{RMS(B)}]$ with A a clean EEG segment, B a muscle artifact segment. In total, 80 combination of the clean segments and artifacted segments are possible and those results were averaged.

In Figure B.1 a clean seizure segment and the segment with on top muscle artifacts are shown.

B.1.3 Results and discussion

Figure B.2 shows the results. It can be seen that the MWF has the lowest RRMSE and highest correlation, expecially for high SNRs. The rest of the filter



(a) Clean seizure segment (10s)

(b) Clean seizure segment with an artifacted segment on top with an SNR of 0.77

Figure B.1: Examples of EEG signals

techniques are similar expect the CCA approach, having a higher RRMSE and lower correlation. WCCA seems slightly better compared to a BP filter.

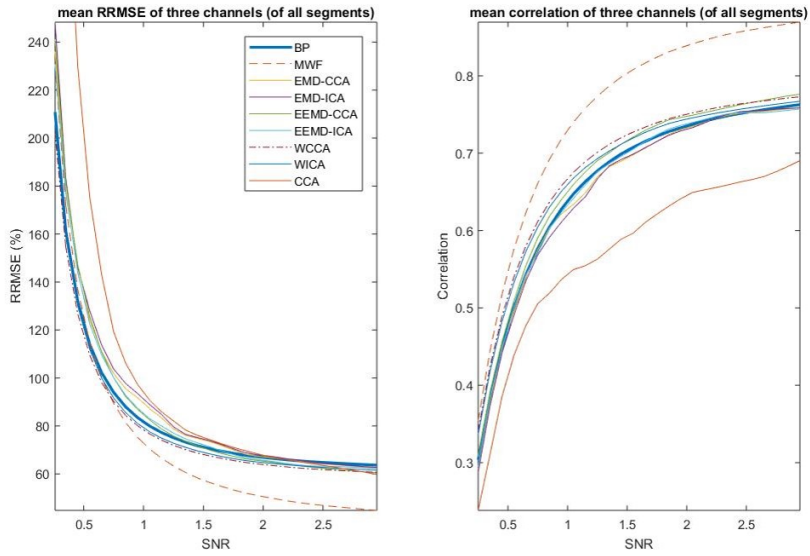


Figure B.2: Results of the simulation study: RMSSA [left] and correlation [right] between the reconstructed signal and the clean EEG signal

Table B.1: Seizure detection results: comparison of different filtering techniques

	Average results	
	Sensitivity (%)	FAR/hour
BP	79	0.96
MWF	81	1.34
WCCA	68	1.43
	Median results	
	Sensitivity (%)	FAR/hour
BP	85	0.27
MWF	88	0.45
WCCA	79	0.66

B.2 Application to seizure detection

The WMF and WCCA filtering techniques had a better performance in the simulation study. Those filtering techniques were tested with the current EEG-based algorithm pipeline in comparison with the BP filter.

B.2.1 Methods

The used patient-specific EEG-based seizure detection algorithm was an earlier version of the one presented in Chapter 7. There are three main differences: First, the extracted features are the ones listed in table 7.1 without the HF and entropy-related features. Second, the median decaying memory method was not applied. Third, the optimization of the hyperparameters was different. In Chapter 7 the hyperparameters were selected with a patient-independent approach with a grid search minimizing the F1-score. Here, the hyperparameters were selected per patient using a grid search selecting the hyperparameters with a sensitivity of at least 80% and the lowest possible FAR on the training set.

B.2.2 Results and discussion

Table B.1 gives the average and median results of the MWF and WCCA filtering techniques in comparison with the BP filter (baseline method). For the MWF, the average and median sensitivity was higher but also the FAR was higher. For the WCCA, the sensitivity was lower and FAR higher.

B.3 Conclusion

No real improvements were seen for the different filtering techniques compared to a bandpass filter. Further research is needed to determine why those approaches didn't work. To further investigate the MWF method, it could be interesting to start from full channel and make a simulation of the performance in function of the number of channels. It is unknown how much channels we need to apply MWF.

Appendix C

Multimodal seizure detection: Appendix

C.1 The unimodal ECG-based algorithm: Comparison with state-of-the-art

C.1.1 Methods

The performance of our developed ECG-based seizure detection algorithm was compared with two other ECG-based seizure detection algorithms, De Cooman and colleagues [53] and Fürbass and colleagues [37]. Note that the developed algorithm is designed for offline usage and the state-of-the-algorithms [53, 37] can be used for real-time alarming. The Epilepsia - Freiburg database was used for comparison, since this data was not used for the algorithm development (in order to avoid any overfit concern). To compare the ECG-based algorithm with state-of-the-art patient-independent algorithms, a 'sensitivity in function of FAR' was constructed. The performance of the whole dataset was calculated for every cut-off probability value.

C.1.2 Results

In Figure C.1, the performance is compared to two state-of-the-art ECG-based seizure detection algorithms. Fürbass and colleagues [82] achieved a sensitivity of 39.35% with an FAR of 0.18 per hour. With the same FAR, our algorithm

had a sensitivity of 48.7%. De Cooman and colleagues [53] achieved a sensitivity of 71.02% with 2.43 FP/hour, whereas our algorithm had a sensitivity of 84.1% with the same FAR.

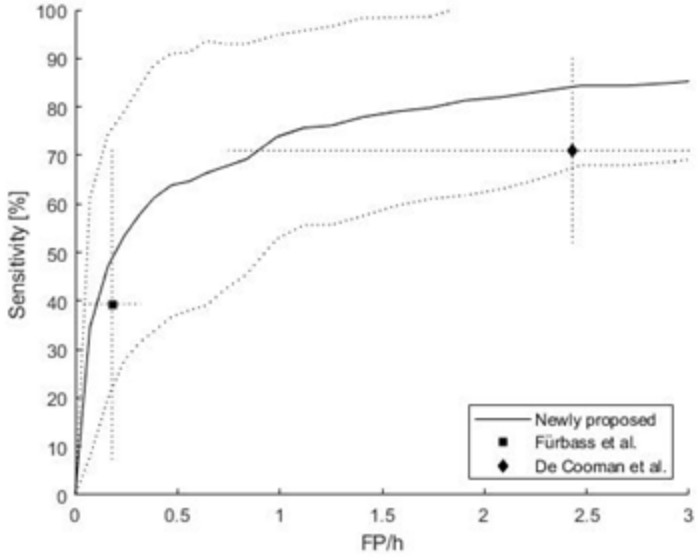


Figure C.1: Performance comparison of our proposed ECG-based seizure detection algorithm. The sensitivity versus FAR is plotted together with the standard deviation on the sensitivity [dotted lines]. The sensitivity and FAR is shown for two state-of-the-art solutions: Fürbass [82] and De Cooman et al. [53], the dotted lines indicate the standard deviation in two directions: the FAR and sensitivity.

C.1.3 Discussion

Increased sensitivities were observed by comparing to two state-of-the-art algorithms with the same FARs.

C.2 The unimodal ECG-based algorithm: Extracted features

We list here the used features for the proposed ECG-based seizure detection. Please refer to the given references for detailed descriptions of the different mentioned features.

C.2.1 Time domain HRV features

Each R-peak is detected and the so-called normal-to-normal (NN) intervals, which are the time intervals between adjecent Rpeaks)

1. The mean NN interval
2. The standard deviation of the NN intervals (SDNN)
3. The ratio of the standard deiation of NN intervals and mean NN interval
4. The difference between feature value 1 of the current window and its value of the previous window
5. The difference between feature value 2 of the current window and its value of the previous window
6. The difference between feature value 3 of the current window and its value of the previous window
7. The root mean squre of successive difference (RMSSD) of the NN intervals
8. Percentage of the difference in two successive NN intervals that is larger than 0.005 seconds
9. Percentage of the difference in two successive NN intervals that is larger than 0.01 seconds
10. Percentage of the difference in two successive NN intervals that is larger than 0.015 seconds
11. Percentage of the difference in two successive NN intervals that is larger than 0.02 seconds
12. Percentage of the difference in two successive NN intervals that is larger than 0.025 seconds

13. The standard deviation of the successive differences between adjecent NN intervals
14. The maximum value of the successive differences between adjecent NN intervals
15. Feature 1 of the previous window
16. Feature 2 of the previous window
17. Feature 3 of the previous window
18. Feature 7 of the previous window
19. Feature 8 of the previous window
20. Feature 9 of the previous window
21. Feature 10 of the previous window
22. Feature 11 of the previous window
23. Feature 12 of the previous window
24. Feature 13 of the previous window
25. Feature 14 of the previous window
26. Feature 15 of the previous window
27. Feature 1 of the next window
28. Feature 2 of the next window
29. Feature 3 of the next window
30. Feature 7 of the next window
31. Feature 8 of the next window
32. Feature 9 of the next window
33. Feature 10 of the next window
34. Feature 11 of the next window
35. Feature 12 of the next window
36. Feature 13 of the next window
37. Feature 14 of the next window
38. Feature 15 of the next window

C.2.2 Frequency domain HRV features

39. The absolute power in the very low frequency (VLF) component (0-0.04 Hz).
40. The absolute power in the low frequency (LF) component (0.04 - 0.15 Hz).
41. The absolute power in the high frequency (HF) component (0.15 - 0.4 Hz).
42. The logarithm of the total power.
43. The ratio between LF and HF.
44. The ratio between VLF and HF.
45. The shannon entropy of the NN intervals
46. The shannon entropy on the power spectral density values of the ECG signal
47. features 46 of the previous window
48. features 47 of the previous window
49. features 48 of the previous window
50. features 49 of the previous window
51. features 50 of the previous window
52. features 51 of the previous window
53. features 52 of the previous window
54. features 53 of the previous window
55. features 46 of the next window
56. features 47 of the next window
57. features 48 of the next window
58. features 49 of the next window
59. features 50 of the next window
60. features 51 of the next window
61. features 52 of the next window
62. features 53 of the next window

C.2.3 Features Jeppesen et al. [115]

Features were derived from the Lorenz plot (or Poincare plot).

63. The standard deviation SD1 of the transverse direction of the Lorenz plot.
64. The standard deviation SD2 of the longitudinal direction of the Lorenz plot.
65. The ratio of SD2 and SD1
66. The logarithm of the product of SD1 and SD2
67. The modified cardiac sympathetic index (CSI), Calculated by L^2/T with T four times the standard deviation of the spreak in the transverse axis and L four times the standard deviation of the spread in the longitudinal axis

C.2.4 Features Doyle et al. [64]

68. The del_+ feature is computed using sequential trend analysis, which involves plotting the first derivative of the NN intervals as a function of the immediately preceding one. Del_+ is the concentration of points in the first quandrant (+/+ axis)
69. The del_- feature is the concentration of points in the 3rd quadrant (-/- axis)
70. The line length of the ECG signal
71. The number of zero-crossings of the ECG signal

C.2.5 Features De Cooman et al. [53]

Features were derived from the heart rate increases (HRI), occuring in the specific time window.

72. The maximal duration of the HRI in number of heart beats
73. The maximal slope (or heart rate gradient) during the HRI
74. The maximal HR obtained during the HRI

75. The signal qualitity index, based on RR matching [180]
76. The heart rate at the start of the HRI
77. The duration of HRI in seconds
78. The ratio of the maximum heart rate and the average heart rate during the HRI
79. The difference between the peak heart rate and the heart rate at the start of the HRI
80. The heart rate at the end of the HRI
81. The mean heart rate after the HRI when the new baseline is reached
82. The needed time to reach the new baseline
83. The average HR before the HRI
84. The ratio of the mean HR after the HRI and mean HR before the HRI
85. The number of heart beats higher than 110% of the mean HR before the HRI
86. The number of heart beats higher than 120% of the mean HR before the HRI
87. The number of heart beats higher than 130% of the mean HR before the HRI
88. The number of heart beats higher than 140% of the mean HR before the HRI
89. The number of heart beats higher than 150% of the mean HR before the HRI
90. The number of heart beats higher than 160% of the mean HR before the HRI
91. The number of heart beats higher than 20 bpm + mean HR before HRI
92. The number of heart beats higher than 30 bpm + mean HR before HRI
93. The number of heart beats higher than 40 bpm + mean HR before HRI
94. The number of heart beats higher than 50 bpm + mean HR before HRI
95. The number of heart beats higher than 60 bpm + mean HR before HRI

C.2.6 Circadian Rhythm Features

Heart rate characteristics fluctuate throughout the day which is called the circadian rhythm. Circadian features are extracted.

96. The mean value of the circadian NN intervals
97. The standard deviation of the circadian NN intervals
98. The ratio between feature 98 and 97
99. The root mean square of successive differences of the circadian NN intervals
100. The standard deviation of successive differences of the circadian NN intervals
101. The mean value of successive differences of the circadian NN intervals
102. the maximum value of the successive differences of the circadian NN intervals

C.2.7 Features related to the noise level [180]

103. The maximum value of the kurtosis, calculated based on the previous 10 seconds
104. The minimum value of the kurtosis, calculated based on the previous 10 seconds
105. The mean value of the krutosis, computed on 10 seconds windows
106. The fusion signal quality index (FSQI) determines whether the ECG segment is of low or high quality based on the level of agreement of two heart peak detectors [120].
107. The relative power of the powerline interference at 50Hz and harmonics
108. The relative power of the high frequency noise
109. The ECGSQI provides a signal quality estimate of an ECG signals [87].

C.2.8 Point process features [40]

110. The mean spectral power.
111. The maximum spectral low-frequency power.
112. The maximum spectral high-frequency power.
113. The maximum value of the ratio of the spectral low-frequency power and the spectral high-frequency power
114. The maximum spectral power.
115. The mean very low frequency (VLF) power.
116. The mean low frequency (LF) power.
117. The mean high frequency (HF) power.
118. The ratio of the mean low frequency (LF) power and mean high frequency (HF) power.

C.2.9 Features Osorio et al. [181, 182]

119. The maximum threshold value for the R peak detection of the ECG signal
120. The duration in which the HR in the current window is higher than 115% of the average HR in the reference window in the past
121. The duration in which the HR in the current window is higher than 120% of the average HR in the reference window in the past
122. The duration in which the HR in the current window is higher than 125% of the average HR in the reference window in the past
123. The duration in which the HR in the current window is higher than 130% of the average HR in the reference window in the past
124. The maximum value of the short-term window.
125. The average value of the heart rate in a long-term window
126. The standard deviation of the heart rate in a long-term window

C.2.10 Features Ungureanu et al. [244]

119. The age of the patient
120. The maximum value of a tachycardiac event (CS+)
121. The minimum value of a bradycardic event (CS-)
122. The threshold of the algorithm based on age
123. The maximum duration of positive values exceeding a positive threshold
124. The maximum duration of negative values exceeding a negative threshold

C.3 Detected seizures in function of seizure type and localization

Figure C.2 shows the percentage of detected seizures at a FAR of 1/hour for the modalities in function of seizure type (A) and localization (B). The percentage of seizures detected both with EEG and ECG was the highest for F-BTC seizures (74%) and the lowest for FA seizures (32%). The percentage detected with EEG only was the highest for UC seizures (34%), for ECG only this percentage was the highest for the FA group (13%). FA seizures have also the highest percentage of seizures not detected with any of the two modalities (26%). The percentage of seizures detected both with EEG and ECG was the highest for seizures with a (fronto/temporo)-parietal origin (60%), followed with the temporal (59%) and (temporo/parieto)-occipital origin (59%). Seizures with a frontal origin have the highest percentage of seizures detected with EEG only (41%), whereas the lowest percentage with ECG only (3%). The seizures with an unclear origin have the highest percentage of seizures not detected with any of the two modalities (20%), followed by the fronto-temporal seizures (18%) and (fronto/temporo)-parietal seizures (18%).

C.4 Probable reasons why seizures are not detected with EEG, while they are detected with ECG

53 seizures (6%) were detected only with ECG, which exhibits the added value of ECG in this study. 28 seizures (10%), 12 seizures (7%) and 13 seizures (3%) were detected only with ECG from Epilepsiae-Freiburg, SeizeIT1 and

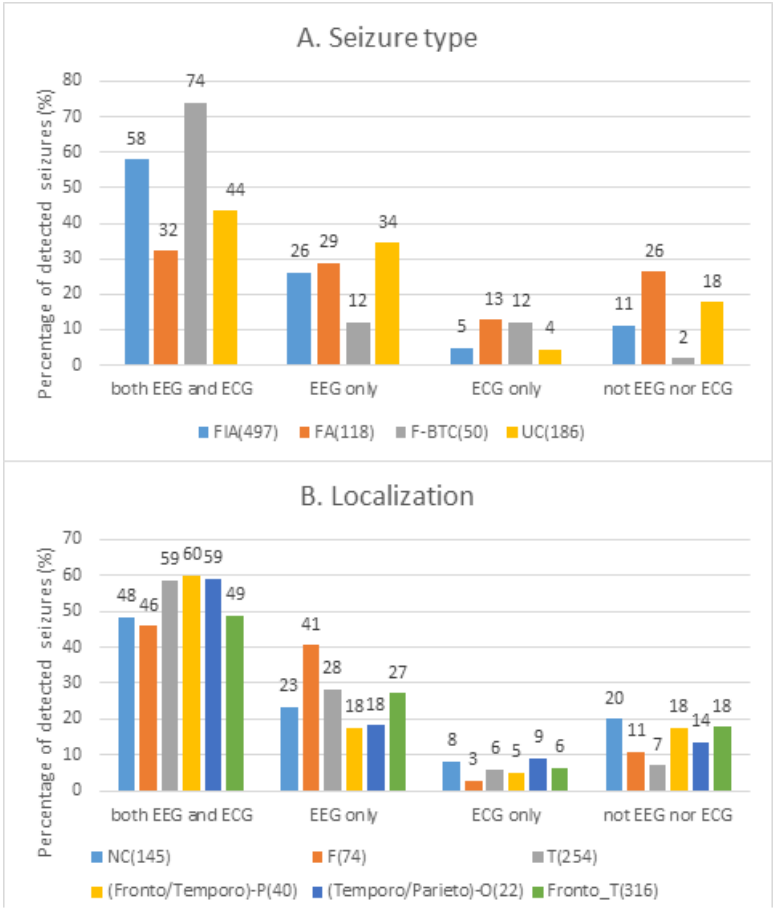


Figure C.2: Percentage of detected seizures at a FAR of 1/hour is displayed for the four groups: Seizures detected with both EEG and ECG, only with EEG, only with ECG or seizures not detected neither with EEG nor with ECG in function of Seizure type (A) and in function of localization (B). The number of seizures in each group is indicated in the legend.

Epilepsiae-Paris. Probable reasons why those seizures could not be picked up with EEG are listed.

- Artifacts were present (14 seizures): strong artifacts with electrode disconnection was observed during 1 seizure, strong artifacts without

visible ictal patterns were present during 5 seizures, artifacts with some ictal patterns could be seen during 8 seizures.

- No typical ictal pattern could be observed or the difference with the background EEG was minimal (11 seizures).
- No EEG correlates were observed (10 seizures). Only in the Epilepsiae - Freiburg database, seizures were present without any EEG correlates on full scalp.
- Seizures were not visible on the behind-the-ear electrodes, marked by a neurologist (5 seizures).
- There was no propagation to the temporal lobe, which was annotated in the Epilepsiae database (4 seizures).
- The seizure duration was shorter than 10 seconds. Due to the postprocessing rules, those seizures will be not detected (3 seizures).
- Some patterns are difficult to detect (for example: low amplitude fast activity). This is especially difficult when the majority of the patients' seizures have other patterns (3 seizures).
- Only 2 seizures were available per patient, as a result only one seizure is available to train the model and overfitting occurs (3 seizures).

Appendix D

Artifact detection of wrist photplethysmograph signals

The content of this chapter is taken from Vandecasteele et al. [256].

D.1 Abstract

There is a growing interest in monitoring of vital signs through wearable devices, such as heart rate (HR). A comfortable and non-invasive technique to measure the HR is pulse photoplethysmography (PPG) with the use of a smartwatch. This watch records also triaxial accelerometry (ACM). However, it is well known that motion and noise artifacts (MNA) are present. A MNA detection method, which classifies into a clean or MNA segment, is trained and tested on a dataset of 17 patients, each with a recording duration of 24 hours. PPG- and ACM-derived features are extracted and classified with a LS-SVM classifier. A sensitivity and specificity of respectively 85.50 % and 92.36 % are obtained. For this dataset, the ACM features do not improve the performance, suggesting that ACM recording could be avoided from the point of view for detecting MNA in PPG signals during daily life.

D.2 Introduction

There is a growing interest in wearable and continuous monitoring of vital signs, such as heart rate (HR). A comfortable and non-invasive technique to measure the HR is pulse photoplethysmography (PPG). PPG makes use of reflected or transmitted light through the skin to measure a pulsatile physiological waveform caused by changes in the blood volume due to a heart beat. Common PPG recording locations include fingers, ears, toes, forehead or wrist [6]. The wrist is a possible recording location. An advantage is that the PPG sensor can be embedded in a watch. However, it is well known that motion and noise artifacts (MNA) can distort the signal [189]. Those MNA are caused by 1) the movement of venous blood as well as other non-pulsatile components 2) variations in the optical coupling between the sensor and the skin [11, 239]. The MNA can be particularly challenging when computing derived features from the PPG waveform such as HR. Various design approaches to reduce MNA have been proposed [143]. With these improvements, MNA are stil present. Therefore, algorithm-based MNA reduction methods were proposed [241, 134, 81, 184, 241, 270, 202, 137, 237, 241, 124]. These MNA reduction algorithms operate also on clean parts of the signal, which is unnecessary computation and can cause distortion of the signal. Therefore an algorithm which can distinguish clean parts from MNA is desired. MNA detection algorithms are designed with the use of waveform morphologies [230, 144, 147, 73] or filtered output [172, 122]. Statistical measures, such as skewness, kurtosis, shannon entropy and Renyi's entropy have been shown useful for automatic detection of MNA [218, 128]. Another approach, using Hjorth parameters was proposed [89]. Other methods were published, which perform classification with a support vector machine (SVM) with time-domain features [38] or time-frequency spectrum analysis [44] .

To the best of our knowledge, all these methods are tested and validated for PPG recorded on the ears, fingers or forehead, but none have been validated on the wrist. Moreover, these methods are never tested on 24 hour recordings. In our paper, we propose an automated computer-based method for the detection of MNA in PPG signals, recorded with a wrist watch. The method is validated on 24-hour data recordings. The classification is performed with a LS-SVM model using previously published features [218, 89, 38], together with new features. Additional to the PPG signals, most smart watches also record the accelerometry (ACM). Therefore, it is investigated if the ACM improves the MNA detection method. A backwards wrapper feature selection is implemented to determine which features are the most discriminative ones. The goal of the paper is to provide a reliable MNA detection method, validated for wrist PPG signals, and additionally to evaluate whether the ACM improves the detection

performance.

D.3 Methodology

The methodology consists of five parts. Firstly, the data collection is described. Secondly, the extracted features from the PPG signal, are summarized. Thirdly, a LS-SVM-based classifier is discussed. Fourthly, a feature selection method is explained, which selects the most discriminative features. Lastly, the labelling process is explained. With the use of a reference signal, a label (Clean or MNA) is given to each PPG segment.

D.3.1 Data acquisition

The dataset, used in this experiment, contains recordings of 17 epilepsy patients, each with a duration around 24 hours. The epilepsy patients were recorded with a wired conventional multi-channel scalp EEG. Additionally to the standard clinical equipment, recordings were made with a wearable ECG device: the 180^o eMotion Faros [23], and a wrist-worn PPG device: the E4 Empatica wristband [70]. The Faros ECG was used in a single-channel configuration. The Empatica E4 measures reflective PPG using a green and a red LED on the wrist. The device returns a single channel which is obtained by combining the green and the red channels using Empatica's proprietary algorithm. Additional to the 1-channel PPG, the triaxial ACM is recorded. Considering that the intravenous insertion, used to administer medication in clinical practice, is routinely placed at the non-dominant wrist, the patients wore the Empatica watch on the dominant hand. The sampling rate of the Faros and Empatica (PPG/ACM) device are respectively 500Hz and 64Hz (PPG)/32 Hz (ACM).

D.3.2 Feature extraction

Features are extracted from both the PPG signal and ACM signal. Features from literature, which are previously shown to be useful, are combined with our own features. First, the PPG signal was preprocessed by a 5th order bandpass butterworth filter [0.5 - 12 Hz]. The ACM was preprocessed by a 3th order butterworth filter [0.2 - 10Hz]. The PPG signal and corresponding ACM data are segmented in 7 seconds, because it was reported to be the optimal segment length for MNA detection [38].

PPG

The following features were extracted from the PPG segments:

- Standard Deviation of Pulse-to-Pulse Interval (STD_{HR}), Standard Deviation of Pulse-to-Pulse Amplitude (STD_{amp}), Standard Deviation of Systolic and Diastolic Ratio (STD_{SD}) and Mean-Standard Deviation of Pulse Shape (STD_{WAV}), which are described in [38]
- Kurtosis (K) and Shannon Entropy (SE), which are described in [218]
- Variance (Var) of the signal segment
- The frequency of the first/second/third-largest peak in the power spectrum (FLP/SLP/TLP), which are expected to be around 1Hz (the HR frequency)/ 2Hz (the first harmonic)/ 3Hz (the second harmonic) for a clean segment
- Spectral Shannon entropy (SSE), which is the shannon entropy of the power spectrum
- Hjorth parameters: H1 and H2, which represents respectively the central frequency and half of the bandwidth [89]

In order to calculate the features STD_{HR} and STD_{amp}, the location and amplitude of the pulse peaks are needed. The feature STD_{SD} requires the systolic and diastolic time, which are respectively the rising time from valley to peak and the falling time from peak to the next valley. The feature STD_{WAV} require the alignment of the pulses in a segment, which is done with the peak location. To calculate the location and amplitude of the pulse peaks and pulse valleys, an algorithm developed in [136] is used. This algorithm consists of two phases: a linear filtering transformation and an adaptive thresholding operation. The filtering step consists of a linear-phase FIR low-pass-differentiator filter, which is used to accentuate the abrupt upslopes of the PPG pulses. The abrupt upslopes correspond to peaks in the filtered signal, which are detected by an adaptive thresholding operation. Once the peaks in the filtered signal are found, the maximum and minimum point in the original PPG signal are found.

ACM

The following features were extracted from each direction and Euclidean norm of the ACM segments:

1. The maximal value of the rectified segment (max_x,max_y,max_z and max_{norm})
2. The 90th percentile of the rectified segment (90_x,90_y,90_z and 90_{norm})
3. The Variance of the segment (Var_x,Var_y,Var_z and Var_{norm})
4. The mean absolute deviation of the segment (MAD_x,MAD_y,MAD_z and MAD_{norm})
5. The norm of the segment ($Norm_x$,$Norm_y$,$Norm_z$ and $Norm_{norm}$)

D.3.3 LS-SVM based classification of MNA

The classification is done with a LS-SVM (Least Squares Support Vector Machines) classifier [45] using a linear kernel. The classifier is trained and tested within a leave-one-patient-out cross-validation (LOPO-CV) approach. In this way, no data of the patient itself is used for the training. To evaluate the classifier, the sensitivity (proportion of MNA segments that are correctly classified), the specificity (the proportion of clean segments that are correctly classified) and the accuracy are calculated. The classifier is tested with only PPG features, only ACC features and all the features together.

D.3.4 Feature selection

In order to investigate which features are discriminative for clean and MNA PPG segments, a backwards wrapper feature selection method is implemented. In Figure D.1 a flow diagram of the method is shown. At the start, the total feature set is used to train and test the classifier within a LOPO-CV approach. As evaluation criteria, the F1-score is calculated, which is the harmonic mean of the sensitivity and the specificity. In a next step, new feature sets are created by leaving out each feature one time. So, if there are N features, N new feature sets are created. Again the classifier is trained and tested with these new feature sets within a LOPO-CV approach and the F1-scores are calculated. Next, the maximal F1-score, corresponding to the best new feature set, is compared with the original F1-score. If this F1-score is higher or equal, this feature doesn't improve the classification problem and is removed. Whole the procedure is calculated again by starting with the new feature set, corresponding to the highest F1-score. With every iteration only 1 feature can be removed. The method will stop when all the new F1-scores are lower.

The feature selection procedure was performed on the PPG features, ACM features and all the features together.

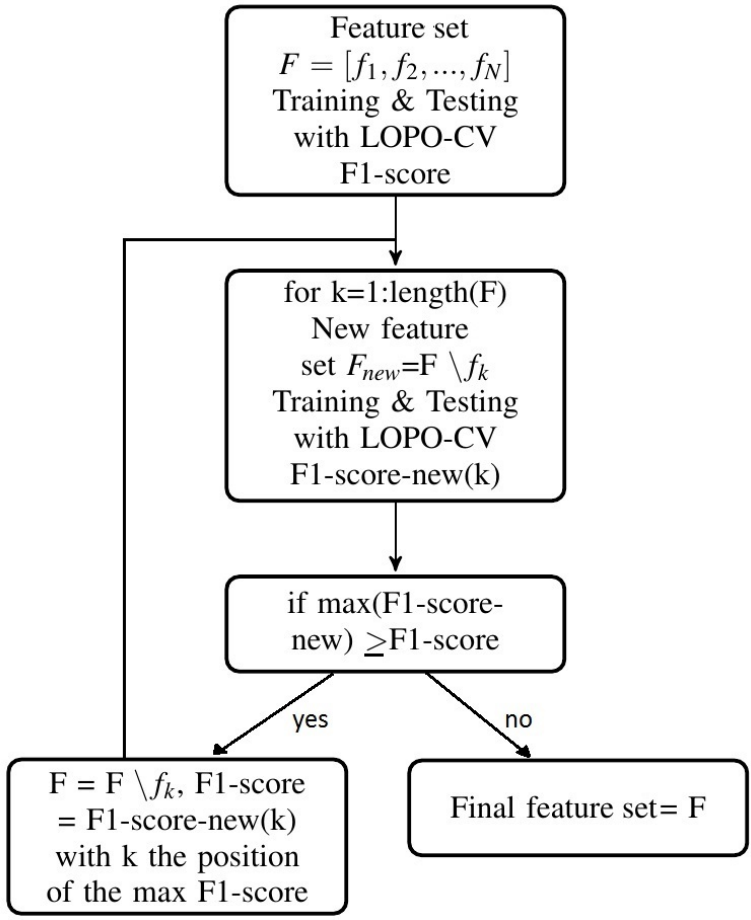


Figure D.1: Flowchart: Backwards wrapper feature selection

D.3.5 Reference signal: ECG

In order to train and test a classifier, labels for each segment are needed. A visual reference is avoided because it's very subjective, i.e. different visual inspectors annotate the segments differently. Furthermore, it would be very time consuming to annotate a whole dataset of 408 hours (17*24 hours). Instead, we performed an automatic labelling procedure based on the reference electrocardiography (ECG) signal, similarly as in [38]. The heart rate variability (HRV) is calculated, by finding the location of the R-peaks [260]. For each PPG segment and

corresponding ECG segment, the mean RR-interval (RR_{ECG}) and mean PP-interval (PP_{PPG}) and standard deviation of the RR- and PP-interval (STD_{ECG} and STD_{PPG}) are calculated. A segment is classified as MNA, if $|RR_{ECG} - PP_{PPG}| > 150ms$ or $|STD_{ECG} - STD_{PPG}| > 100ms$. These thresholds are set empirically based on a subset of the data.

D.4 Results and discussion

D.4.1 Feature selection

In table D.1, D.2 and D.3 the selected features are shown in bold, starting from respectively the PPG, ACM and all the features. From the newly proposed PPG features, 3 features are retained by the feature selection: the variance, the frequency of the second and third largest peak in the power spectrum. These 3 features do have an added value for the MNA detection algorithm. The feature selection process with the ACM features shows that all features which make use of the y-direction are left out. The y-direction is the direction along the lower arm, from wrist towards the elbow, as shown in Fig. D.2. The accelerometry in this direction doesn't have an added value for the algorithm for this dataset.

It might be that motion in the y-direction, which is along the direction of the lower arm, causes less MNA than the other directions. Another reason can be that this direction is less present during daily motion compared to the other directions. The feature selection process with all the features shows that 4 from the 13 PPG-derived and 10 from the 20 ACM-derived features are removed. It seems that the ACM-features have an added value, but this added value is only minor. With all the resulting features, a F1-score of 0.8841 is obtained. If 1 of those PPG-derived features is removed, a F1-score between 0.8474 and 0.8836 is obtained. If one of the ACM-derived features is removed, a F1-score between 0.8831 and 0.8841 is obtained. So leaving out a ACM-feature would only decrease the F1-score slightly.

D.4.2 Classification performance

In Figure D.3 the sensitivities (Sens), specificities (Spec) and accuracies (Acc) are plotted for all the patients. The sensitivity (specificity) is the proportion of MNA (clean) segments that are correctly classified. The accuracy is the proportion of segments that are correctly classified. In Table D.4 the average values $\pm$ standard deviations are shown.

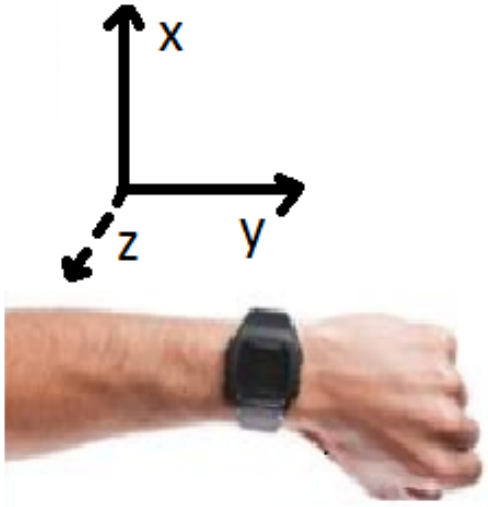


Figure D.2: ACM axis

Table D.1: Feature selection PPG

Standard Deviation of Pulse-to-pulse Interval/Amplitude
Standard Deviation of Systolic and Diastolic rate
Mean-standard deviation of Pulse shape
Kurtosis and Shannon Entropy
Variance
Frequency of the first/second/third-largest peak in the PSD
Spectral Shannon Entropy
Hjorth parameters: H1 and H2

Table D.2: Feature selection ACC

max_x, max_y, max_z and $\mathbf{max_{norm}}$
$\mathbf{90_x}$, 90_y, $\mathbf{90_z}$ and $\mathbf{90_{norm}}$
$\mathbf{Var_x}$, Var_y, $\mathbf{Var_z}$ and $\mathbf{Var_{norm}}$
$\mathbf{MAD_x}$, MAD_y, $\mathbf{MAD_z}$ and $\mathbf{MAD_{norm}}$
$Norm_x$, $Norm_y$, $Norm_z$ and $\mathbf{Norm_{norm}}$

Table D.3: Feature selection ALL

$\mathbf{STD_{HR}}$, $\mathbf{STD_{amp}}$, $\mathbf{STD_{SD}}$ and $\mathbf{STD_{WAV}}$
K and SE
Var
FLP, **SLP** and **TLP**
SSE
H1 and H2
$\mathbf{max_x}$, max_y, max_z and $\mathbf{max_{norm}}$
90_x, $\mathbf{90_y}$, $\mathbf{90_z}$ and $\mathbf{90_{norm}}$
Var_x, Var_y, Var_z and Var_{norm}
MAD_x, MAD_y, $\mathbf{MAD_z}$ and $\mathbf{MAD_{norm}}$
$\mathbf{Norm_x}$, $Norm_y$, $\mathbf{Norm_z}$ and $\mathbf{Norm_{norm}}$

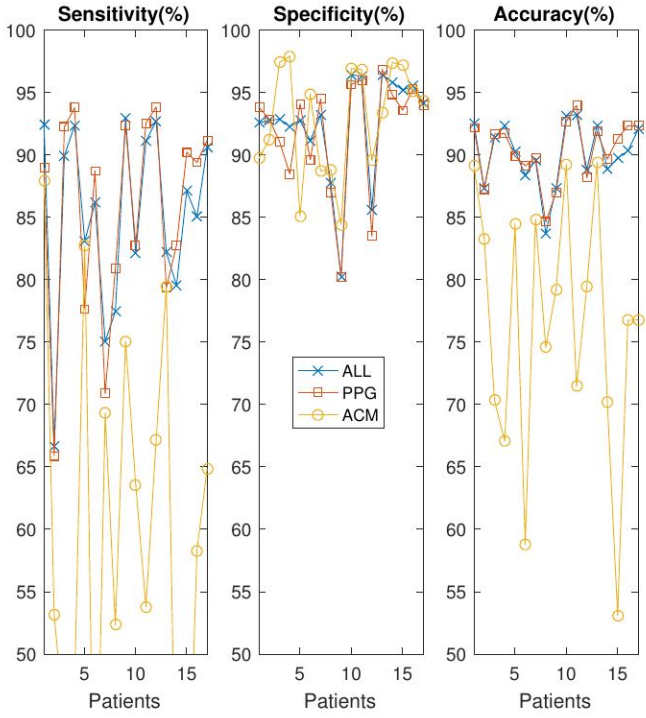


Figure D.3: Classification performance

The performance with PPG features is similar as the performance with all features. Adding the ACM features to the classification does not increase the

Table D.4: Classification performance

	PPG	ACM	ALL
Sens (%)	85.50 ± 8	58.04 ± 18	85.50 ± 7
Spec (%)	91.84 ± 5	93.01 ± 4	92.36 ± 4
Acc (%)	90.33 ± 2	76.23 ± 11	90.23 ± 3

performance. The reason is that the PPG signal has already enough information on itself. The MNA segments show large differences with clean segments, which is illustrated in Figure D.4.

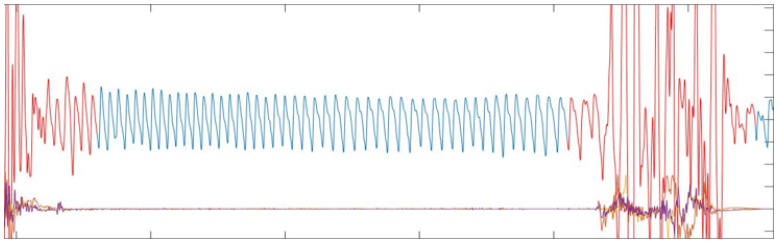


Figure D.4: Example: Clean (blue) and MNA (red) PPG segments with 3 axis ACM

By using only the ACM features, a low sensitivity is obtained. This is due to the fact that not all kind of MNA are caused by wrist motion. For example subtle finger motion, which is shown in Figure D.5, or bad positioning of the sensor cause MNA, but there is no corresponding ACM activation.

In table D.5 previous experiments and results from literature are summarized. In all the studies reflective PPG with infrared light is recorded. The dataset and sensor type are different for each study, which makes it difficult to compare quantitatively the results.

D.4.3 Overall data quality

In total 44.26% ± 16.20% of the data is labeled as MNA based on the reference signal, 43.38% ± 15.62% of the data is detected as MNA by the algorithm. This means that close to half of the measured data are contaminated with MNA, so that the heart rate variability cannot be reliably estimated by the algorithm [136] from the recorded signals. Note that our dataset was acquired from patients in a hospital environment. The patients are continuously monitored with wired

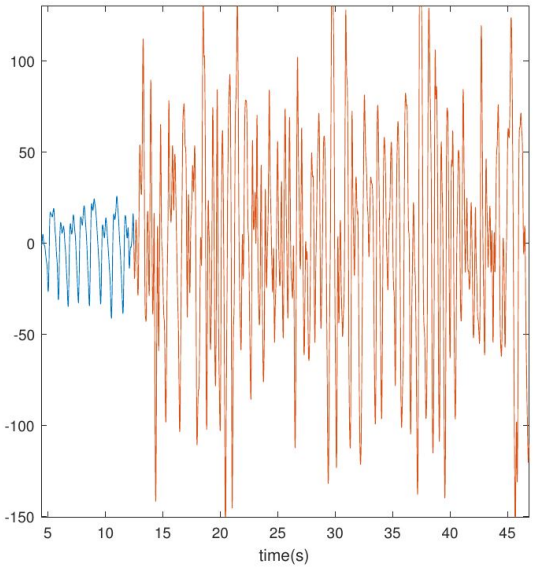


Figure D.5: Example: Clean (blue) and MNA, caused by finger motion, (red) PPG

EEG, which limit their mobility. Outside the hospital these percentages are probably even higher.

D.4.4 Limitations and further work

The algorithm is tested on a data set, recorded in the hospital. The algorithm should also be tested on daily life data, recorded outside the hospital.

Only one type of sensor is tested (wrist reflective PPG). It should be extended to other sensors. In order to compare the different studies, the MNA detection algorithms should be tested on the same data sets.

The MNA detection method, explained in this paper, makes use of a fixed window length of 7s. A method should be investigated to automatically determine the length of the MNA.

Other models should be tested for this classification problem, for example deep neural networks.

Extracting HR and HRV is more challenging during these artifactual segments

Table D.5: Comparison with literature [Rec.=Recording, Acc=Accuracy, Se=Sensitivity, Sp=Specificity, Results are in %].

No. subjects	Sensor type	Type of movement	Results
Sukor et al., 2011			
13 (8 min)	Finger	Hand movements	Acc: 83 ± 11 Se: 89 ± 10 Sp: 77 ± 19
Selvaraj et al., 2011			
10 (5 - 20 min)	Ear/ Finger/ Forehead	Involuntary movements	Acc: 99.0/94.8/93.3 Se: 100/99.3/96.3 Sp: 98.9/93.8/91.9
14 (10 min)	Finger	Voluntary movements	Acc: 88.8 Se: 86.9 Sp: 98.3
Chong et al., 2014			
11 (10 min)	Forehead	Head movement	Acc: 94.4 ± 3.3 Se: 94.7 ± 3.4 Sp: 94.7 ± 4.5
9 (10 min)	Finger	Finger movement	Acc: 93.4 ± 3.5 Se: 88.8 ± 7.9 Sp: 96.7 ± 3.0
9 (45 min)	Finger/Forehead	Stair-climbing	Acc: 93.7 ± 2.7 Se: 93.9 ± 5.0 Sp: 91.4 ± 2.0
Dao et al., 2016			
11 (10 min)	Forehead	Head movement	Acc: 95.7 ± 0.82 Se: 93.0 ± 5.75 Sp: 96.6 ± 1.48
11 (10 min)	Finger	Finger movement	Acc: 97.5 ± 1.50 Se: 96.4 ± 2.34 Sp: 98.1 ± 1.43
10	Forehead	UMMC hospital	Acc: 95.3 ± 1.34 Se: 90.8 ± 2.83 Sp: 98.7 ± 1.07
10	Finger	UMMC hospital	Acc: 94.3 ± 1.64 Se: 88.5 ± 2.23 Sp: 96.9 ± 1.86

and further signal processing techniques are needed. Further studies must be elaborated to assess how these MNA affect to the different HRV indices.

D.5 Conclusions

The goal of the paper is to provide a reliable motion and noise artifact (MNA) detection method for PPG signals, recorded with a wrist watch. PPG- and ACM-derived features are extracted and classified with a LS-SVM classifier. For

this dataset, the ACM features do not improve the performance, suggesting that ACM recording could be avoided from the point of view for detecting MNAs in PPG signals.

Bibliography

[1] Flanders AI Research program. https://airesearchflanders.be/, 2021. [Online; accessed 25-January-2021].

[2] Aboukhalil, A., Nielsen, L., Saeed, M., Mark, R. G., and Clifford, G. D. Reducing false alarm rates for critical arrhythmias using the arterial blood pressure waveform. *Journal of biomedical informatics 41*, 3 (2008), 442–451.

[3] Acharya, U. R., Oh, S. L., Hagiwara, Y., Tan, J. H., and Adeli, H. Deep convolutional neural network for the automated detection and diagnosis of seizure using eeg signals. *Computers in biology and medicine 100* (2018), 270–278.

[4] Akbani, R., Kwek, S., and Japkowicz, N. Applying support vector machines to imbalanced datasets. In *Machine Learning: ECML 2004*. Springer, 2004, pp. 39–50.

[5] Akbani, R., Kwek, S., and Japkowicz, N. Applying support vector machines to imbalanced datasets. In *European conference on machine learning* (2004), Springer, pp. 39–50.

[6] Allen, J. Photoplethysmography and its application in clinical physiological measurement. *Physiol. Meas. 28*, 3 (2007), R1–R39.

[7] Altaf, F., Islam, S. M., Akhtar, N., and Janjua, N. K. Going deep in medical image analysis: concepts, methods, challenges, and future directions. *IEEE Access 7* (2019), 99540–99572.

[8] Ammanuel, S. G., Kleen, J. K., Leonard, M. K., and Chang, E. F. Interictal epileptiform discharges and the quality of human intracranial neurophysiology data. *Frontiers in Human Neuroscience 14* (2020).

[9] Ansari, A. H., Cherian, P. J., Caicedo, A., Naulaers, G., De Vos, M., and Van Huffel, S. Neonatal seizure detection using deep convolutional neural networks. *International journal of neural systems 29*, 04 (2019), 1850011.

[10] Arends, J., Thijs, R. D., Gutter, T., Ungureanu, C., Cluitmans, P., Van Dijk, J., van Andel, J., Tan, F., de Weerd, A., Vledder, B., et al. Multimodal nocturnal seizure detection in a residential care setting: A long-term prospective trial. *Neurology 91*, 21 (2018), e2010–e2019.

[11] Barker, S.J, and Shah, N.K. The effects of motion on the performance of pulse oximeters in volunteers (revised publication). *Anesthesiology*, 86 (1997), 101–108.

[12] Baumgartner, C., and Koren, J. P. Seizure detection using scalp-eeg. *Epilepsia 59* (2018), 14–22.

[13] Becker, T., Vandecasteele, K., Chatzichristos, C., Van Paesschen, W., Valkenborg, D., Van Huffel, S., and De Vos, M. Classification with a deferral option and low-trust filtering for automated seizure detection. *Sensors 21*, 4 (2021), 1046.

[14] Behar, J., Oster, J., Li, Q., and Clifford, G. A single channel ecg quality metric. In *2012 Computing in Cardiology* (2012), IEEE, pp. 381–384.

[15] Behar, J., Oster, J., Li, Q., and Clifford, G. D. Ecg signal quality during arrhythmia and its application to false alarm reduction. *IEEE transactions on biomedical engineering 60*, 6 (2013), 1660–1666.

[16] Ben-Menachem, E. Vagus-nerve stimulation for the treatment of epilepsy. *The Lancet Neurology 1*, 8 (2002), 477–482.

[17] Beniczky, S., Conradsen, I., Henning, O., Fabricius, M., and Wolf, P. Automated real-time detection of tonic-clonic seizures using a wearable emg device. *Neurology 90*, 5 (2018), e428–e434.

[18] Beniczky, S., Karoly, P., Nurse, E., Ryvlin, P., and Cook, M. Machine learning and wearable devices of the future. *Epilepsia* (2020).

[19] Beniczky, S., Polster, T., Kjaer, T. W., and Hjalgrim, H. Detection of generalized tonic–clonic seizures by a wireless wrist accelerometer: a prospective, multicenter study. *Epilepsia 54*, 4 (2013), e58–e61.

[20] Beniczky, S., and Ryvlin, P. Standards for testing and clinical validation of seizure detection devices. *Epilepsia 59* (2018), 9–13.

[21] Bennis, F. C., Geertsema, E. E., Velis, D. N., Reus, E. E., and Visser, G. H. The use of single bipolar scalp derivation for the detection of ictal events during long-term eeg monitoring. *Epileptic Disorders 19*, 3 (2017), 307–314.

[22] Biau, G., and Scornet, E. A random forest guided tour. *Test 25*, 2 (2016), 197–227.

[23] Bittium Biosignals Ltd. eMotion Faros 180. `http://www.megaemg.com/products/faros/`, 2017. [Online; accessed 22-August-2017].

[24] Bleichner, M. G., and Debener, S. Concealed, unobtrusive ear-centered eeg acquisition: ceegrids for transparent eeg. *Frontiers in human neuroscience 11* (2017), 163.

[25] Blum, D., Eskola, J., Bortz, J., and Fisher, R. Patient awareness of seizures. *Neurology 47*, 1 (1996), 260–264.

[26] Boeckx, S., Van Paesschen, W., Bonte, B., and Dan, J. Live demonstration: Seizeit-a wearable multimodal epileptic seizure detection device. In *2018 IEEE Biomedical Circuits and Systems Conference (BioCAS)* (2018), IEEE, pp. 1–1.

[27] Boon, P., Vonck, K., van Rijckevorsel, K., El Tahry, R., Elger, C. E., Mullatti, N., Schulze-Bonhage, A., Wagner, L., Diehl, B., Hamer, H., et al. A prospective, multicenter study of cardiac-based seizure detection to activate vagus nerve stimulation. *Seizure 32* (2015), 52–61.

[28] Boon, P., Vonck, K., van Rijckevorsel, K., El Tahry, R., Elger, C. E., Mullatti, N., Schulze-Bonhage, A., Wagner, L., Diehl, B., Hamer, H., et al. A prospective, multicenter study of cardiac-based seizure detection to activate vagus nerve stimulation. *Seizure 32* (2015), 52–61.

[29] Boonyakitanont, P., Lek-Uthai, A., Chomtho, K., and Songsiri, J. A review of feature extraction and performance evaluation in epileptic seizure detection using eeg. *Biomedical Signal Processing and Control 57* (2020), 101702.

[30] Breningstall, G. N. Mortality in pediatric epilepsy. *Pediatric neurology 25*, 1 (2001), 9–16.

[31] Britton, J. W., Frey, L. C., Hopp, J. L., Korb, P., Koubeissi, M. Z., Lievens, W. E., Pestana-Knight, E. M., and St, E. L. *Electroencephalography (EEG): An introductory text and atlas of normal and abnormal findings in adults, children, and infants.* American Epilepsy Society, Chicago, 2016.

[32] Byteflies. Byteflies. `https://www.byteflies.com/`, 2021. [Online; accessed January 2021].

[33] Callaerts, J. *Transfer learning in deep neural networks for epileptic seizure detection.* PhD thesis, KU Leuven, 2020.

[34] Cascino, G. D. Surgical treatment for epilepsy. *Epilepsy research 60*, 2-3 (2004), 179–186.

[35] Castiglioni, P., Meriggi, P., Faini, A., and Di Rienzo, M. Cepstral based approach for online quantification of ecg quality in freely moving subjects. In *2011 Computing in Cardiology* (2011), IEEE, pp. 625–628.

[36] Chatzichristos, C., Dan, J., Narayanan, A. M., Seeuws, N., Vandecasteele, K., De Vos, M., Bertrand, A., and Van Huffel, S. Epileptic seizure detection in eeg via fusion of multi-view attention-gated u-net deep neural networks. In *Proceedings of the IEEE Signal Processing in Medicine and Biology Symposium (SPMB)* (2020), p. 7.

[37] Chen, W., Guo, C.-L., Zhang, P.-S., Liu, C., Qiao, H., Zhang, J.-G., and Meng, F.-G. Heart rate changes in partial seizures: analysis of influencing factors among refractory patients. *BMC neurology 14*, 1 (2014), 135.

[38] Chong, J. W., Dao, D. K., Salehizadeh, S. M., McManus, D. D., Darling, C. E., Chon, K. H., and Mendelson, Y. Photoplethysmograph Signal Reconstruction Based on a Novel Hybrid Motion Artifact Detection – Reduction Approach. Part I: Motion and Noise Artifact Detection. *Ann. Biomed. Eng. 42*, 11 (2014), 2238–2250.

[39] Chudáček, V., Zach, L., Kužílek, J., Spilka, J., and Lhotská, L. Simple scoring system for ecg quality assessment on android platform. In *2011 Computing in Cardiology* (2011), IEEE, pp. 449–451.

[40] Citi, L., Klerman, E., Brown, E. N., and Barbieri, R. Point process heart rate variability assessment during sleep deprivation. In *2010 Computing in Cardiology* (2010), IEEE, pp. 721–724.

[41] Clifford, G., Behar, J., Li, Q., and Rezek, I. Signal quality indices and data fusion for determining clinical acceptability of electrocardiograms. *Physiological measurement 33*, 9 (2012), 1419.

[42] Cogan, D., Birjandtalab, J., Nourani, M., Harvey, J., and Nagaraddi, V. Multi-biosignal analysis for epileptic seizure monitoring. *International journal of neural systems 27*, 01 (2017), 1650031.

[43] Cogan, D., Heydarzadeh, M., and Nourani, M. Personalization of noneeg-based seizure detection systems. In *Engineering in Medicine and Biology Society (EMBC), 2016 IEEE 38th Annual International Conference of the* (2016), IEEE, pp. 6349–6352.

[44] Dao, D., Salehizadeh, S. M. A., Noj, Y., Chong, J. W., Cho, C., Mcmanus, D., Darling, C. E., Mendelson, Y., and Chon, K. H. A Robust Motion Artifact Detection Algorithm for Accurate Detection of Heart Rates from Photoplethysmographic Signals using Time-Frequency Spectral Features. *IEEE J. Biomed. Heal. informatics 21*, 5 (2016), 1242–1253.

[45] De Brabanter, K., Karsmakers, P., Ojeda, F., Alzate, C., De Brabanter, J., Pelckmans, K., De Moor, B., Vandewalle, J., and Suykens, J. a. K. LS-SVMlab Toolbox User's Guide. *Pattern Recognit. Lett. 3*, February (2003), 179–202.

[46] De Clercq, W., Vergult, A., Vanrumste, B., Van Paesschen, W., and Van Huffel, S. Canonical correlation analysis applied to remove muscle artifacts from the electroencephalogram. *IEEE transactions on Biomedical Engineering 53*, 12 (2006), 2583–2587.

[47] De Cooman, T. *Epileptic Seizure Detection in a Home Environment.* PhD thesis, KU Leuven, 2018.

[48] De Cooman, T., Carrette, E., Boon, P., Meurs, A., and Van Huffel, S. Online seizure detection in adults with temporal lobe epilepsy using single-lead ECG.

[49] De Cooman, T., Goovaerts, G., Varon, C., Widjaja, D., Willemen, T., and Van Huffel, S. Heart beat detection in multimodal data using automatic relevant signal detection. *Physiological measurement 36*, 8 (2015), 1691.

[50] De Cooman, T., Kjær, T. W., Van Huffel, S., and Sorensen, H. B. Adaptive heart rate-based epileptic seizure detection using real-time user feedback. *Physiological measurement 39*, 1 (2018), 014005.

[51] De Cooman, T., Van De Vel, A., Ceulemans, B., Lagae, L., Vanrumste, B., and Van Huffel, S. Online detection of tonic-clonic seizures in pediatric patients using ECG and low-complexity incremental novelty detection. In *Proc. Annu. Int. Conf. IEEE Eng. Med. Biol. Soc. EMBS* (2015).

[52] De Cooman, T., Vandecasteele, K., Varon, C., Hunyadi, B., Cleeren, E., Van Paesschen, W., and Van Huffel, S. Personalizing heart rate-based seizure detection using supervised svm transfer learning. *Frontiers in Neurology 11* (2020), 145.

[53] De Cooman, T., Varon, C., Hunyadi, B., Van Paesschen, W., Lagae, L., Huffel, S. V., and Van Huffel, S. Online automated seizure detection in temporal lobe epilepsy patients using single-lead ECG. *Int. J. Neural Syst. 27*, 0 (2017), 1–17.

[54] De Cooman, T., Varon, C., Van de Vel, A., Ceulemans, B., Lagae, L., and Van Huffel, S. Comparison and combination of electrocardiogram, electromyogram and accelerometry for tonic-clonic seizure detection in children. In *2018 IEEE EMBS International Conference on Biomedical & Health Informatics (BHI)* (2018), IEEE, pp. 438–441.

[55] De Cooman, T., Varon, C., Van de Vel, A., Jansen, K., Ceulemans, B., Lagae, L., and Van Huffel, S. Adaptive nocturnal seizure detection using heart rate and low-complexity novelty detection. *Seizure 59* (2018), 48–53.

[56] Debener, S., Emkes, R., De Vos, M., and Bleichner, M. Unobtrusive ambulatory eeg using a smartphone and flexible printed electrodes around the ear. *Scientific reports 5* (2015), 16743.

[57] Debener, S., Minow, F., Emkes, R., Gandras, K., and De Vos, M. How about taking a low-cost, small, and wireless eeg for a walk? *Psychophysiology 49*, 11 (2012), 1617–1621.

[58] del Rio, B. A. S., Lopetegi, T., and Romero, I. Assessment of different methods to estimate electrocardiogram signal quality. In *2011 Computing in Cardiology* (2011), IEEE, pp. 609–612.

[59] Delorme, A., and Makeig, S. Eeglab: an open source toolbox for analysis of single-trial eeg dynamics including independent component analysis. *Journal of neuroscience methods 134*, 1 (2004), 9–21.

[60] Deviaene, M., Testelmans, D., Borzée, P., Buyse, B., Van Huffel, S., and Varon, C. Feature selection algorithm based on random forest applied to sleep apnea detection. In *2019 41st Annual International Conference of the IEEE Engineering in Medicine and Biology Society (EMBC)* (2019), IEEE, pp. 2580–2583.

[61] Devinsky, O., Kelley, K., Porter, R. J., and Theodore, W. H. Clinical and electroencephalographic features of simple partial seizures. *Neurology 38*, 9 (1988), 1347–1347.

[62] Di Gennaro, G., Quarato, P. P., Sebastiano, F., Esposito, V., Onorati, P., Grammaldo, L. G., Meldolesi, G. N., Mascia, A., Falco, C., Scoppetta, C., Eusebi, F., Manfredi, M., and Cantore, G. Ictal heart rate increase precedes EEG discharge in drug-resistant mesial temporal lobe seizures. *Clin. Neurophysiol. 115*, 5 (2004), 1169–1177.

[63] Dileep, R., Nair, M. D., and ODwyer, M. D. *Epilepsy: An Atlas of Investigation and Management*. Oxford Centre for Innovation, 2010. ISBN-13 978 1 904392 54 5.

[64] Doyle, O., Temko, A., Marnane, W., Lightbody, G., and Boylan, G. Heart rate based automatic seizure detection in the newborn. *Medical engineering & physics 32*, 8 (2010), 829–839.

[65] Duun-Henriksen, J., Baud, M., Richardson, M. P., Cook, M., Kouvas, G., Heasman, J. M., Friedman, D., Peltola, J., Zibrandtsen, I. C., and Kjaer, T. W. A new era in electroencephalographic monitoring? subscalp devices for ultra–long-term recordings. *Epilepsia 61*, 9 (2020), 1805–1817.

[66] Eggleston, K. S., Olin, B. D., and Fisher, R. S. Ictal tachycardia: the head–heart connection. *Seizure 23*, 7 (2014), 496–505.

[67] EIT Health. SeizeIT2. `https://www.eithealth.eu/seizeit2`, 2018. [Online; accessed 29-Septembert-2019].

[68] El Atrache, R., Tamilia, E., Mohammadpour Touserkani, F., Hammond, S., Papadelis, C., Kapur, K., Jackson, M., Bucciarelli, B., Tsuboyama, M., Sarkis, R. A., et al. Photoplethysmography: A measure for the function of the autonomic nervous system in focal impaired awareness seizures. *Epilepsia 61*, 8 (2020), 1617–1626.

[69] Elger, C. E., and Mormann, F. Seizure prediction and documentation—two important problems. *The Lancet Neurology 12*, 6 (2013), 531–532.

[70] Empatica Inc. Empatica E4 wristband. `https://www.empatica.com/e4-wristband`, 2017. [Online; accessed 22-August-2017].

[71] Epilepsy.org. epilepsy.org. `https://www.epilepsy.org.uk/info/seizures/focal-seizures`. Accessed: 2020-12-09.

[72] Falk, T. H., Maier, M., et al. Ms-qi: A modulation spectrum-based ecg quality index for telehealth applications. *IEEE Transactions on Biomedical Engineering 63*, 8 (2014), 1613–1622.

[73] Fischer, C., Domer, B., Wibmer, T., and Penzel, T. An algorithm for real-time pulse waveform segmentation and artifact detection in photoplethysmograms. *IEEE J. Biomed. Heal. Informatics 21*, 2 (2017), 372–381.

[74] Fisher, R. S., Acevedo, C., Arzimanoglou, A., Bogacz, A., Cross, J. H., Elger, C. E., Jr, J. E., Forsgren, L., French, J. A., Glynn, M., Hesdorffer, D. C., Lee, B., Mathern, G. W., Moshe, S. L., Perucca, E., Scheffer, I. E., Tomson, T., Watanabe, M., and Wiebe, S. A practical clinical definition of epilepsy. *Epilepsia, 55(4):475-482* (2014). doi: 10.1111/epi.12550.

[75] Fisher, R. S., Blum, D. E., DiVentura, B., Vannest, J., Hixson, J. D., Moss, R., Herman, S. T., Fureman, B. E., and French, J. A. Seizure diaries for clinical research and practice: limitations and future prospects. *Epilepsy Behav. 24*, 3 (2012), 304–310.

[76] Fisher, R. S., Cross, J. H., French, J. A., Higurashi, N., Hirsch, E., Jansen, F. E., Lagae, L., Moshé, S. L., Peltola, J., Roulet Perez, E., et al. Operational classification of seizure types by the international league against epilepsy: Position paper of the ilae commission for classification and terminology. *Epilepsia 58*, 4 (2017), 522–530.

[77] Fisher, R. S., and Velasco, A. L. Electrical brain stimulation for epilepsy. *Nature Reviews Neurology 10*, 5 (2014), 261–270.

[78] Foldvary, N., Klem, G., Hammel, J., Bingaman, W., Najm, I., and Lüders, H. The localizing value of ictal eeg in focal epilepsy. *Neurology 57*, 11 (2001), 2022–2028.

[79] Forsgren, L., Beghi, E., Oun, A., and Sillanpää, M. The epidemiology of epilepsy in europe–a systematic review. *European Journal of Neurology 12*, 4 (2005), 245–253.

[80] French, J. A. Refractory epilepsy: Clinical overview. *Epilepsia 48*, SUPPL. 1 (2007), 3–7.

[81] Fukushima, H., Kawanaka, H., Bhuiyan, M. S., and Oguri, K. Estimating heart rate using wrist-type photoplethysmography and acceleration sensor while running. In *Engineering in Medicine and Biology Society (EMBC), 2012 Annual International Conference of the IEEE* (2012), IEEE, pp. 2901–2904.

[82] Fürbass, F., Kampusch, S., Kaniusas, E., Koren, J., Pirker, S., Hopfengärtner, R., Stefan, H., Kluge, T., and Baumgartner,

C. Automatic multimodal detection for long-term seizure documentation in epilepsy. *Clinical Neurophysiology 128*, 8 (2017), 1466–1472.

[83] Fürbass, F., Ossenblok, P., Hartmann, M., Perko, H., Skupch, A., Lindinger, G., Elezi, L., Pataraia, E., Colon, A., Baumgartner, C., et al. Prospective multi-center study of an automatic online seizure detection system for epilepsy monitoring units. *Clinical Neurophysiology 126*, 6 (2015), 1124–1131.

[84] Gabor, A. Seizure detection using a self-organizing neural network: validation and comparison with other detection strategies. *Electroencephalography and clinical Neurophysiology 107*, 1 (1998), 27–32.

[85] Gabor, A., Leach, R., and Dowla, F. Automated seizure detection using a self-organizing neural network. *Electroencephalography and clinical Neurophysiology 99*, 3 (1996), 257–266.

[86] Gaitatzis, A., and Sander, J. W. The mortality of epilepsy revisited. *Epileptic disorders 6*, 1 (2004), 3–13.

[87] Ganeshapillai, G., Liu, J. F., and Guttag, J. Reconstruction of ecg signals in presence of corruption. In *2011 Annual International Conference of the IEEE Engineering in Medicine and Biology Society* (2011), IEEE, pp. 3764–3767.

[88] Gao, X. Non-invasive detection and compression of fetal electrocardiogram. *Interpreting Cardiac Electrograms-From Skin to Endocardium, InTechOpen* (2017), 53–74.

[89] Gil, E., María Vergara, J., and Laguna, P. Detection of decreases in the amplitude fluctuation of pulse photoplethysmography signal as indication of obstructive sleep apnea syndrome in children. *Biomed. Signal Process. Control 3*, 3 (jul 2008), 267–277.

[90] Golmohammadi, M., Shah, V., Obeid, I., and Picone, J. Deep learning approaches for automated seizure detection from scalp electroencephalograms. In *Signal Processing in Medicine and Biology*. Springer, 2020, pp. 235–276.

[91] Golmohammadi, M., Ziyabari, S., Shah, V., Von Weltin, E., Campbell, C., Obeid, I., and Picone, J. Gated recurrent networks for seizure detection. In *2017 IEEE Signal Processing in Medicine and Biology Symposium (SPMB)* (2017), IEEE, pp. 1–5.

[92] Gotman, J. Automatic recognition of epileptic seizures in the eeg. *Electroencephalography and clinical Neurophysiology 54*, 5 (1982), 530–540.

[93] Goverdovsky, V., Looney, D., Kidmose, P., and Mandic, D. P. In-ear eeg from viscoelastic generic earpieces: Robust and unobtrusive 24/7 monitoring. *IEEE Sensors Journal 16*, 1 (2015), 271–277.

[94] Greene, B., Faul, S., Marnane, W., Lightbody, G., Korotchikova, I., and Boylan, G. A comparison of quantitative eeg features for neonatal seizure detection. *Clinical Neurophysiology 119*, 6 (2008), 1248–1261.

[95] Greene, B. R., Boylan, G. B., Reilly, R. B., de Chazal, P., and Connolly, S. Combination of eeg and ecg for improved automatic neonatal seizure detection. *Clinical neurophysiology 118*, 6 (2007), 1348–1359.

[96] Gu, Y., Cleeren, E., Dan, J., Claes, K., Van Paesschen, W., Van Huffel, S., and Hunyadi, B. Comparison between scalp eeg and behind-the-ear eeg for development of a wearable seizure detection system for patients with focal epilepsy. *Sensors 18*, 1 (2018), 29.

[97] Halford, J. J., Sperling, M. R., Nair, D. R., Dlugos, D. J., Tatum, W. O., Harvey, J., French, J. A., Pollard, J. R., Faught, E., Noe, K. H., et al. Detection of generalized tonic–clonic seizures using surface electromyographic monitoring. *Epilepsia 58*, 11 (2017), 1861–1869.

[98] Hartmann, M. M., Fürbass, F., Perko, H., Skupch, A., Lackmayer, K., Baumgartner, C., and Kluge, T. Episcan: online seizure detection for epilepsy monitoring units. In *2011 Annual International Conference of the IEEE Engineering in Medicine and Biology Society* (2011), IEEE, pp. 6096–6099.

[99] Hayn, D., Jammerbund, B., and Schreier, G. Ecg quality assessment for patient empowerment in mhealth applications. In *2011 Computing in Cardiology* (2011), IEEE, pp. 353–356.

[100] Hayn, D., Jammerbund, B., and Schreier, G. Qrs detection based ecg quality assessment. *Physiological measurement 33*, 9 (2012), 1449.

[101] Hopfengärtner, R., Kasper, B. S., Graf, W., Gollwitzer, S., Kreiselmeyer, G., Stefan, H., and Hamer, H. Automatic seizure detection in long-term scalp eeg using an adaptive thresholding technique: a validation study for clinical routine. *Clinical Neurophysiology 125*, 7 (2014), 1346–1352.

[102] Hopfengärtner, R., Kerling, F., Bauer, V., and Stefan, H. An efficient, robust and fast method for the offline detection of epileptic

seizures in long-term scalp eeg recordings. *Clinical Neurophysiology 118*, 11 (2007), 2332–2343.

[103] Hoppe, C., Poepel, A., and Elger, C. E. Epilepsy: accuracy of patient seizure counts. *Archives of neurology 64*, 11 (2007), 1595–1599.

[104] https://seizeit.eubuild.redcapcloud.com/. RedCap cloud. `https://seizeit.eubuild.redcapcloud.com/`, 2020. [Online; accessed 30-December-2020].

[105] Hunyadi, B., De Vos, M., Van Paesschen, W., and Van Huffel, S. A mimicking approach for human epileptic seizure detection. In *Proc. of the International Biosignal Processing Conference* (2010), pp. 1–4.

[106] Hunyadi, B., Signoretto, M., Van Paesschen, W., Suykens, J. A., Van Huffel, S., and De Vos, M. Incorporating structural information from the multichannel eeg improves patient-specific seizure detection. *Clinical Neurophysiology 123*, 12 (2012), 2352–2361.

[107] Hussein, R., Palangi, H., Ward, R. K., and Wang, Z. J. Optimized deep neural network architecture for robust detection of epileptic seizures using eeg signals. *Clinical Neurophysiology 130*, 1 (2019), 25–37.

[108] Ihle, M., Feldwisch-Drentrup, H., Teixeira, C. A., Witon, A., Schelter, B., Timmer, J., and Schulze-Bonhage, A. Epilepsiae–a european epilepsy database. *Computer methods and programs in biomedicine 106*, 3 (2012), 127–138.

[109] Institute, N. C. Seer training modules. `https://training.seer.cancer.gov/images/anatomy/nervous/neuron-structure.jpg`, 2020. [Online; accessed January 2021].

[110] Jain, A., Fandango, A., and Kapoor, A. *TensorFlow Machine Learning Projects: Build 13 real-world projects with advanced numerical computations using the Python ecosystem*. Packt Publishing Ltd, 2018.

[111] Jansen, K., and Lagae, L. Cardiac changes in epilepsy. *Seizure 19*, 8 (oct 2010), 455–460.

[112] Jekova, I., Krasteva, V., Christov, I., and Abächerli, R. Threshold-based system for noise detection in multilead ecg recordings. *Physiological measurement 33*, 9 (2012), 1463.

[113] Jekova, I., Krasteva, V., Dotsinsky, I., Christov, I., and Abächerli, R. Recognition of diagnostically useful ecg recordings: alert for corrupted or interchanged leads. In *2011 Computing in Cardiology* (2011), IEEE, pp. 429–432.

[114] Jeppesen, J., Beniczky, S., Johansen, P., Sidenius, P., and Fuglsang-Frederiksen, A. Using lorenz plot and cardiac sympathetic index of heart rate variability for detecting seizures for patients with epilepsy. In *2014 36th Annual International Conference of the IEEE Engineering in Medicine and Biology Society* (2014), IEEE, pp. 4563–4566.

[115] Jeppesen, J., Beniczky, S., Johansen, P., Sidenius, P., and Fuglsang-Frederiksen, A. Detection of epileptic seizures with a modified heart rate variability algorithm based on lorenz plot. *Seizure 24* (2015), 1–7.

[116] Jeppesen, J., Fuglsang-Frederiksen, A., Johansen, P., Christensen, J., Wüstenhagen, S., Tankisi, H., Qerama, E., Hess, A., and Beniczky, S. O-45 automated seizure detection for epilepsy patients using wearable ecg-device. *Clinical Neurophysiology 130*, 7 (2019), e36.

[117] Jiang, Y., Wu, D., Deng, Z., Qian, P., Wang, J., Wang, G., Chung, F.-L., Choi, K.-S., and Wang, S. Seizure classification from eeg signals using transfer learning, semi-supervised learning and tsk fuzzy system. *IEEE Transactions on Neural Systems and Rehabilitation Engineering 25*, 12 (2017), 2270–2284.

[118] Johannesen, L. Assessment of ecg quality on an android platform. In *2011 Computing in Cardiology* (2011), IEEE, pp. 433–436.

[119] Johannesen, L., and Galeotti, L. Automatic ecg quality scoring methodology: mimicking human annotators. *Physiological measurement 33*, 9 (2012), 1479.

[120] Johnson, A. E., Behar, J., Andreotti, F., Clifford, G. D., and Oster, J. Multimodal heart beat detection using signal quality indices. *Physiological measurement 36*, 8 (2015), 1665.

[121] Kahane, P., and Depaulis, A. Deep brain stimulation in epilepsy: what is next? *Current opinion in neurology 23*, 2 (2010), 177–182.

[122] Karlen, W., Kobayashi, K., Ansermino, J. M., and Dumont, G. A. Photoplethysmogram signal quality estimation using repeated Gaussian filters and cross-correlation. *Physiol. Meas. 33*, 10 (2012), 1617–1629.

[123] Kelly, K., Shiau, D., Kern, R., Chien, J., Yang, M., Yandora, K., Valeriano, J., Halford, J., and Sackellares, J. Assessment of a scalp eeg-based automated seizure detection system. *Clinical Neurophysiology 121*, 11 (2010), 1832–1843.

[124] Kim, B. S., and Yoo, S. K. Motion artifact reduction in photoplethysmography using independent component analysis. *IEEE Trans. Biomed. Eng. 53*, 3 (2006), 566–568.

[125] Kjaer, T. W., Sorensen, H. B., Groenborg, S., Pedersen, C. R., and Duun-Henriksen, J. Detection of paroxysms in long-term, single-channel eeg-monitoring of patients with typical absence seizures. *IEEE journal of translational engineering in health and medicine 5* (2017), 1–8.

[126] Klatt, J., Feldwisch-Drentrup, H., Ihle, M., Navarro, V., Neufang, M., Teixeira, C., Adam, C., Valderrama, M., Alvarado-Rojas, C., Witon, A., et al. The epilepsiae database: An extensive electroencephalography database of epilepsy patients. *Epilepsia 53*, 9 (2012), 1669–1676.

[127] Koubeissi, M. Z., and Azar, N. J. *Epilepsy Board Review*. Springer, 2017.

[128] Krishnan, R., Natarajan, B., and Warren, S. Analysis and detection of motion artifact in photoplethysmographic data using higher order statistics. In *Acoustics, Speech and Signal Processing, 2008. ICASSP 2008. IEEE International Conference on* (2008), IEEE, pp. 613–616.

[129] Kristensen, O., and Sindrup, E. H. Sphenoidal electrodes their use and value in the electroencephalographic investigation of complex partial epilepsy. *Acta Neurologica Scandinavica 58*, 3 (1978), 157–166.

[130] Kuhlmann, L., Burkitt, A. N., Cook, M. J., Fuller, K., Grayden, D. B., Seiderer, L., and Mareels, I. M. Seizure detection using seizure probability estimation: Comparison of features used to detect seizures. *Annals of biomedical engineering 37*, 10 (2009), 2129–2145.

[131] Kuhlmann, L., Lehnertz, K., Richardson, M. P., Schelter, B., and Zaveri, H. P. Seizure prediction—ready for a new era. *Nature Reviews Neurology 14*, 10 (2018), 618–630.

[132] Kurada, A. V., Srinivasan, T., Hammond, S., Ulate-Campos, A., and Bidwell, J. Seizure detection devices for use in antiseizure medication clinical trials: A systematic review. *Seizure 66* (2019), 61–69.

[133] Kužílek, J., Huptych, M., Chudáček, V., Spilka, J., and Lhotská, L. Data driven approach to ecg signal quality assessment using multistep svm classification. In *2011 Computing in Cardiology* (2011), IEEE, pp. 453–455.

[134] Lai, P., and Kim, I. Lightweight wrist photoplethysmography for heavy exercise: motion robust heart rate monitoring algorithm. *Healthcare Technology Letters 2*, 1 (2015), 6–11.

[135] Langley, P., Di Marco, L. Y., King, S., Duncan, D., Di Maria, C., Duan, W., Bojarnejad, M., Zheng, D., Allen, J., and Murray, A. An algorithm for assessment of quality of ecgs acquired via mobile telephones. In *2011 Computing in Cardiology* (2011), IEEE, pp. 281–284.

[136] Lázaro, J., Gil, E., Vergara, J. M., and Laguna, P. Pulse rate variability analysis for discrimination of sleep-apnea-related decreases in the amplitude fluctuations of pulse photoplethysmographic signal in children. *IEEE J. Biomed. Heal. Informatics* (2014), 240–6.

[137] Lee, B., Han, J., Baek, H. J., Shin, J. H., Park, K. S., and Yi, W. J. Improved elimination of motion artifacts from a photoplethysmographic signal using a kalman smoother with simultaneous accelerometry. *Physiol Meas 31*, 12 (2010), 1585–603.

[138] Lee, J., McManus, D. D., Merchant, S., and Chon, K. H. Automatic motion and noise artifact detection in holter ecg data using empirical mode decomposition and statistical approaches. *IEEE Transactions on Biomedical Engineering 59*, 6 (2011), 1499–1506.

[139] Leijten, F. S., Consortium, D. T., van Andel, J., Ungureanu, C., Arends, J., Tan, F., van Dijk, J., Petkov, G., Kalitzin, S., Gutter, T., et al. Multimodal seizure detection: a review. *Epilepsia 59* (2018), 42–47.

[140] Leutmezer, F., Schernthaner, C., Lurger, S., Pötzelberger, K., and Baumgartner, C. Electrocardiographic changes at the onset of epileptic seizures. *Epilepsia 44*, 3 (2003), 348–354.

[141] LeVan, P., Urrestarazu, E., and Gotman, J. A system for automatic artifact removal in ictal scalp eeg based on independent component analysis and bayesian classification. *Clinical Neurophysiology 117*, 4 (2006), 912–927.

[142] Li, C., Zheng, C., and Tai, C. Detection of ecg characteristic points using wavelet transforms. *IEEE Transactions on biomedical Engineering 42*, 1 (1995), 21–28.

[143] Li, K., and Warren, S. A wireless reflectance pulse oximeter with digital baseline control for unfiltered photoplethysmograms. *IEEE Trans. Biomed. Circuits Syst. 6*, 3 (2012), 269–278.

[144] Li, K., Warren, S., and Natarajan, B. Onboard tagging for real-time quality assessment of photoplethysmograms acquired by a wireless reflectance pulse oximeter. *IEEE Trans. Biomed. Circuits Syst. 6*, 1 (2012), 54–63.

[145] Li, Q., and Clifford, G. D. Signal quality and data fusion for false alarm reduction in the intensive care unit. *Journal of electrocardiology 45*, 6 (2012), 596–603.

[146] Li, Q., Mark, R. G., and Clifford, G. D. Robust heart rate estimation from multiple asynchronous noisy sources using signal quality indices and a kalman filter. *Physiological measurement 29*, 1 (2007), 15.

[147] Li, Q., Mark, R. G., and Clifford, G. D. Robust heart rate estimation from multiple asynchronous noisy sources. *Physiol. Meas. 29*, 1 (2008), 15–32.

[148] Li, Q., Mark, R. G., and Clifford, G. D. Artificial arterial blood pressure artifact models and an evaluation of a robust blood pressure and heart rate estimator. *Biomedical engineering online 8*, 1 (2009), 13.

[149] Liu, C., Li, P., Zhao, L., Liu, F., and Wang, R. Real-time signal quality assessment for ecgs collected using mobile phones. In *2011 Computing in Cardiology* (2011), IEEE, pp. 357–360.

[150] Logesparan, L., Rodriguez-Villegas, E., and Casson, A. J. The impact of signal normalization on seizure detection using line length features. *Medical & biological engineering & computing 53*, 10 (2015), 929–942.

[151] Looney, D., Park, C., Kidmose, P., Rank, M. L., Ungstrup, M., Rosenkranz, K., and Mandic, D. P. An in-the-ear platform for recording electroencephalogram. In *2011 Annual International Conference of the IEEE Engineering in Medicine and Biology Society* (2011), IEEE, pp. 6882–6885.

[152] Low, P. Merck manual consumer version. `https://www.merckmanuals.com/home/brain,-spinal-cord,-and-nerve-disorders/autonomic-nervous-system-disorders/overview-of-the-autonomic-nervous-system`, 2020. [Online; accessed January 2021].

[153] Maan, A. C., van Zwet, E. W., Man, S., Oliveira-Martens, S. M., Schalij, M. J., and Swenne, C. A. Assessment of signal quality and electrode placement in ecgs using a reconstruction matrix. In *2011 Computing in Cardiology* (2011), IEEE, pp. 289–292.

[154] Maeda, Y., Sekine, M., and Tamura, T. Relationship between measurement site and motion artifacts in wearable reflected photoplethysmography. *Journal of medical systems 35*, 5 (2011), 969–976.

[155] Mann, S. A., and Orglmeister, R. A flexible pca-based ecg-reconstruction algorithm with confidence estimation for ecg during exercise. In *Computing in Cardiology 2014* (2014), IEEE, pp. 33–36.

[156] Manzouri, F., Heller, S., Dümpelmann, M., Woias, P., and Schulze-Bonhage, A. A comparison of machine learning classifiers for energy-efficient implementation of seizure detection. *Frontiers in systems neuroscience 12* (2018), 43.

[157] Martinez-Tabares, F., Espinosa-Oviedo, J., and Castellanos-Dominguez, G. Improvement of ecg signal quality measurement using correlation and diversity-based approaches. In *2012 Annual International Conference of the IEEE Engineering in Medicine and Biology Society* (2012), IEEE, pp. 4295–4298.

[158] Massé, F., van Bussel, M.J.P, Serteyn, A.A.M, Arends, J.B.A.M, and Penders, J. Miniaturized wireless ECG monitor for real-time detection of epileptic seizures. *ACM Trans. Embed. Comput. Syst. 12*, 4 (2013), 1.

[159] Mayoclinic. Mayoclinic. `https://www.mayoclinic.org/diseases-conditions/frontal-lobe-seizures/symptoms-causes/syc-20353958`. Accessed: 2020-12-09.

[160] McCorry, L. K. Physiology of the autonomic nervous system. *American journal of pharmaceutical education 71*, 4 (2007).

[161] Medium.com. Understanding recurrent neural networks in 6 minutes. `https://medium.com/x8-the-ai-community/understanding-recurrent-neural-networks-in-6-minutes-967ab51b94fe`. Accessed: 2021-01-27.

[162] Meritam, P., Ryvlin, P., and Beniczky, S. User-based evaluation of applicability and usability of a wearable accelerometer device for detecting bilateral tonic–clonic seizures: A field study. *Epilepsia 59* (2018), 48–52.

[163] Mijović, B., De Vos, M., Gligorijević, I., Taelman, J., and Van Huffel, S. Source separation from single-channel recordings by combining empirical-mode decomposition and independent component analysis. *IEEE transactions on biomedical engineering 57*, 9 (2010), 2188–2196.

[164] Milošević, M., Van de Vel, A., Bonroy, B., Ceulemans, B., Lagae, L., Vanrumste, B., and Van Huffel, S. Automated detection of tonic–clonic seizures using 3-d accelerometry and surface electromyography in pediatric patients. *IEEE journal of biomedical and health informatics 20*, 5 (2015), 1333–1341.

[165] Moeyersons, J., Smets, E., Morales, J., Villa, A., De Raedt, W., Testelmans, D., Buyse, B., Van Hoof, C., Willems, R., Van Huffel, S., et al. Artefact detection and quality assessment of ambulatory ecg signals. *Computer methods and programs in biomedicine 182* (2019), 105050.

[166] Mohri, M., Rostamizadeh, A., and Talwalkar, A. *Foundations of machine learning*. MIT press, 2018.

[167] Moody, B. E. Rule-based methods for ecg quality control. In *2011 Computing in Cardiology* (2011), IEEE, pp. 361–363.

[168] Morgado, E., Alonso-Atienza, F., Santiago-Mozos, R., Barquero-Pérez, Ó., Silva, I., Ramos, J., and Mark, R. Quality estimation of the electrocardiogram using cross-correlation among leads. *Biomedical engineering online 14*, 1 (2015), 59.

[169] Moridani, M., and Farhadi, H. Heart rate variability as a biomarker for epilepsy seizure prediction. *Clin. Study 3*, 8 (2017).

[170] Mormann, F., Andrzejak, R. G., Elger, C. E., and Lehnertz, K. Seizure prediction: the long and winding road. *Brain 130*, 2 (2006), 314–333.

[171] N. Neurotech and NeuroTechX. NeurekaTM 2020 epilepsy challenge. `https://neureka-challenge.com/`, 2020. [Online; accessed 30-December-2020].

[172] Nakajima, K., Tamura, T., and Miike, H. Monitoring of heart and respiratory rates by photoplethysmography using a digital filtering technique. *Med. Eng. Phys. 18*, 5 (1996), 365–372.

[173] Naseri, H., and Homaeinezhad, M. Electrocardiogram signal quality assessment using an artificially reconstructed target lead. *Computer methods in biomechanics and biomedical engineering 18*, 10 (2015), 1126–1141.

[174] Neal, E. G., Chaffe, H., Schwartz, R. H., Lawson, M. S., Edwards, N., Fitzsimmons, G., Whitney, A., and Cross, J. H. The ketogenic diet for the treatment of childhood epilepsy: a randomised controlled trial. *The Lancet Neurology 7*, 6 (2008), 500–506.

[175] Nemati, S., Malhotra, A., and Clifford, G. D. Data fusion for improved respiration rate estimation. *EURASIP journal on advances in signal processing 2010*, 1 (2010), 926305.

[176] Noponen, K., Karsikas, M., Tiinanen, S., Kortelainen, J., Huikuri, H., and Seppänen, T. Electrocardiogram quality classification based on robust best subsets linear prediction error. In *2011 Computing in Cardiology* (2011), IEEE, pp. 365–368.

[177] Obeid, I., and Picone, J. The temple university hospital eeg data corpus. *Frontiers in neuroscience 10* (2016), 196.

[178] Oh, S. *A new quality measure in electrocardiogram signal*. PhD thesis, University of Florida, 2004.

[179] Onorati, F., Regalia, G., Caborni, C., Migliorini, M., Bender, D., Poh, M.-Z., Frazier, C., Kovitch Thropp, E., Mynatt, E. D., Bidwell, J., et al. Multicenter clinical assessment of improved wearable multimodal convulsive seizure detectors. *Epilepsia 58*, 11 (2017), 1870–1879.

[180] Orphanidou, C., Bonnici, T., Charlton, P., Clifton, D., Vallance, D., and Tarassenko, L. Signal-quality indices for the electrocardiogram and photoplethysmogram: Derivation and applications to wireless monitoring. *IEEE journal of biomedical and health informatics 19*, 3 (2014), 832–838.

[181] Osorio, I. Automated seizure detection using ekg. *International Journal of Neural Systems 24*, 02 (2014), 1450001. PMID: 24475899.

[182] Osorio, I., and Manly, B. Is seizure detection based on ekg clinically relevant? *Clinical Neurophysiology 125*, 10 (2014), 1946–1951.

[183] Page, A., Shea, C., and Mohsenin, T. Wearable seizure detection using convolutional neural networks with transfer learning. In *2016 IEEE International Symposium on Circuits and Systems (ISCAS)* (2016), IEEE, pp. 1086–1089.

[184] Pan, H., Temel, D., and AlRegib, G. Heartbeat: Heart beat estimation through adaptive tracking. In *Biomedical and Health Informatics (BHI), 2016 IEEE-EMBS International Conference on* (2016), IEEE, pp. 587–590.

[185] Pauri, F., Pierelli, F., Chatrian, G.-E., and Erdly, W. W. Long-term eeg-video-audio monitoring: computer detection of focal eeg seizure patterns. *Electroencephalography and clinical Neurophysiology 82*, 1 (1992), 1–9.

[186] Pavei, J., Heinzen, R. G., Novakova, B., Walz, R., Serra, A. J., Reuber, M., Ponnusamy, A., and Marques, J. L. Early seizure detection based on cardiac autonomic regulation dynamics. *Frontiers in physiology 8* (2017), 765.

[187] Petersen, O. H. *Lecture notes: Human physiology.* John Wiley & Sons, 2019.

[188] Petrosian, A., Prokhorov, D., Homan, R., Dasheiff, R., and Wunsch II, D. Recurrent neural network based prediction of epileptic seizures in intra-and extracranial eeg. *Neurocomputing 30*, 1-4 (2000), 201–218.

[189] Petterson, M. T., Begnoche, V. L., and Graybeal, J. M. The effect of motion on pulse oximetry and its clinical significance. *Anesth. Analg. 105*, 6 suppl. (2007), S78–84.

[190] Petty, B. G. *Basic electrocardiography.* Springer Nature, 2020.

[191] Phan, H., Chén, O. Y., Koch, P., Lu, Z., McLoughlin, I., Mertins, A., and De Vos, M. Towards more accurate automatic sleep staging via deep transfer learning. *IEEE Transactions on Biomedical Engineering* (2020).

[192] Pion-Tonachini, L., Kreutz-Delgado, K., and Makeig, S. Iclabel: An automated electroencephalographic independent component classifier, dataset, and website. *NeuroImage 198* (2019), 181–197.

[193] Poh, M.-Z., Loddenkemper, T., Reinsberger, C., Swenson, N. C., Goyal, S., Sabtala, M. C., Madsen, J. R., and Picard, R. W. Convulsive seizure detection using a wrist-worn electrodermal activity and accelerometry biosensor. *Epilepsia 53*, 5 (2012), e93–e97.

[194] Polikar, R. Ensemble learning. In *Ensemble machine learning.* Springer, 2012, pp. 1–34.

[195] Poochikian-Sarkissian, S., Tai, P., Andrade, D., Carlen, P., Valiante, T., Wennberg, R., et al. Patient awareness of seizures as documented in the epilepsy monitoring unit. *Canadian journal of neuroscience nursing 31*, 4 (2009), 22–23.

[196] Princeton brain, s., and sports medicine. Brain anatomy. `https://www.princetonbrainandspine.com/resources/learning-center/brain-anatomy/`, 2020. [Online; accessed January 2021].

[197] Qaraqe, M., Ismail, M., Serpedin, E., and Zulfi, H. Epileptic seizure onset detection based on eeg and ecg data fusion. *Epilepsy & Behavior 58* (2016), 48–60.

[198] Qu, H., and Gotman, J. A patient-specific algorithm for the detection of seizure onset in long-term eeg monitoring: possible use as a warning device. *IEEE transactions on biomedical engineering 44*, 2 (1997), 115–122.

[199] Quesnel, P. X., Chan, A. D., and Yang, H. Real-time biosignal quality analysis of ambulatory ecg for detection of myocardial ischemia. In *2013 IEEE International Symposium on Medical Measurements and Applications (MeMeA)* (2013), IEEE, pp. 1–5.

[200] Quesnel, P. X., Chan, A. D., and Yang, H. Signal quality and false myocardial ischemia alarms in ambulatory electrocardiograms. In *2014 IEEE International Symposium on Medical Measurements and Applications (MeMeA)* (2014), IEEE, pp. 1–5.

[201] R, M., H, D., A, S.-B., and A., A. Detecting epileptic seizures in long-term human eeg: a new approach to automatic online and real-time detection and classification of polymorphic seizure patterns. *J Clin Neurophysiol 25*, 3 (2008), 119–31.

[202] Ram, M., Madhav, K. V., Krishna, E. H., Komalla, N. R., and Reddy, K. A. A novel approach for motion artifact reduction in ppg signals based on as-lms adaptive filter. *IEEE Trans Intrum Meas 16* (2012), 1445–1457.

[203] Redmond, S. J., Lovell, N. H., Basilakis, J., and Celler, B. G. Ecg quality measures in telecare monitoring. In *2008 30th Annual International Conference of the IEEE Engineering in Medicine and Biology Society* (2008), IEEE, pp. 2869–2872.

[204] Redmond, S. J., Xie, Y., Chang, D., Basilakis, J., and Lovell, N. H. Electrocardiogram signal quality measures for unsupervised telehealth environments. *Physiological Measurement 33*, 9 (2012), 1517.

[205] Regalia, G., Onorati, F., Lai, M., Caborni, C., and Picard, R. W. Multimodal wrist-worn devices for seizure detection and advancing research: focus on the empatica wristbands. *Epilepsy research 153* (2019), 79–82.

[206] Ronneberger, O., Fischer, P., and Brox, T. U-net: Convolutional networks for biomedical image segmentation. In *International Conference on Medical image computing and computer-assisted intervention* (2015), Springer, pp. 234–241.

[207] Roy, Y., Banville, H., Albuquerque, I., Gramfort, A., Falk, T. H., and Faubert, J. Deep learning-based electroencephalography analysis: a systematic review. *Journal of neural engineering 16*, 5 (2019), 051001.

[208] Saab, M., and Gotman, J. A system to detect the onset of epileptic seizures in scalp eeg. *Clinical Neurophysiology 116*, 2 (2005), 427–442.

[209] Salas-Puig, X., Iniesta, M., Abraira, L., Puig, J., study group, Q.-G., et al. Accidental injuries in patients with generalized tonic–clonic seizures. a multicenter, observational, cross-sectional study (quin-gtc study). *Epilepsy & Behavior 92* (2019), 135–139.

[210] Salehizadeh, S. M. A., Dao, D. K., Chong, J. W., McManus, D., Darling, C., Mendelson, Y., and Chon, K. H. Photoplethysmograph signal reconstruction based on a novel motion artifact detection-reduction approach. part ii: Motion and noise artifact removal. *Annals of Biomedical Engineering 42*, 11 (Nov 2014), 2251–2263.

[211] Satija, U., Ramkumar, B., and Manikandan, M. S. A review of signal processing techniques for electrocardiogram signal quality assessment. *IEEE reviews in biomedical engineering 11* (2018), 36–52.

[212] Scheffer, I. E., Berkovic, S., Capovilla, G., Connolly, M. B., French, J., Guilhoto, L., Hirsch, E., Jain, S., Mathern, G. W., Moshé, S. L., et al. Ilae classification of the epilepsies: position paper of the ilae commission for classification and terminology. *Epilepsia 58*, 4 (2017), 512–521.

[213] Schelter, B., Winterhalder, M., Maiwald, T., Brandt, A., Schad, A., Schulze-Bonhage, A., and Timmer, J. Testing statistical significance of multivariate time series analysis techniques for epileptic seizure prediction. *Chaos: An Interdisciplinary Journal of Nonlinear Science 16*, 1 (2006), 013108.

[214] Schlemper, J., Oktay, O., Schaap, M., Heinrich, M., Kainz, B., Glocker, B., and Rueckert, D. Attention gated networks: Learning to leverage salient regions in medical images. *Medical image analysis 53* (2019), 197–207.

[215] Schumm, J. *Quality assessment of physiological signals during ambulatory measurements*. ETH Zurich, 2010.

[216] Seeck, M., Koessler, L., Bast, T., Leijten, F., Michel, C., Baumgartner, C., He, B., and Beniczky, S. The standardized eeg electrode array of the ifcn. *Clinical Neurophysiology 128*, 10 (2017), 2070–2077.

[217] Seeuws, N., De Vos, M., and Bertrand, A. Electrocardiogram quality assessment usingunsupervised deep learning. *IEEE Transactions on Biomedical Engineering (TBME) submitted in December 2020*.

[218] Selvaraj, N., Mendelson, Y., Shelley, K. H., Silverman, D. G., and Chon, K. H. Statistical Approach for the Detection of Motion / Noise Artifacts in Photoplethysmogram. *Conf Proc IEEE Eng Med Biol Soc.* (2011), 4972–4975.

[219] Shah, V., Von Weltin, E., Lopez, S., McHugh, J. R., Veloso, L., Golmohammadi, M., Obeid, I., and Picone, J. The temple university hospital seizure detection corpus. *Frontiers in neuroinformatics 12* (2018), 83.

[220] Shoeibi, A., Ghassemi, N., Khodatars, M., Jafari, M., Hussain, S., Alizadehsani, R., Moridian, P., Khosravi, A., Hosseini-Nejad, H., Rouhani, M., et al. Epileptic seizure detection using deep learning techniques: A review. *arXiv preprint arXiv:2007.01276* (2020).

[221] Silva, I., Lee, J., and Mark, R. G. Signal quality estimation with multichannel adaptive filtering in intensive care settings. *IEEE Transactions on Biomedical Engineering 59*, 9 (2012), 2476–2485.

[222] Sim, I. Mobile devices and health. *New England Journal of Medicine 381*, 10 (2019), 956–968.

[223] Simonyan, K., and Zisserman, A. Very deep convolutional networks for large-scale image recognition. *arXiv preprint arXiv:1409.1556* (2014).

[224] Somers, B., Francart, T., and Bertrand, A. A generic eeg artifact removal algorithm based on the multi-channel wiener filter. *Journal of neural engineering 15*, 3 (2018), 036007.

[225] Somers, B., Francart, T. and Bertrand, A. MWF toolbox for EEG artifact removal. `http://www.github.com/exporl/mwf-artifact-removal`, 2017. [Online; accessed 2018].

[226] Song, Y., Liò, P., et al. A new approach for epileptic seizure detection: sample entropy based feature extraction and extreme learning machine. *Journal of Biomedical Science and Engineering 3*, 06 (2010), 556.

[227] Sopic, D., Aminifar, A., and Atienza, D. e-glass: A wearable system for real-time detection of epileptic seizures. In *2018 IEEE International Symposium on Circuits and Systems (ISCAS)* (2018), IEEE, pp. 1–5.

[228] Spencer, S. S., Williamson, P. D., Bridgers, S. L., Mattson, R. H., Cicchetti, D. V., and Spencer, D. D. Reliability and accuracy of localization by scalp ictal eeg. *Neurology 35*, 11 (1985), 1567–1567.

[229] Stern, J. M. *Atlas of EEG patterns*. Lippincott Williams & Wilkins, 2005.

[230] Sukor, J. A., Redmond, S. J., and Lovell, N. H. Signal quality measures for pulse oximetry through waveform morphology analysis. *Physiol. Meas. 32*, 3 (2011), 369–384.

[231] Surges, R., Thijs, R. D., Tan, H. L., and Sander, J. W. Sudden unexpected death in epilepsy: risk factors and potential pathomechanisms. *Nature Reviews Neurology 5*, 9 (2009), 492.

[232] Sveinsson, O., Andersson, T., Mattsson, P., Carlsson, S., and Tomson, T. Clinical risk factors in sudep: A nationwide population-based case-control study. *Neurology 94*, 4 (2020), e419–e429.

[233] Takagi, T., and Sugeno, M. Fuzzy identification of systems and its applications to modeling and control. *IEEE transactions on systems, man, and cybernetics*, 1 (1985), 116–132.

[234] Tamura, T., Maeda, Y., Sekine, M., and Yoshida, M. Wearable photoplethysmographic sensors—past and present. *Electronics 3*, 2 (2014), 282–302.

[235] Tat, T. H. C., Xiang, C., and Thiam, L. E. Physionet challenge 2011: improving the quality of electrocardiography data collected using real time qrs-complex and t-wave detection. In *2011 Computing in Cardiology* (2011), IEEE, pp. 441–444.

[236] Tatum IV, W. O., Winters, L., Gieron, M., Passaro, E. A., Benbadis, S., Ferreira, J., and Liporace, J. Outpatient seizure identification: results of 502 patients using computer-assisted ambulatory eeg. *Journal of Clinical Neurophysiology 18*, 1 (2001), 14–19.

[237] Temko, A. Accurate heart rate monitoring during physical exercises using ppg. *IEEE Trans Biomed Eng. 64*, 9 (2017), 2016–2024.

[238] Thodoroff, P., Pineau, J., and Lim, A. Learning robust features using deep learning for automatic seizure detection. In *Machine learning for healthcare conference* (2016), pp. 178–190.

[239] Tobin, R. M., Pologe, J. A., and Batchelder, P. B. A characterization of motion affecting pulse oximetry in 350 patients. *Anesth. Analg.*, 94 (2002), S54–S61.

[240] Tobón, D. P., and Falk, T. H. Online ecg quality assessment for context-aware wireless body area networks. In *2015 IEEE 28th Canadian Conference on Electrical and Computer Engineering (CCECE)* (2015), IEEE, pp. 587–592.

[241] Torres, J. M. M., Ghosh, A., Stepanov, E. A., and Riccardi, G. Heal-t: An efficient ppg-based heart-rate and ibi estimation method during physical exercise. *24th European Signal Processing Conference (EUSIPCO)* (2016).

[242] towardsdatascience.com. A comprehensive guide to convolutional neural networks — the eli5 way. `https://medium.com/x8-the-ai-community/understanding-recurrent-neural-networks-in-6-minutes-967ab51b94fe`. Accessed: 2021-01-27.

[243] Ullah, I., Hussain, M., Aboalsamh, H., et al. An automated system for epilepsy detection using eeg brain signals based on deep learning approach. *Expert Systems with Applications 107* (2018), 61–71.

[244] Ungureanu, C.; Bui, V.; Roosmalen, W.; Aarts, R.M.; Arends, J.B.A.M.; Verhoeven,R.; Lukkien, J.J. A wearable monitoring system for nocturnal epileptic seizures. *Med. Inf. Commun. Technol. 8th Int. Symp.* (2014), 3–7.

[245] Vaglio, M., Isola, L., Gates, G., and Badilini, F. Use of ecg quality metrics in clinical trials. In *2010 Computing in Cardiology* (2010), IEEE, pp. 505–508.

[246] van Andel, J., Ungureanu, C., Aarts, R.M, Leijten, F., and Arends, J.B.A.M. Using photoplethysmography in heart rate monitoring of patients with epilepsy. *Epilepsy Behav. 45* (apr 2015), 142–145.

[247] van Andel, J., Ungureanu, C., Arends, J., Tan, F., Van Dijk, J., Petkov, G., Kalitzin, S., Gutter, T., de Weerd, A., Vledder, B., et al. Multimodal, automated detection of nocturnal motor seizures at home: Is a reliable seizure detector feasible? *Epilepsia Open 2*, 4 (2017), 424–431.

[248] Van De Vel, A., Cuppens, K., Bonroy, B., Milosevic, M., Jansen, K., Van Huffel, S., Vanrumste, B., Lagae, L., and Ceulemans, B. Non-EEG seizure-detection systems and potential SUDEP prevention: State of the art. *Seizure 22*, 5 (2013), 345–355.

[249] Van de Vel, A., Cuppens, K., Bonroy, B., Milosevic, M., Van Huffel, S., Vanrumste, B., Lagae, L., and Ceulemans, B. Long-term home monitoring of hypermotor seizures by patient-worn accelerometers. *Epilepsy & Behavior 26*, 1 (2013), 118–125.

[250] van Elmpt, W.J.C, Nijsen, T.M.E, Griep, P.A.M, and Arends, J.B.A.M. A model of heart rate changes to detect seizures in severe epilepsy. *Seizure 15*, 6 (sep 2006), 366–375.

[251] van Elmpt,W.J.C., Nijsen,T.M.E., Griep,P.A.M., and Arends, J. B. A. M. A model of heart rate changes to detect seizures in severe epilepsy. *Seizure* (2006).

[252] van Westrhenen, A., De Cooman, T., Lazeron, R. H., Van Huffel, S., and Thijs, R. D. Ictal autonomic changes as a tool for seizure detection: a systematic review. *Clinical Autonomic Research 29*, 2 (2019), 161–181.

[253] Vandecasteele, K., De Cooman, T., Chatzichristos, C., Cleeren, E., Swinnen, L., Ortiz, J. M., Van Huffel, S., Dümpelmann, M., Schulze-Bonhage, A., De Vos, M., Van Paesschen, W., and Hunyadi, B. The power of ecg in multimodal patient-specific seizure monitoring: added value to an eeg-based detector using limited channels. *Epilepsia revised version submitted in March 2021*.

[254] Vandecasteele, K., De Cooman, T., Dan, J., Cleeren, E., Van Huffel, S., Hunyadi, B., and Van Paesschen, W. Visual seizure annotation and automated seizure detection using behind-the-ear electroencephalographic channels. *Epilepsia 61*, 4 (2020), 766–775.

[255] Vandecasteele, K., De Cooman, T., Gu, Y., Cleeren, E., Claes, K., Van Paesschen, W., Van Huffel, S., and Hunyadi, B. Automated epileptic seizure detection based on wearable ecg and ppg in a hospital environment. *Sensors 17*, 10 (2017), 2338.

[256] Vandecasteele, K., Lázaro, J., Cleeren, E., Claes, K., Van Paesschen, W., Van Huffel, S., and Hunyadi, B. Artifact detection of wrist photoplethysmograph signals. In *Biostec (Biosignals), Funchal, Madeira - Portugal* (19-21 January, 2018), pp. 182–189.

[257] Vanherck, A. *Quality assessment and automated artefact detection in wearable PPG signals at different body places*. PhD thesis, KU Leuven, 2019.

[258] Varon, C. *Mining the ECG: algorithms and applications*. PhD thesis, KU Leuven, 2015.

[259] Varon, C., Caicedo, A., Testelmans, D., Buyse, B., and Van Huffel, S. A novel algorithm for the automatic detection of sleep apnea from single-lead ecg. *IEEE Transactions on Biomedical Engineering 62*, 9 (2015), 2269–2278.

[260] Varon, C., Jansen, K., Lagae, L., and Van Huffel, S. Can ECG monitoring identify seizures? *J. Electrocardiol.* (2015), 1069–1074.

[261] Verdru, J., and Van Paesschen, W. Wearable seizure detection devices in refractory epilepsy. *Acta Neurologica Belgica* (2020), 1–11.

[262] Vergult, A., De Clercq, W., Palmini, A., Vanrumste, B., Dupont, P., Van Huffel, S., and Van Paesschen, W. Improving the interpretation of ictal scalp eeg: Bss–cca algorithm for muscle artifact removal. *Epilepsia 48*, 5 (2007), 950–958.

[263] Walczak, T. S., Radtke, R. A., and Lewis, D. V. Accuracy and interobserver reliability of scalp ictal eeg. *Neurology 42*, 12 (1992), 2279–2279.

[264] Wan, Z., Yang, R., Huang, M., Zeng, N., and Liu, X. A review on transfer learning in eeg signal analysis. *Neurocomputing 421* (2020), 1–14.

[265] Wang, J. A new method for evaluating ecg signal quality for multi-lead arrhythmia analysis. In *Computers in Cardiology* (2002), IEEE, pp. 85–88.

[266] Wilson, S. B., Scheuer, M. L., Emerson, R. G., and Gabor, A. J. Seizure detection: evaluation of the reveal algorithm. *Clinical neurophysiology 115*, 10 (2004), 2280–2291.

[267] Xia, H., Garcia, G. A., McBride, J. C., Sullivan, A., De Bock, T., Bains, J., Wortham, D. C., and Zhao, X. Computer algorithms for evaluating the quality of ecgs in real time. In *2011 Computing in Cardiology* (2011), IEEE, pp. 369–372.

[268] Xie, Y., Redmond, S. J., Basilakis, J., and Lovell, N. H. Effect of ecg quality measures on piecewise-linear trend detection for telehealth decision support systems. In *2010 Annual International Conference of the IEEE Engineering in Medicine and Biology* (2010), IEEE, pp. 2877–2880.

[269] You, S., Cho, B. H., Yook, S., Kim, J. Y., Shon, Y.-M., Seo, D.-W., and Kim, I. Y. Unsupervised automatic seizure detection for focal-onset seizures recorded with behind-the-ear eeg using an anomaly-detecting generative adversarial network. *Computer Methods and Programs in Biomedicine* (2020), 105472.

[270] Yousefi, R., Nourani, M., Ostadobbas, S., and Panahi, I. A motion-tolerant adaptive algorithm for wearable photoplethysmographic biosensors. *IEEE J Biomed Health 18*, 2 (2012), 670–681.

[271] Yu, C., Liu, Z., McKenna, T., Reisner, A. T., and Reifman, J. A method for automatic identification of reliable heart rates calculated from ecg and ppg waveforms. *Journal of the American Medical Informatics Association 13*, 3 (2006), 309–320.

[272] Zaunseder, S., Huhle, R., and Malberg, H. Cinc challenge—assessing the usability of ecg by ensemble decision trees. In *2011 Computing in Cardiology* (2011), IEEE, pp. 277–280.

[273] Zhang, Y., Wei, S., Long, Y., and Liu, C. Performance analysis of multiscale entropy for the assessment of ecg signal quality. *Journal of Electrical and Computer Engineering 2015* (2015).

[274] Zhou, M., Tian, C., Cao, R., Wang, B., Niu, Y., Hu, T., Guo, H., and Xiang, J. Epileptic seizure detection based on eeg signals and cnn. *Frontiers in neuroinformatics 12* (2018), 95.

[275] Zibrandtsen, I., Kidmose, P., Christensen, C. B., and Kjaer, T. Ear-eeg detects ictal and interictal abnormalities in focal and generalized epilepsy–a comparison with scalp eeg monitoring. *Clinical Neurophysiology 128*, 12 (2017), 2454–2461.

[276] Zibrandtsen, I., Kidmose, P., and Kjaer, T. Detection of generalized tonic-clonic seizures from ear-eeg based on emg analysis. *Seizure 59* (2018), 54–59.

[277] Zijlmans, M., Flanagan, D., and Gotman, J. Heart rate changes and ECG abnormalities during epileptic seizures: Prevalence and definition of an objective clinical sign. *Epilepsia 43*, 8 (2002), 847–854.

[278] Ziyabari, S., Shah, V., Golmohammadi, M., Obeid, I., and Picone, J. Objective evaluation metrics for automatic classification of eeg events. *arXiv preprint arXiv:1712.10107* (2017).

Curriculum vitae

Kaat Vandecasteele was born in UZ Leuven, Belgium on July 7th, 1993. In 2014, she received the bachelor's degree in Bioscience Engineering and in 2016, the master degree in Biomedical Enginereering. Her thesis was in the field of Biomedical Data Processing with topic 'Online epileptic seizure detection for children at home using a multimodal approach' under supervision of Dr. Thomas de Cooman, Prof. dr. ir. Sabine Van Huffel and Prof. dr. Lieven Lagae. In the summer of 2015, she did an internship at Transtimulation Research Inc. and Johns Hopkins University, US, Baltimore on 'Intestinal electrical stimulation to treat diabetes and obesity'. In the summer of 2016, she did an internship at Manipal University, Karnataka, India on 'Segmentation of a brain tumor using MR images'. From September 2016, she has been working towards the PhD degree in the Department of Electrical Engineering (ESAT-STADIUS) of the KU Leuven under the supervision of Prof. dr. ir. Borbála Hunyadi, Prof. dr. ir. Sabine Van Huffel and Prof. dr. Wim Van Paesschen.

List of publications

Papers in international journals

1. **Vandecasteele K.**, De Cooman T., Gu Y., Cleeren E., Claes K., Van Paesschen W., Van Huffel S., Hunyadi B., "Automated Epileptic Seizure Detection Based on Wearable ECG and PPG in a Hospital Environment", Sensors, Special Issue on Wearable and Ambient Sensors for Healthcare and Wellness Applications, vol. 17, no. 10, Oct. 2017, pp. 1 - 12.

2. De Cooman T.*, **Vandecasteele K.***, Varon C., Hunyadi B., Cleeren E., Van Paesschen W., Van Huffel S., "Personalizing Heart Rate-Based Seizure Detection Using Supervised SVM Transfer Learning", Frontiers in Neurology, vol. 11, no. 145, Feb. 2020, pp. 1-13. [Authors [*] contributed equally to the work.]

3. **Vandecasteele K.**, De Cooman T., Dan J., Cleeren E., Van Huffel S., Hunyadi B., Van Paesschen W., "Visual seizure annotation and automated seizure detection using behind-the-ear electroencephalographic channels", Epilepsia, vol. 61, no. 4, Apr. 2020, pp. 766-775.

4. Becker, T., **Vandecasteele, K.**, Chatzichristos, C., Van Paesschen, W., Valkenborg, D., Van Huffel, S., De Vos, M. "Classification with a Deferral Option and Low-Trust Filtering for Automated Seizure Detection", Sensors, Special issue on Healthcare Monitoring and Management with Artificial Intelligence, vol. 21, no. 4., February 2021, 1046.

Papers submitted to international journals

1. **Vandecasteele, K.**, De Cooman, T., Chatzichristos, C., Cleeren, E., Swinnen, L., Ortiz, J. M., Van Huffel, S., Dümpelmann, M., Schulze-Bonhage, A., De Vos, M., Van Paesschen, W., Hunyadi, B., "The power

of ecg in multimodal seizure monitoring: visual recognition and added value to an eeg-based detector using limited channels", Epilepsia, revised version submitted in March 2021 (ESAT-Stadius report number: 21-03).

Papers in proceedings of international conferences

1. **Vandecasteele K.**, Lázaro J., Cleeren E., Claes K., Van Paesschen W., Van Huffel S., Hunyadi B., "Artifact detection of wrist photoplethysmograph signals", Biostec (Biosignals), Funchal, Madeira - Portugal, 19-21 January 2018, 8 p.

2. Chatzichristos C.*, Dan J.*, Narayanan A. M.*, Seeuws N.*, **Vandecasteele K.***, De Vos M., Bertrand A., Van Huffel S., "Epileptic Seizure Detection in EEG via Fusion of Multi-View Attention-Gated U-net Deep Neural Networks", The 2020 IEEE Signal Processing in Medicine and Biology Symposium (SPMB), Philadelphia, USA, 2020.7p. [Authors [*] contributed equally to the work. This paper received the SPMB best paper award.]



FACULTY OF ENGINEERING SCIENCE
DEPARTMENT OF ELECTRICAL ENGINEERING
STADIUS
Kasteelpark Arenberg 10 box 2446, B-3001 Leuven (Belgium)
B-3001 Leuven
kaat.vandecasteele@esat.kuleuven.be